OFFICIAL JOURNAL OF THE SCIENTIFIC SOCIETY OF ANATOMISTS, HISTOLOGISTS, EMBRYOLOGISTS AND TOPOGRAPHIC ANATOMISTS OF UKRAINE

DOI: 10.31393
ISSN 1818-1295
eISSN 2616-6194

ВІСНИК МОРФОЛОГІЇ
REPORTS OF MORPHOLOGY

Vol. 28, №2, 2022

Scientific peer-reviewed journal in the fields of normal and pathological anatomy, histology, cytology and embryology, topographical anatomy and operative surgery, biomedical anthropology, ecology, molecular biology, biology of development

Published since 1993
Periodicity: 4 times a year

Vinnytsya · 2022

ВІСНИК МОРФОЛОГІЇ - REPORTS OF MORPHOLOGY

Founded by the "Scientific Society of Anatomists, Histologists, Embryologists, and Topographic Anatomists of Ukraine" and National Pyrogov Memorial Medical University, Vinnytsya in 1993

Certificate of state registration КВ №9310 from 02.11.2004

Professional scientific publication of Ukraine in the field of medical sciences in specialties 221, 222, 228, 229
According to the list of professional scientific publications of Ukraine, approved by the order of the Ministry of Education and Science of Ukraine No. 1188 of 24.09.2020
Professional scientific publication of Ukraine in the field of biological sciences in specialty 091
According to the list of professional scientific publications of Ukraine, approved by the order of the Ministry of Education and Science of Ukraine No. 1471 of 26.11.2020

Approved by the Academic Council of National Pyrogov Memorial Medical University, Vinnytsya, protocol №8 from 26.05.2022.

Indexation: CrossRef, Index Copernicus, Google Schoolar Metrics, National Library of Ukraine Vernadsky

Address editors and publisher:
Pyrogov Str. 56,
Vinnytsya, Ukraine - 21018
Tel.: +38 (0432) 553959
E-mail: nila@vnmu.edu.ua

Computer page-proofs - Klopotovska L.O.
Translator - Gunas V.I.
Technical support - Levenchuk S.S.
Scientific editing - editorship

The site of the magazine - https://morphology-journal.com

CONTENT

DOI: 10.31393/morphology-journal-2022-28(2)-01 Reports of Morphology, Vol. 28, №2, Pages 5-12

ISSN 1818-1295 eISSN 2616-6194

REPORTS OF MORPHOLOGY

Official Journal of the Scientific Society of Anatomists, Histologists, Embryologists and Topographic Anatomists of Ukraine

journal homepage: https://morphology-journal.com

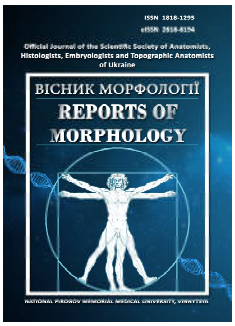

Cephalometric parameters of the upper and lower jaws according to the COGS method in Ukrainian young men and young women with orthognathic occlusion depending on the type of face

Nesterenko Ye. A., Shinkaruk-Dykovytska M. M., Chaika V. H., Dudik O. P., Gunas I. V.
National Pirogov Memorial Medical University, Vinnytsya, Ukraine

ARTICLE INFO
Received: 28 December 2021
Accepted: 03 February 2022

UDC: 616.714.1-071.3(477)

CORRESPONDING AUTHOR
e-mail: tikhonova_123@ukr.net
Nesterenko Ye. A.

CONFLICT OF INTEREST
The authors have no conflicts of interest to declare.

FUNDING
Not applicable.

The key to successful orthodontic treatment is the use of a delicate, modern, accurate and scientifically sound method of intervention planning. In addition, it is critical that this method takes into account as many variables as possible that may affect the final result. Given these criteria, the most appropriate for planning orthodontic treatment is cephalometric analysis of lateral teleradiograms, which, however, requires preliminary clinical trials to adapt it to the local population. The aim of the study was to establish the features of cephalometric parameters of the upper and lower jaws, determined according to the COGS method, in Ukrainian young men and young women with orthognathic occlusion depending on the type of face. According to the COGS method, cephalometry was performed for 46 young men (aged 17 to 21) and 72 young women (aged 16 to 20) who belonged in three generations to Caucasian residents of Ukraine and had an orthognathic bite. OnyxCeph³TM software, 3DPro version, Image Instruments GmbH, Germany was used for cephalometric analysis of the upper and lower jaws. Determination of the type of face of young men and young women was carried out according to the values of the morphological index of Garson. Statistical processing of the obtained results was performed in the license package "Statistica 6.0" using non-parametric evaluation methods. The following significant or tendencies of differences between linear and angular parameters of the upper and lower jaws were found between young women with different face types: in young women with a very wide face type - lower values of ANS-Me distance and N-A-Pog, MP-HP angles (compared to other types face) and Ar-Go-Gn (compared to medium and narrow face types), as well as larger values of the distances N-B and N-Pog (compared to other face types); in young women with medium face type - smaller the values of the distances N-A (compared to other face types), N-B and N-Pog (compared to wide and narrow face types), Go-Pog (compared to very wide face type), A-B (compared to a wide face type), as well as larger values of the distance B-Pog and angles MP-HP and Ar-Go-Gn (compared to a wide face type); representatives with a narrow face type have higher values of the distances N-ANS (compared to other face types), B-Pog (compared to very wide and wide face types), PNS-N (compared to a wide face type). The following significant or tendencies of differences between linear and angular indicators of the upper and lower jaws were found between young men with different face types: representatives with very wide face type have higher values of N-B, N-Pog, ANS-PNS distances (compared to average face type), Ar-Go (compared to wide and medium face types), A-B (compared to medium and narrow face types) and N-A (compared to narrow face types), as well as smaller MP-HP angle values (compared to other face types); representatives with a narrow face type have larger values of PNS-N (compared to other face types) and N-ANS (compared to very wide and wide face types), as well as smaller values of N-A-Pog angle (compared to average face type); representatives with medium face type have only smaller values of the ANS-PNS distance (compared to wide face type). Young men with different face types also have larger upper linear dimensions of the upper and lower jaws than in young women with different face types; and in young women mainly with narrow and medium face types - angular indicators of the upper and lower jaws.

Keywords: *cone-beam computed tomography, teleradiography, COGS cephalometry, cephalometry, upper and lower jaws, young men, young women, orthognathic occlusion, facial types, sex differences.*

Introduction

Aesthetic and balanced facial profile from the point of view of modern medicine has certain, specific parameters that can be calculated in order to plan surgery or therapeutic intervention. What is important, a key component that influences the formation of a balanced facial profile is a person's smile. The condition of the dental and maxillary apparatus, thus, is the focus of various areas of dentistry [26].

At the same time, current data on the prevalence of pathology of the dental and maxillofacial system are not comforting.

In Saudi Arabia, bite pathologies of class I, II and III were found in 52.8 %, 31.8 % and 15.4 % of 500 randomized subjects, respectively. Also, within this sample, 23.4 % showed excessive occlusion, and 12.2 % reduced occlusion [16].

A survey of 1,200 children in India found a prevalence of occlusal pathology in 53.7 % of young men and 32.8 % of young women. 6.8 % have a high risk of caries and 38.1 % have a moderate risk of caries [17].

During the dental examination, 671 adults, residents of Spain, observed orthodontic pathology in 31.3 % of the examined. Of these, only 21.1 % agreed that the identified pathology is really relevant to them. In particular, women agreed to a greater extent than men (23.9 % and 14.4 %, respectively) [4].

374 12-year-old children were examined in Ethiopia for orthodontic pathology. According to the analysis of scientists, almost 50 % of subjects had pathology of the dental and maxillofacial system. The most common pathologies were crowding of teeth and overbite (23.3 % and 30.8 %, respectively) [24].

Given this problem, it is necessary to take into account all possible parameters that may affect the predisposition to the formation of a pathology. An important parameter influencing the formation of the dental-maxillary system is the type of human face [13]. Thus, Duan J. and others [12] drew attention to the fact that parameters such as the angle between the axis of the first premolar of the mandible and the buccal surface of the cheek, vestibular angle and vestibular arc are much higher in people with short face type.

Individuals with brachycephalic facial type are more sensitive to orthodontic treatment and have better sagittal lip contractions [18].

Cephalometric analysis allows to apply the obtained anthropometric data in practice, in order to directly help patients.

Since its introduction to the general public, the cephalometric method of analysis has not remained out of the active attention of the world scientific community. This powerful tool for planning orthodontic treatment has found its place in various fields of medicine - the treatment of ENT diseases, personal identification in forensic medicine, maxillofacial surgery, etc. [14]. However, at the same time, this method requires the use of adaptation of normative indicators for different variables. This can be sex, age, nationality, facial type and other parameters, which will help to maximize the effectiveness of planning the patient's treatment, which in turn will improve the end result - a beautiful and harmonious smile. The wide range of different methods of analysis of lateral teleradiograms, which is the result of almost a century of evolution of the method still does not allow researchers from around the world to fully capture and adapt them. In addition, even preliminary data need to be revised due to the active migration processes taking place in the modern world [25].

A similar problem exists in Ukraine and needs to be addressed in order to implement cephalometric analysis as soon as possible.

The aim of the study was to establish the features of cephalometric parameters of the upper and lower jaws, determined according to the COGS method, in Ukrainian young men and young women with orthognathic occlusion depending on the type of face.

Materials and methods

Cephalometric examination of lateral teleradiograms (obtained using a dental cone-beam tomograph Veraviewepocs 3D Morita) of 46 young men (aged 17 to 21 years) and 72 young women (aged 16 to 20 years) taken from the database of the research center and Department of Pediatric Dentistry National Pirogov Memorial Medical University, Vinnytsya. All young men and young women applied to Vinintermed Private Dental Clinic for a diagnostic examination, belonged in three generations to Caucasian Ukrainians, and had a physiological bite that was as close as possible to orthognathic (orthognathic bite). Committee on Bioethics of National Pirogov Memorial Medical University, Vinnytsya (protocol № 8 From 30.09.2021) found that the studies do not contradict the basic bioethical standards of the Declaration of Helsinki, the Council of Europe Convention on Human Rights and Biomedicine (1977), the relevant WHO regulations and laws of Ukraine.

Cephalometric analysis was performed according to the COGS-method [5], which was performed using OnyxCeph^{3}™ software, 3DPro version, Image Instruments GmbH, Germany (license for software №URSQ-1799 registered to M. O. Dmitriev).

Determination of facial type was performed according to the values of the Garson morphological index [20]. The distribution of persons by the value of the Garson index

was: young men - 5 with a very wide face, 22 with a wide face, 11 with a medium face, 8 with a narrow face; young women - 25 with a very wide face, 25 with a wide face, 10 with a medium face, 12 with a narrow face.

For the convenience of clinical use and correct modeling of a large array of metric characteristics, we used the distribution of teleradiographic indicators proposed by Dmitriev M. O. [6, 7, 8], according to which the second group includes indicators of the dental system, which often need to focus on orthodontic treatment of patients who are in the process of growth, as well as in persons with a formed skeleton, which with the help of orthognathic surgery can change the width, length, angles and positions of the upper and lower jaws.

The main cephalometric points and measurements included in the second group of indicators (Fig. 1, 2):

A (subspinale) - the most posterior point of the anterior contour of the upper jaw;

ANS (spina nazalis anterior) - point at the apex of the anterior nasal spine;

apOcP (anterior point of occlusal plane, anterior Downs point) - the middle of the line connecting the cutting edges of the upper middle **Is1u** and lower **Is1L** cutters;

Ar (articulare) - intersection of the anterior surface of the main part of the occipital bone with the posterior surface of the neck of the mandible;

B (submentale) - the deepest point of the anterior contour of the mandible;

Me (menton) - the lowest point of the symphysis of the mandible;

N (nasion) - the most anterior point of the frontal-nasal suture;

PNS (spina nazalis posterior) - point at the apex of the posterior nasal spine;

Pog (pogonion) - the foremost point of the chin protrusion;

ppOcP (posterior point of occlusal plane) - the point is located in the place of the most posterior contact of the first molars;

tGo (tangens gonion) - projection point at the angle of the mandible, formed at the intersection of lines, one of which is a tangent line to the posterior edge of the mandibular branch from the point **Ar**, the second is a tangent line to the lower edge of the mandible from the point **Me**. It is usually a few millimeters below and distal to the **Go** point;

distance **A-B** (distance of **A** to **B** on occl. Plane, the distance from point **A** to point **B** on the closing plane) - distance from point **A** and **B** defined along the line **Occl. Plane**, which passes through the points **apOcP** and **ppOcP** (mm);

distance **ANS-PNS** (maxillary length, PNS-ANS) - distance from the point **ANS** to point PNS parallel to the horizontal line HR-Line (mm);

distance **ANS-Me** (anterior lower facial height, ANS-Gn) - distance from the point **ANS** to point **Me** (mm);

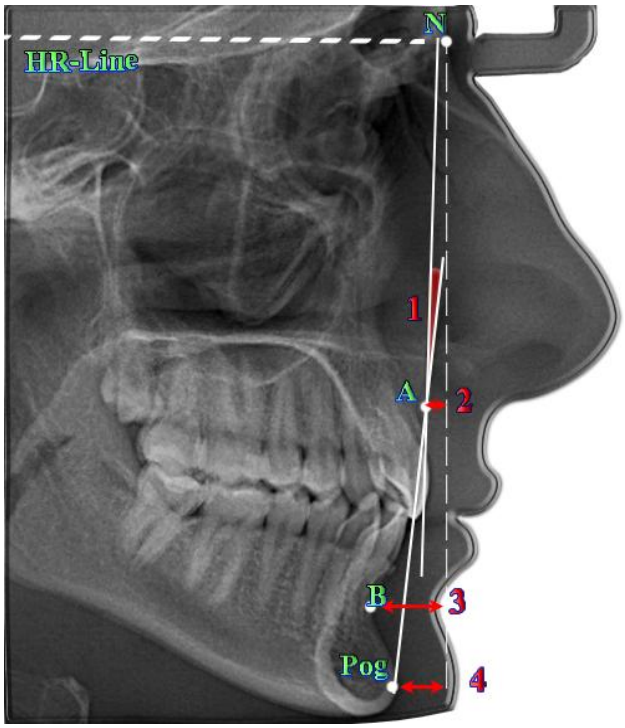

Fig. 1. The main cephalometric points and measurements included in the second group of indicators of the COGS method. 1 - angle **N-A-Pog**; 2 - distance **N-A**; 3 - distance **N-B**; 4 - distance **N-Pog**.

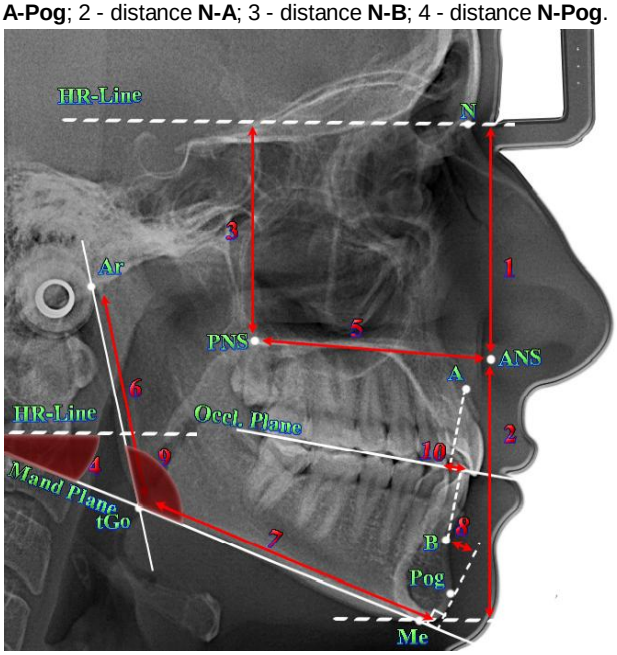

Fig. 2. The main cephalometric points and measurements included in the second group of indicators of the COGS method. 1 - distance **N-ANS**; 2 - distance **ANS-Me**; 3 - distance **PNS-N**; 4 - angle **MP-HP**; 5 - distance **ANS-PNS**; 6 - distance **Ar-Go**; 7 - distance **Go-Pog**; 8 - distance **B-Pog**; 9 - angle **Ar-Go-Gn**; 10 - distance **A-B**.

distance **Ar-Go** (ramus length, the length of the mandible ramus, distance ar-Go) - distance from the point **Ar** to point **tGo** (mm);

distance **B-Pog** - distance from the point **Pog** to point **B**

parallel to the mandibular plane, line **tGo-Me** (mm);

distance **Go-Pog** (mandibular length, the length of the base of the mandible) - distance from the point **Pog** to point **tGo** (mm);

distance **N-A** (maxillary position) - distance between points **N** and **A**, defined along the line HR-Line (HR-Line - the line is drawn through the point **N** and seven degrees above the line **S-N** (mm);

distance **N-ANS** (anterior upper facial height) - distance from the point **N** to point **ANS** (mm);

distance **N-B** (mandibular position) - distance between points **N** and **B**, defined along the line HR-Line (mm);

distance **N-Pog** (position of chin) - distance between points **N** and **Pog**, defined along the line HR-Line (mm);

distance **PNS-N** (posterior upper facial height) - distance from the point **PNS** to line HR-Line (mm);

angle **Ar-Go-Gn** (gonial angle) - the angle is formed by lines **Ar-tGo** and **tGo-Me** (°);

angle **MP-HP** (angle of mandibular to horizontal plane) - the angle formed by the mandibular plane **tGo-Me** and line HR-line (°);

angle **N-A-Pog** (convexity, angle of facial convexity) - the angle is formed by lines **N-A** and **A-Pog** (°).

Statistical processing of the obtained results was performed in the license package "Statistica 6.0" using non-parametric evaluation methods. Mean values and standard deviation were determined for each trait. The reliability of the difference between the values between the independent quantitative values was determined using the U-Mann-Whitney test.

Results

Tables 1 and 2 present the results of the linear and angular values of the upper and lower jaws in young men or young women with orthognathic occlusion, depending on the type of face.

We also found sex differences in the value of these indicators, namely significantly higher or trends toward higher values:

in young men - values of distances N-A (with very wide, p=0.075 and medium face, p=0.067), N-B (with medium face, p<0.05), N-Pog (with wide, p=0.062 and medium face, p<0.05), N-ANS (with wide, p<0.001, medium, p<0.05 and narrow face, p=0.082), ANS-Me (with wide, p<0.01 and narrow face, p=0.097), PNS-N (with wide, p<0.001, average, p=0.067 and narrow face, p<0.01), ANS-PNS (with very wide, p<0.01, wide, p<0.001 and narrow face, p=0.054), Ar-Go (with very wide, p<0.001, wide, p<0.001, medium, p<0.05 and narrow face, p<0.01), Go-Pog (with very wide, p<0.01, wide, p<0.01, medium, p<0.01 and narrow face, p<0.01), B-Pog (with wide face, p<0.001) and A-B (with very wide, p<0.01 and medium face, p=0.078), and angle N-A-Pog (with very wide face p=0.075);

in young women - values of angles N-A-Pog (with a narrow face p<0.05), MP-HP (with very wide, p<0.01, medium, p<0.05 and narrow face, p<0.01) and Ar-Go-Gn with medium, p=0.091 and narrow face, p=0.054).

Discussion

Analysis of 23 indicators of 100 teleradiograms (including 50 men and women aged 20, ethnic Bangladesh) using the COGS method allowed to adapt

Table 1. The magnitude of the linear and angular parameters of the upper and lower jaws in young men with different face types (M±σ).

Indicator	Face type				p_{1-2}	p_{1-3}	p_{1-4}	p_{2-3}	p_{2-4}	p_{3-4}
	Very wide (1)	Wide (2)	Average (3)	Narrow (4)						
Angle N-A-Pog	3.020±5.119	1.659±5.202	2.618±5.642	-1.538±4.378	>0.05	>0.05	>0.05	>0.05	>0.05	**=0.076**
Distance N-A	3.600±4.888	0.305±3.644	-0.427±3.267	-0.850±3.127	>0.05	>0.05	**=0.079**	>0.05	>0.05	>0.05
Distance N-B	1.580±7.088	-3.355±6.825	-4.409±4.382	-3.688±3.841	>0.05	**=0.062**	>0.05	>0.05	>0.05	>0.05
Distance N-Pog	4.900±7.635	-1.005±8.121	-2.464±5.542	-0.450±5.792	>0.05	**=0.079**	>0.05	>0.05	>0.05	>0.05
Distance N-ANS	47.34±6.50	50.90±2.72	51.85±3.21	53.55±2.09	>0.05	>0.05	**=0.079**	>0.05	<0.05	>0.05
Distance ANS-Me	60.74±7.33	62.89±3.93	63.41±3.56	62.81±3.66	>0.05	>0.05	>0.05	>0.05	>0.05	>0.05
Distance PNS-N	49.34±2.51	51.36±2.63	50.47±2.84	54.06±2.55	>0.05	>0.05	**<0.05**	>0.05	**<0.05**	**<0.05**
Angle MP-HP	11.38±4.20	18.70±6.71	20.97±4.98	17.33±5.64	**<0.05**	**<0.01**	**=0.079**	>0.05	>0.05	>0.05
Distance ANS-PNS	57.02±4.57	54.65±2.90	52.49±3.61	53.20±3.06	>0.05	**=0.070**	>0.05	**=0.089**	>0.05	>0.05
Distance Ar-Go	56.38±2.80	52.67±5.13	51.37±4.22	53.59±3.37	**=0.066**	**=0.054**	>0.05	>0.05	>0.05	>0.05
Distance Go-Pog	81.66±5.49	77.51±5.38	78.80±5.12	79.10±6.01	>0.05	>0.05	>0.05	>0.05	>0.05	>0.05
Distance B-Pog	6.360±2.620	7.191±1.685	7.632±1.462	7.825±1.440	>0.05	>0.05	>0.05	>0.05	>0.05	>0.05
Angle Ar-Go-Gn	114.5±7.6	119.7±6.6	118.9±4.6	117.0±4.7	>0.05	>0.05	>0.05	>0.05	>0.05	>0.05
Distance A-B	1.880±1.359	0.118±2.692	-0.773±2.763	-0.088±2.234	>0.05	**<0.05**	**=0.057**	>0.05	>0.05	>0.05

Notes: here and in the following table, M±σ - average sample ± standard deviation; $p(_{1-2}, _{1-3}, _{1-4}, _{2-3}, _{2-4}, _{3-4})$ - the reliability of the differences between the respective types of faces in young men or young women.

Table 2. The magnitude of linear and angular parameters of the upper and lower jaws in young women with different face types (M±σ).

Indicator	Face type				p_{1-2}	p_{1-3}	p_{1-4}	p_{2-3}	p_{2-4}	p_{3-4}
	Very wide (1)	Wide (2)	Average (3)	Narrow (4)						
Angle N-A-Pog	-1.188±4.718	2.600±6.150	2.200±3.207	3.858±3.487	**<0.05**	**<0.05**	**<0.01**	>0.05	>0.05	>0.05
Distance N-A	-0.472±3.476	-1.196±3.738	-3.180±2.538	-0.608±3.734	>0.05	**<0.05**	>0.05	**=0.062**	>0.05	**=0.065**
Distance N-B	-2.200±5.302	-5.268±5.046	-8.290±3.089	-5.317±4.822	**=0.068**	**<0.001**	**<0.05**	<0.05	>0.05	**=0.093**
Distance N-Pog	0.160±5.945	-4.484±5.594	-7.980±4.195	-4.342±5.863	**<0.05**	**<0.001**	**<0.05**	**=0.093**	>0.05	**=0.087**
Distance N-ANS	47.77±2.88	47.56±2.55	48.97±3.37	51.23±2.99	>0.05	>0.05	**<0.01**	>0.05	**<0.001**	**=0.099**
Distance ANS-Me	57.06±2.93	59.96±3.78	61.87±5.24	60.09±3.53	**<0.01**	**<0.01**	**<0.05**	>0.05	>0.05	>0.05
Distance PNS-N	48.56±2.58	47.87±2.11	48.02±2.92	49.38±2.03	>0.05	>0.05	>0.05	>0.05	**<0.05**	>0.05
Angle MP-HP	18.38±4.89	21.89±4.17	25.97±3.64	24.65±3.90	**<0.05**	**<0.001**	**<0.001**	**<0.01**	>0.05	>0.05
Distance ANS-PNS	50.38±2.19	50.78±2.49	50.75±4.07	50.28±2.72	>0.05	>0.05	>0.05	>0.05	>0.05	>0.05
Distance Ar-Go	47.97±5.89	47.20±6.46	46.69±4.27	47.61±3.50	>0.05	>0.05	>0.05	>0.05	>0.05	>0.05
Distance Go-Pog	74.32±3.44	72.81±3.40	70.85±4.16	72.32±3.67	>0.05	**<0.05**	>0.05	>0.05	>0.05	>0.05
Distance B-Pog	6.464±1.412	5.856±1.235	6.890±1.593	7.192±1.196	>0.05	>0.05	**=0.062**	**=0.068**	<0.01	>0.05
Angle Ar-Go-Gn	117.8±6.6	118.7±7.2	123.2±5.4	123.0±6.4	>0.05	**<0.05**	**<0.05**	**=0.065**	>0.05	>0.05
Distance A-B	-1.628±2.331	-0.808±2.686	-2.140±1.688	-0.792±2.944	>0.05	>0.05	>0.05	**=0.080**	>0.05	>0.05

this method for the local population. According to the results of the study - 15 indicators had pronounced manifestations of sexual dimorphism [1].

A similar study was performed using COGS analysis for residents of Saudi Arabia (160 people). The results of 38 measurements were selected for statistical processing. In this study, the manifestations of sexual dimorphism were not detected. But at the same time there are significant differences with European regulatory indicators [2]. These data are confirmed by the work of another team of authors, where the sample was 500 people aged 18-30 years [21].

There are also significant differences in the normative indicators of the COGS analysis for Sudanese residents. In particular, the latter have smaller values of height, length of the upper jaw, shorter base of the skull. In addition, significant manifestations of sexual dimorphism have been identified [15].

Residents of Kerala (India) also have significant differences with European data, which was made possible by studying their lateral teleradiograms using the COGS method [19]. Another study, however, already conducted in a sample of 100 indigenous peoples in northern India, also found significant differences with regulatory data and also found differences in the rates of men and women [22].

Also positive results were obtained when surveying people living in the central regions of India. This contingent found a decrease in the height of the upper and lower incisors, the height of the upper third of the face and the length of the anterior base of the skull [23]

A COGS survey of ethnic Malaysians and Chinese living in Malaysia was conducted. Of the 38 indicators, statistically significant differences between the sexes were found in 4 indicators of Malaysian Chinese and 18 Malaysians. There was also a significant difference between ethnic groups in 16 indicators [3].

When comparing between young men or young women with orthognathic occlusion with different face types of linear and angular indicators of the upper and lower jaws, determined by the COGS method, more pronounced differences were found between young women with different face types, namely:

in women with a very wide face type significantly smaller, or a tendency to lower values of the distance ANS-Me and angles N-A-Pog, MP-HP (compared to other face types) and Ar-Go-Gn (compared to medium and narrow face types), as well as significantly higher values of the distances N-B and N-Pog (compared to other types of faces);

in young women with medium face type significantly smaller, or tendencies to smaller values of distances N-A (compared to other face types), N-B and N-Pog (compared to wide and narrow face types), Go-Pog (compared to very wide face type), A-B (compared to a wide face type), as well as significantly larger, or tendencies to larger values of the distance B-Pog and angles MP-HP and Ar-Go-Gn (compared to a wide face type);

in women with a narrow face type significantly greater, or tendencies to greater values of the distances N-ANS (compared to other face types), B-Pog (compared to very wide and wide face types), PNS-N (compared to a wide face type).

Between young men with different face types, most of the reliable, or tendencies of differences between linear and angular indicators of the upper and lower jaws, determined by the COGS method, are established with

representatives of very wide or narrow face types:

in representatives with a very wide face type significantly greater, or tendencies to greater values of the distances N-B, N-Pog, ANS-PNS (compared to the average face type), Ar-Go (compared to wide and medium face types), A-B (compared with medium and narrow face types) and N-A (compared to narrow face type), as well as significantly smaller, or tendencies to smaller values of the MP-HP angle (compared to other face types);

representatives with a narrow face type have significantly larger, or tend to greater values of the distances PNS-N (compared to other types of faces) and N-ANS (compared to very wide and wide types of faces), as well as a tendency to smaller values of the angle N-A -Pog (compared to the average face type);

representatives with medium face type have only a slight tendency to lower values of the ANS-PNS distance (compared to wide face type).

We also found pronounced manifestations of sexual dimorphism of linear and angular parameters of the upper and lower jaws, determined by COGS-method, namely: in young men with different face types significantly larger or tendencies to larger values of most linear sizes of upper and lower jaws; and in young women, mostly with narrow and medium face types - angular indicators.

It should be noted that in the studies of Drachevskaya I. Yu. and others [9, 10, 11] conducted a survey and found the features of cephalometric indicators for Ukrainian young men and young women with orthognathic occlusion according to the methods of Ricketts, Downs, Steiner, taking into account the type of face of the subject. In particular, in all cases there were manifestations of sexual dimorphism.

Our results of linear and angular parameters of the upper and lower jaws, determined by COGS-method in Ukrainian young men and young women will provide dental care at the current level, taking into account not only age, sex and ethnicity, but also face type.

Conclusion

1. Between young men or young women (more pronounced) with orthognathic occlusion with different face types, numerous significant or tendencies of discrepancies between the linear and angular indices of the upper and lower jaws by the COGS method have been established.

2. Between young men and young women with orthognathic occlusion and the corresponding facial types, there are pronounced manifestations of sexual dimorphism of the upper and lower jaws by COGS-method: in young men - in most cases larger linear dimensions; for young women - angular.

References

[1] Alam, M. K., Basri, R., Purmal, K., Rahman, S. A., Shaari, R., & Haq, M. E. (2013). Cephalometric for orthognathic surgery (COGS) for Bangladeshi population. *Int Med J,* 20(3), 345-348. J-GLOBAL ID:201302294304893441

[2] Alam, M. K., Kassab, M., Alroudhan, I. E., Alabid, M. I. A. I., Alruwaili, M. M. F., Nafea, K., ... & Abdulelah, M. Cephalometrics For Orthognathic Surgery (COGS) Analysis For Saudi Arabian Adults. *European Journal of Molecular & Clinical Medicine,* 7(6), 2020.

[3] Averistus, G., Abdul Razak, N. H., & Alam, M. K. (2019). Cephalometric for orthognathic surgery (COGS): Determination of values applicable to Malaysian Malay and Chinese population. *Archives of Orofacial Science,* 14(1), 40-52.

[4] Bellot-Arcis, C., Montiel-Company, J. M., Manzanera-Pastor, D., & Almerich-Silla, J. M. (2012). Orthodontic treatment need in a Spanish young adult population. *Medicina oral, patologia oral y cirugia bucal,* 17(4), e638-e643. doi: 10.4317/medoral.17722

[5] Burstone, C. J., James, R. B., Legan, H., Murphy, G. A., & Norton, L. A. (1979). Cephalometrics for orthognathic surgery. *J. Oral. Surg,* 36, 269-277. PMID: 273073

[6] Dmitriev, M. O. (2016). Кореляції основних краніальних показників з характеристиками верхньої та нижньої щелеп у мешканців України юнацького віку [Correlations of main cranial index with characteristics of upper and lower jaws among residents in Ukraine of adolescent age]. *Світ медицини та біології - World of Medicine and Biology,* 4(58), 24-29.

[7] Dmitriev, M. O. (2017). Зв'язки кутових міжщелепних показників з характеристиками положення зубів та профілем м'яких тканин лиця у мешканців України юнацького віку [Links of angular inter-jaws indices with the characteristics of the closure plane, the position of the teeth and the soft-tissue profile of the face in the youth of Ukraine]. *Світ медицини та біології - World of Medicine and Biology,* 2(60), 51-59.

[8] Dmitriev, M. O. (2017). Зв'язки основних краніальних показників з характеристиками положення зубів верхньої і нижньої щелеп та профілем м'яких тканин лиця у юнаків і дівчат [Relations of key cranial indicators with the characteristics of the teeth of the upper and lower jaws and profile face soft tissue in boys and girls]. *Вісник морфології - Reports of Morphology,* 23(1), 125-131.

[9] Drachevska, I. Yu., Dmitriev, M. O., Likhitskyi, O. O., Kyrychenko, I. M., & Barylo, O. S. (2021). Determination of normative cephalometric parameters according to the Ricketts method for Ukrainian young men and young women with different face types. *Вісник Вінницького національного медичного університету,* 25(3), 381-388. doi: 10.31393/reports-vnmedical-2021-25(3)-05

[10] Drachevska, I. Yu., Dmitriev, M. O., Likhitskyi, O. M, Perlova, A. V., & Gunas, I. V. (2021). Determination of normative cephalometric parameters according to the Downs method for Ukrainian young men and young women with different face types. *Reports of Morphology*, 27(4), 47-52. doi: 10.31393/morphology-journal-2021-27(4)-07

[11] Drachevska, I. Yu., Dmitriev, M. O., Popova, O. I., Chugu, T. V., & Gunas I. V. (2021). Determination of normative cephalometric parameters according to the Steiner method for Ukrainian young men and young women with different face types. *Український стоматологічний альманах,* (4), 26-33. doi: 10.31718/2409-0255.4.2021.05

[12] Duan, J., Deng, F., Li, W. S., Li, X. L., Zheng, L. L., Li, G. Y., & Bai, Y. J. (2015). Differences in the mandibular premolar positions in Angle Class I subjects with different vertical facial types: A cone-beam computed tomography study. *The korean journal of orthodontics,* 45(4), 180-189. doi: 10.4041/kjod.2015.45.4.180

[13] Franco, F. C. M., Araujo, T. M. D., Vogel, C. J., & Quintao, C. C. A. (2013). Brachycephalic, dolichocephalic and mesocephalic: Is it appropriate to describe the face using skull patterns?. *Dental press journal of orthodontics,* 18(3), 159-163. doi: 10.1590/S2176-94512013000300025

[14] Furche, S., Edwards, S. P., Aronovich, S., Hummon, G., Shah, K. B., & Conley, R. S. (2019). 3D Airway changes using cone beam computed tomography in patients following mandibular advancement surgery with and without constriction. *Orthodontics & Craniofacial Research,* 22, 36-42. doi: 10.1111/ocr.12292

[15] Gilada, W. M., Abuaffan, A. H., & Hamid, M. M. (2021). Orthognathic cephalometric norms for a sample of Sudanese adults. *Journal of Head & Neck Physicians And Surgeons,* 9(1), 20-27. doi: 10.4103/jhnps.jhnps_11_21

[16] Gudipaneni, R. K., Aldahmeshi, R. F., Patil, S. R., & Alam, M. K. (2018). The prevalence of malocclusion and the need for orthodontic treatment among adolescents in the northern border region of Saudi Arabia: an epidemiological study. *BMC oral health*, 18(1), 16. doi: 10.1186/s12903-018-0476-8

[17] Kumar, P., Londhe, S. M., Kotwal, A., & Mitra, R. (2013). Prevalence of malocclusion and orthodontic treatment need in schoolchildren-An epidemiological study. *Medical journal armed forces India*, 69(4), 369-374. doi: 10.1016/j.mjafi.2012.02.003

[18] Martins, L. F., & Vigorito, J. W. (2013). Cone beam tomographic study of facial structures characteristics at rest and wide smile, and their correlation with the facial types. *Dental Press Journal of Orthodontics,* 18, 38-44. doi: 10.1590/S2176-94512013000600007

[19] Nasim, R., Ramakrishnan, R., Alkahtani, Z. M., Ganapathy, S., Vedam, V., & Saluja, P. (2021). A Cross-Sectional Study To Establish Soft Tissue Cephalometric Norms For Orthognathic Surgery In Kerala Population. *European Journal of Molecular and Clinical Medicine*, 8(1), 863-875.

[20] Proffit, U. R., Fildz, G. U., & Saver, D. M. (2006). *Современная ортодонтия* (перевод с английского Д. С. Персина) [*Modern orthodontics* (translation from English by D. S. Persina)]. M.: МЕДпресс-информ - M.: MEDpress-inform.

[21] Siddika, A., Rahman, S. A., & Alam, M. K. (2021). Cephalometric for Orthognathic Surgery (COGS) Analysis for Saudi Population. *Pesquisa Brasileira em Odontopediatria e Clinica Integrada*, 21, e0090. doi: 10.1590/pboci.2021.151

[22] Tikku, T., Khanna, R., Maurya, R. P., Verma, S. L., Srivastava, K., & Kadu, M. (2014). Cephalometric norms for orthognathic surgery in North Indian population using Nemoceph software. *Journal of oral biology and craniofacial research,* 4(2), 94-103. doi: 10.1016/j.jobcr.2014.07.004

[23] Tiwari, M. M., Daigavane, P. S., Kamble, R., Shrivastav, S., Jadhav, V. V., & Tiwari, R. M. (2020). Establishment of Cephalometric Norms for UCLP Cases from Central India Population Falling Under Goslon 1 and 2 Based on Burstone Analysis. *Journal of Evolution of Medical and Dental Sciences,* 9(16), 1365-1369. doi: 10.14260/jemds/2020/297

[24] Tolessa, M., Singel, A. T., & Merga, H. (2020). Epidemiology of orthodontic treatment need in southwestern Ethiopian children: a cross sectional study using the index of orthodontic treatment need. *BMC oral health*, 20(1), 210. doi: 10.1186/s12903-020-01196-2

[25] Turley, P. K. (2015). Evolution of esthetic considerations in orthodontics. *American Journal of Orthodontics and Dentofacial Orthopedics*, 148(3), 374-379. doi: 10.1016/j.ajodo.2015.06.010

[26] Zakaullah, S. (2021). An evaluation of the changes in bite force before and after orthognathic surgical correction of facial skeletal deformities. *University Journal Maxillofacial Surgery And Oral Sciences,* 1(1), 43-43. doi: 10.52977/ujmfs.2021.1.1.9

ОСОБЛИВОСТІ ЦЕФАЛОМЕТРИЧНИХ ПАРАМЕТРІВ ВЕРХНЬОЇ ТА НИЖНЬОЇ ЩЕЛЕП ЗА МЕТОДОМ COGS В УКРАЇНСЬКИХ ЮНАКІВ І ДІВЧАТ ІЗ ОРТОГНАТИЧНИМ ПРИКУСОМ В ЗАЛЕЖНОСТІ ВІД ТИПУ ОБЛИЧЧЯ

Нестеренко Є. А., Шінкарук-Диковицька М. М., Чайка В. Г., Дудік О. П., Гунас І. В.

Ключем до успішного проведення ортодонтичного лікування є застосування делікатного, сучасного, точного та науково обґрунтованого методу планування втручання. Окрім того критично важливо, аби даний метод враховував якомога більшу кількість змінних, що можуть впливати на остаточний результат. З урахуванням даних критеріїв, найбільш доцільним для планування ортодонтичного лікування є цефалометричний аналіз бокових телерентгенограм, який, проте, потребує проведення попередніх клінічних досліджень з метою адаптації його для місцевого населення. Мета дослідження - встановити особливості цефалометричних параметрів верхньої та нижньої щелеп, що визначаються за методом COGS, в українських юнаків і дівчат із ортогнатичним прикусом у залежності від типу обличчя. Згідно COGS-методу проведено цефалометрію 46 юнаків (віком від 17 до 21 років) і 72 дівчат (віком від 16 до 20 років) які належали у трьох колінах до мешканців України європеоїдної раси та мали ортогнатичний прикус. Для проведення цефалометричного аналізу показників верхньої та нижньої щелеп використовувалось програмне забезпечення OnyxCeph³™, версії 3DPro, компанії Image Instruments GmbH, Німеччина. Визначення типу обличчя юнаків і дівчат проводилося відповідно значенням морфологічного індексу Гарсона. Статистичну обробку отриманих результатів проводили в ліцензійному пакеті "Statistica 6.0" з використанням непараметричних методів оцінки. Між дівчатами з різними типами обличчя встановлені наступні достовірні або тенденції відмінностей лінійних і кутових показників верхньої та нижньої щелеп: у представниць із дуже широким типом обличчя - менші значення величини відстані ANS-Me та кутів N-A-Pog, MP-HP (порівняно з іншими типами обличчя) і Ar-Go-Gn (порівняно з середнім і вузьким типами обличчя), а також більші значення величини відстаней N-B і N-Pog (порівняно з іншими типами обличчя); у представниць із середнім типом обличчя - менші значення величини відстаней N-A (порівняно з іншими типами обличчя), N-B і N-Pog (порівняно з широким і вузьким типами обличчя), Go-Pog (порівняно з дуже широким типом обличчя), A-B (порівняно з широким типом обличчя), а також більші значення величини відстані B-Pog і кутів MP-HP та Ar-Go-Gn (порівняно з широким типом обличчя); у представниць із вузьким типом обличчя - більші значення величини відстаней N-ANS (порівняно з іншими типами обличчя), B-Pog (порівняно з дуже широким і широким типами обличчя), PNS-N (порівняно з широким типом обличчя). Між юнаками з різними типами обличчя встановлені наступні достовірні або тенденції відмінностей лінійних і кутових показників верхньої та нижньої щелеп: у представників із дуже широким типом обличчя - більші значення величини відстаней N-B, N-Pog, ANS-PNS (порівняно з середнім типом обличчя), Ar-Go (порівняно з широким і середнім типами обличчя), A-B (порівняно з середнім і вузьким типами обличчя) і N-A (порівняно з вузьким

типом обличчя), а також менші значення величини кута MP-HP (порівняно з іншими типами обличчя); у представників із вузьким типом обличчя - більші, значення величини відстаней PNS-N (порівняно з іншими типами обличчя) і N-ANS (порівняно з дуже широким і широким типами обличчя), а також менші значення величини кута N-A-Pog (порівняно з середнім типом обличчя); у представників із середнім типом обличчя - лише менші значення величини відстані ANS-PNS (порівняно з широким типом обличчя). Також в юнаків із різними типами обличчя встановлені більші значення, ніж у дівчат із відповідними типами обличчя більшості лінійних розмірів верхньої та нижньої щелеп; а у дівчат переважно з вузьким і середнім типами обличчя - кутових показників верхньої та нижньої щелеп.

Ключові слова: *конусно-променева комп'ютерна томографія, телерентгенографія, цефалометрія за COGS-методом, кефалометрія, верхня та нижня щелепи, юнаки, дівчата, ортогнатичний прикус, типи обличчя, статеві розбіжності.*

DOI: 10.31393/morphology-journal-2022-28(2)-02 Reports of Morphology, Vol. 28, №2, Pages 13-19

ISSN 1818-1295 eISSN 2616-6194

REPORTS OF MORPHOLOGY

Official Journal of the Scientific Society of Anatomists, Histologists, Embryologists and Topographic Anatomists of Ukraine

journal homepage: https://morphology-journal.com

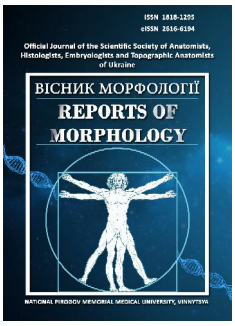

Central retinal artery: branching patterns on the disc of optic nerve

Orlova T. V., Stepanenko O. Yu.
Kharkiv National Medical University, Kharkiv, Ukraine

ARTICLE INFO
Received: 11 January 2022
Accepted: 26 February 2022

UDC: 611.843.1/.2

CORRESPONDING AUTHOR
e-mail: tv.orlova@knmu.edu.ua
Orlova T. V.

CONFLICT OF INTEREST
The authors have no conflicts of interest to declare.

FUNDING
Not applicable.

Vascular pathology of the retina is a common problem among patients with diabetes mellitus, hypertension. There are non-invasive diagnostic methods for retinal examination, which gives an advantage over other research methods. Pathological processes should be differentiated from the normal state of blood vessels without their lesion, so we should understand the pattern and variant anatomy of the vascular bed. The objective was to investigate the nature of the variability of the central retinal artery branching on the disc of optic nerve. We studied 402 images of the ophthalmoscopies from 8 databases that are available on the Internet. It was investigated that central retinal artery goes out to optic disc as one trunk (86.8 %) or two (13.0 %) and three (0.2 %) branches of the first order. One of the most common options is the ramification of two branches of first order - the upper and lower (73.1 %). Three branches were also found: upper, lower, nasal branch - 20.0 %; upper, lower, macular - 3.3 %. Other options were observed, but to a lesser extent. In 1.7 % of cases, four branches ramified from the main trunk: upper, lower, nasal and macular. When describing the variants of artery and vein on optic disc, similar variants of the pattern are observed, which were combined into groups X-shaped pattern of the I (41.3 %), II (7.7 %) and III type (10.2 %), Y-shaped (9.4 %), ζ (dzeta)-shaped pattern I type (8.7 %), ζ (dzeta)-shaped pattern II type (15.0 %) and V-shaped (7.7 %). The classic version can be represented as follows. Most often, the central retinal artery goes to the optic disc as a single trunk. One of the most common options was the ramification of two branches: upper and lower. The most common variant of the pattern of artery and vein at the optic disc was X-shaped pattern of the I type.
Keywords: *human, eye, retina, central retinal artery.*

Introduction

Vascular diseases of the retina are a common complication of diseases such as diabetes, hypertension and more. According to the WHO, the leading causes of blindness in people over the age of 50 in 2020 are age-related macular degeneration (1.8 million) and diabetic retinopathy (0.86 million) [22], among which 3 to 4.1 % of Europeans are affected [18]. By 2020, diabetic retinopathy was detected in 7.9 % of the 5 million subjects [19].

Another extremely serious vascular pathology of the retina is occlusion of the central retinal artery (CRA) and the central retinal vein (CRV). In 2020, among the 5 million studied - 4.4 % had occlusion of the CRV. Annual incidence of the most common retinal diseases (such as diabetic retinopathy, central artery and retinal vein occlusion) continues to increase [19].

The human retina receives blood supply from the CRA, and blood flows through the CRV. Sometimes the cilioretinal artery is involved [1, 14].

The main trunk of the CRA goes to the optic disc, dichotomously branching into two branches of the first order (upper and lower). Then each of the branches forms two branches of the second order: temporal and nasal [10, 16, 17, 20]; upper - upper temporal and upper nasal; lower - respectively, the lower temporal and lower nasal. Temporal branches go arcuate around the macula; they are better seen during ophthalmoscopy. The nasal branches run diagonally and in the opposite direction from the temporal branches; they are harder to see because they are out of sight [9, 23]. However, the sequence of division of CRA into branches is not constant. The variety of variants of CRA branching on the optic disc is the first vector of its individual anatomical variability.

The purpose of the work: to investigate the variant anatomy of the CRA branch on the disc of optic nerve.

Materials and methods

We studied 402 images of the retinal fundus obtained from 8 databases that are publicly available on the Internet

Table 1. Retinal fundus image database.

Database	Link	Number of images used
CHASE	https://www.medicmind.tech/retinal-image-databases	26
DRIVE AV		40
MESSIDOR		98
STARE		29
FIRE	https://projects.ics.forth.gr/cvrl/fire/	41
HRF	https://paperswithcode.com/dataset/hrf	33
INSPIRE	https://medicine.uiowa.edu/eye/inspire-datasets	40
DRIONS	http://www.ia.uned.es/~ejcarmona/DRIONS-DB.html	95
Total:		**402**

[3-5, 7, 11-13, 15, 21]. The data are presented in table 1.

To describe the branching of the CRA, retinal fundus images were processed: the images were added to Microsoft PowerPoint 2016, which created an enlarged image of the optic disc in the form of a circle. Then the images were transferred to Adobe Photoshop CS5, a new layer was added and the course of the artery was drawn in it, repeating their course on the base image. The next step was to hide the first layer of the original photo and leave the layer with the painted vessels. These images were analyzed and classified. Each image was described by the following criteria: the number of main trunks on the optic disc, the number of branches branching from the main trunk within the optic disc, and the types of pattern formed by second-order branches on the optic disc.

Results

The first manifestation of individual anatomical variability of the CRA is variants of its branching within the optic disc to the branches of the first and second order (Fig. 1). The most common variant of the structure is the division of the main trunk of the CRA into two branches of the first order: upper and lower (264 observations, or 73.1 %; see Fig. 1a). Less frequently, on the optic disc, the main trunk of the CRA branched into three branches of the first order, with several variants of branching. More often than others (72, or 20.0 % of observations) there was a variant when the main trunk was divided into upper, lower and nasal branches (see Fig. 1b). Less often (12 or 3.3 %) the division of the main trunk into upper, lower and macular branches was observed (see Fig. 1c). In 6 images, or 1.7 % of cases, four branches branched from the main trunk: upper, lower, nasal and macular (see Fig. 1d, Fig. 2).

Another - the second - manifestation of individual anatomical variability of the CRA is the beginning, or depth, of its branching relative to the optic disc on the next branches of the first order. Most often (355 observations, or 86.8 %), the main trunk of the CRA emerges on the optic disc and already on its surface branches into next branches of the first order (see Figs. 1, 2). But there are variants of the structure, when it branches before the passage of lamina cribrosa into two branches (53 observations, or 13.0 %;

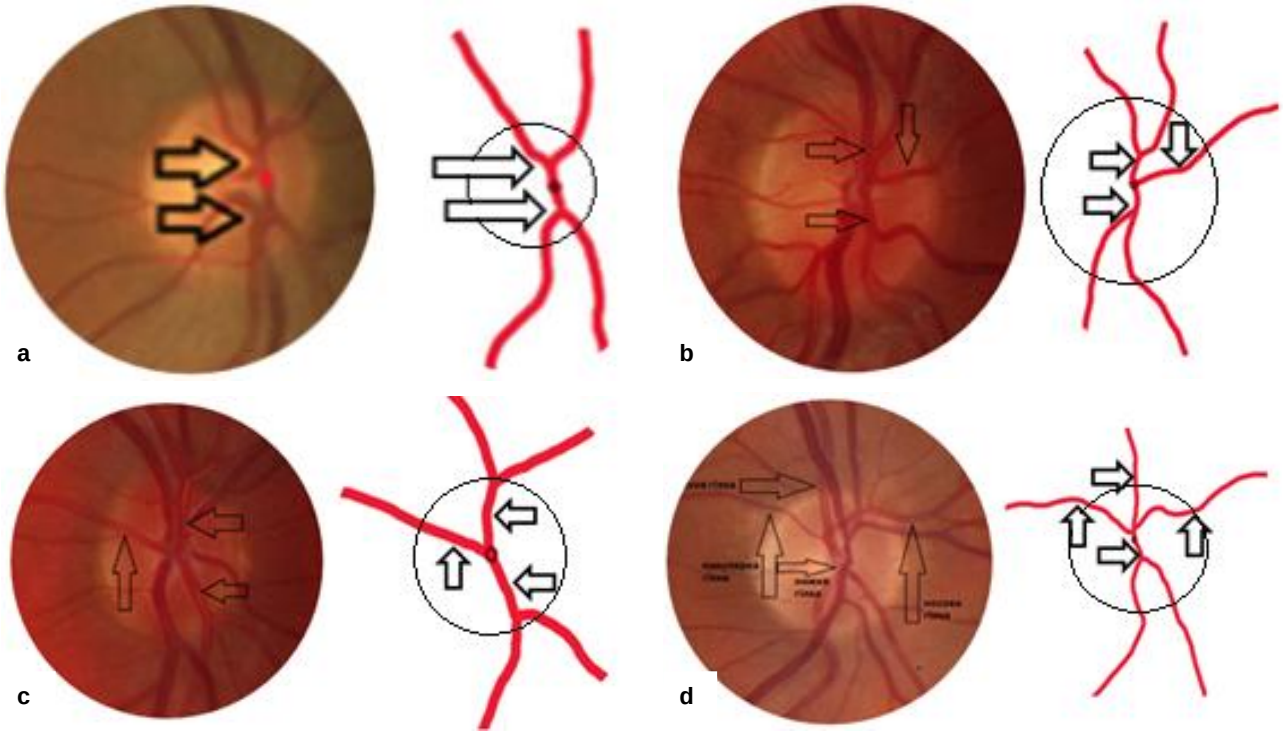

Fig. 1. Variants of division of CRA main trunk into branches of the first order (arrows indicate the branches): a - into 2 branches: upper and lower; b - on 3 branches: upper, lower, nasal; c - on 3 branches: upper, lower, macular; d - on 4 branches: upper, lower, macular, nasal.

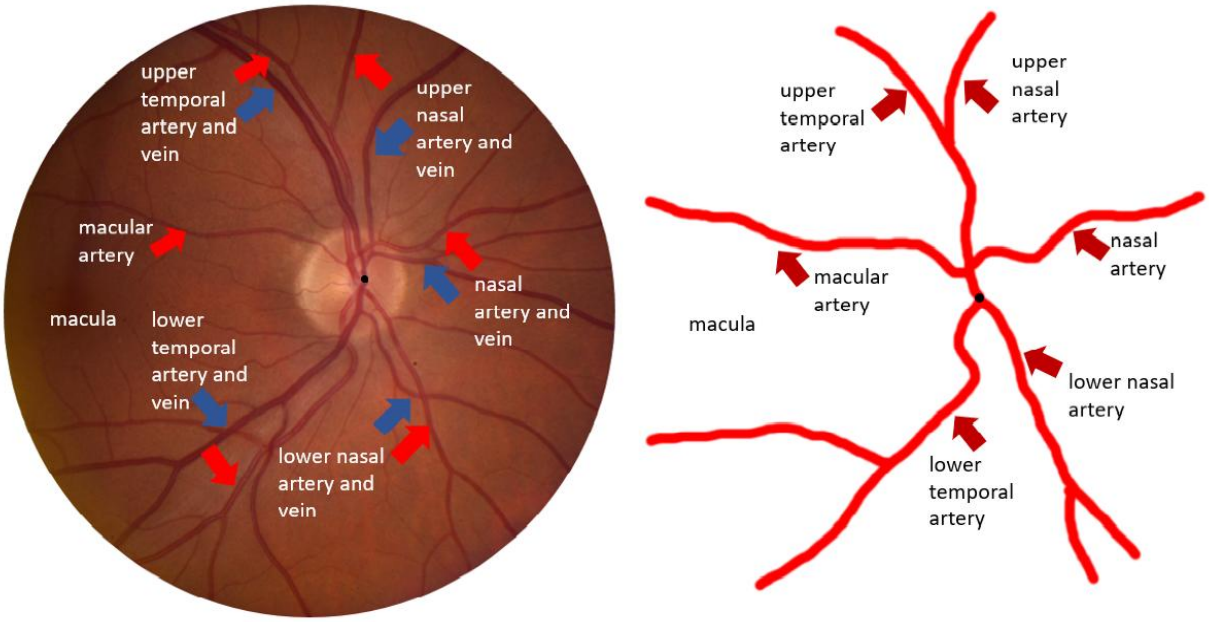

Fig. 2. The main branches of the CRA and CRV of the human retina: upper temporal, upper nasal, lower temporal, lower nasal, macular, nasal.

Fig. 3a, b). In only one case we observe a division into three (1 observation, or 0.2 %) branches of the first order (see Fig. 3c).

When the CRA appears on the surface of the optic disc by two branches of the first order, there are several options for its further branching. As a rule, when entering the optic disc, they are located in such a way that they can be described as the upper and lower branches of the first order. Each of them branches into temporal and nasal (see Fig. 3a); the latter can be considered second-order branches.

Sometimes the branches of the first order differ in the degree of branching; in this case, they can be defined as the main and additional branches of the first order: the main branch into a larger number of branches (see Fig. 3b). The additional branch either does not branch, or at a certain distance from the beginning is divided into two branches. Together, they form the usual number of second-order branches (branching of an additional branch on the surface of the optic disc we consider as second-order branches).

The additional branch, depending on the location relative to the main one, can be described as temporal (Fig. 4a, b) or nasal (Fig. 4c); the first can be described as upper temporal if its trunk emerges in the upper temporal area (see Fig. 4a), or lower temporal if its trunk emerges in the lower temporal area (see Fig. 4b).

The third manifestation of CRA variability is the peculiarity of the division into second-order branches and the pattern they form on the optic disc (Fig. 5).

We have identified the following types:

1) X-shaped pattern of type I - the artery comes to the surface of the optic disc at right angles to its surface and

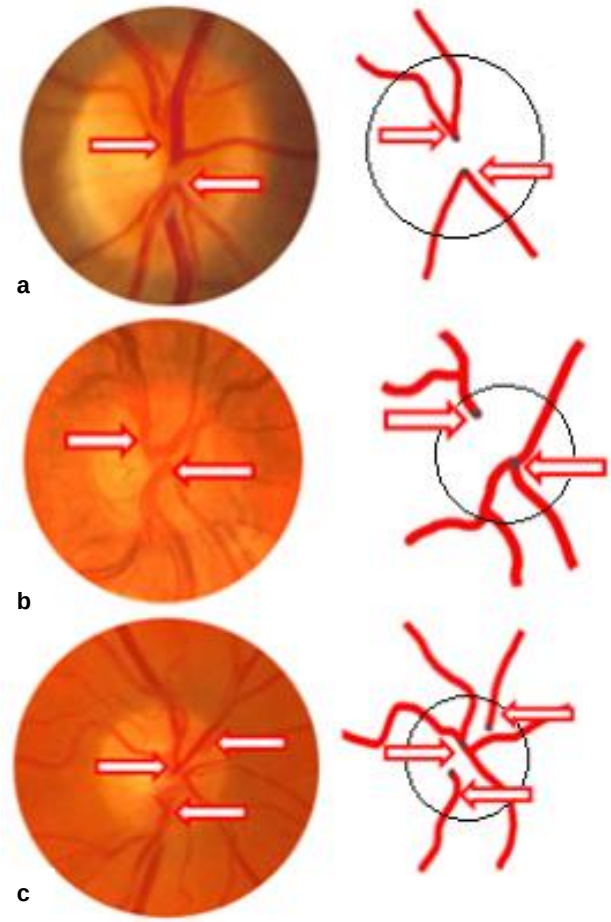

Fig. 3. Options for individual variability of the CRA: enters on the surface of the optic disc as two (a, b), or three (c) branches of the first order (arrows).

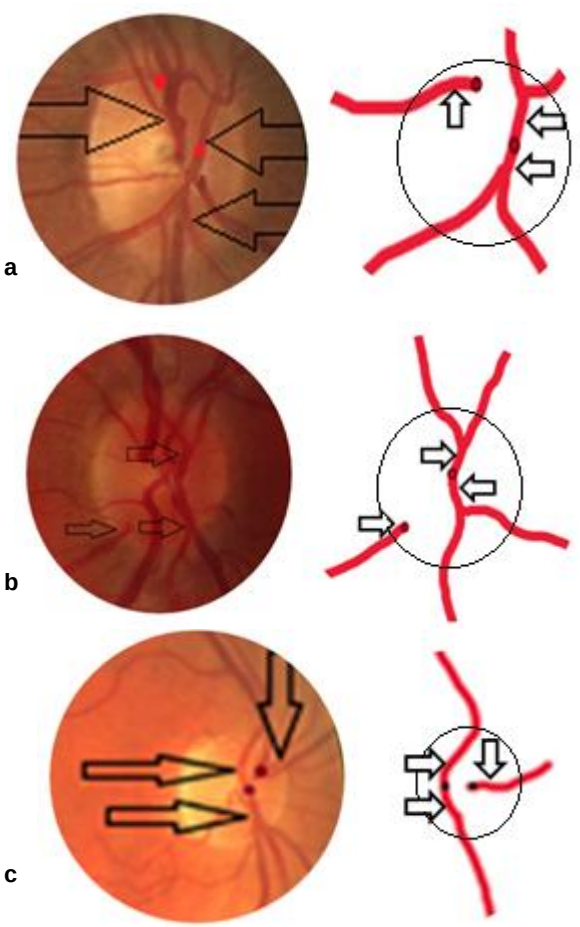

Fig. 4. Variants of individual variability of CRA: the main branch of the first order is divided into upper and lower branches of the first order; the additional branch is located as upper temporal (a), lower temporal (b), upper nasal (c).

branches to clearly visible branches of the first order. Then from each of the branches of the first order branches of the second order are formed. This type of figure is the most common (166 observations, or 41.3 %) (see Figure 5.1);

2) X-shaped pattern of type II - the artery of the optic disc at right angles branches into very short branches of the first order (the length of which is about two diameters of the CRA) and then branches to the branches of the second order (31 observations, or 7.7 %) (see Fig. 5.2);

3) X-shaped pattern type III - the artery emerges from the optic disc at right angles and immediately branches to the branches of the second order, ie branches of the first order are almost absent (41 observations, or 10.2 %) (see Fig. 5.3);

4) Y-shaped pattern - in the place of branching there is the formation of two upper branches of the second order (or there is a very short upper branch of the first order, which immediately branches) and there is one lower branch of the first order (see Fig. 5.4). Thus, the CRA on the optic disc is represented by three branches: the upper temporal and upper nasal and lower. This figure resembles the letter

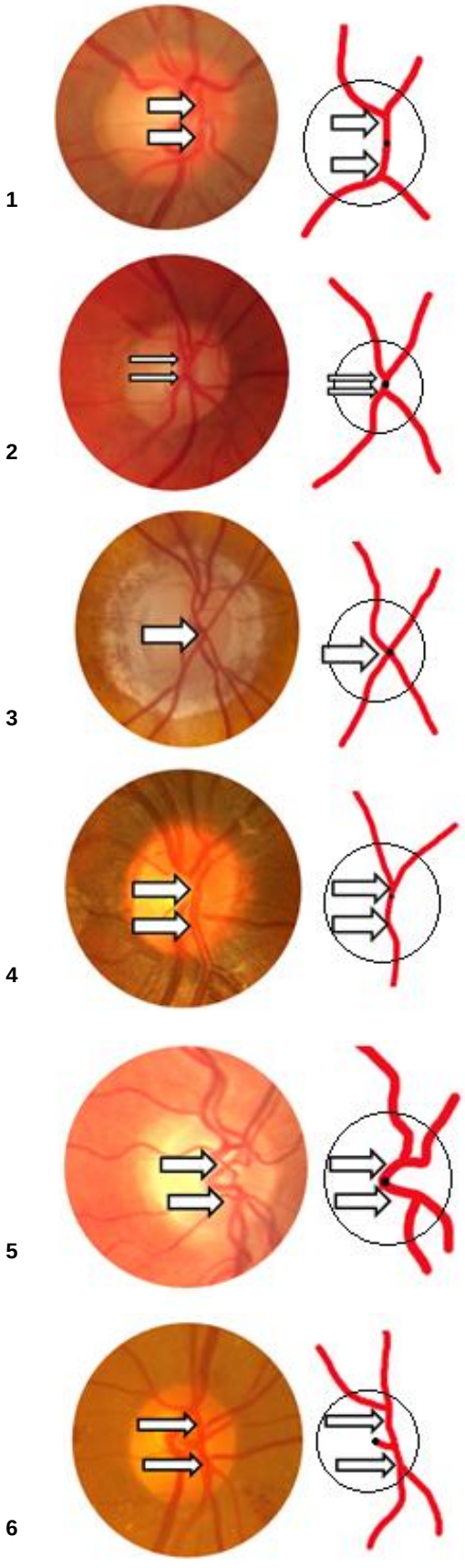

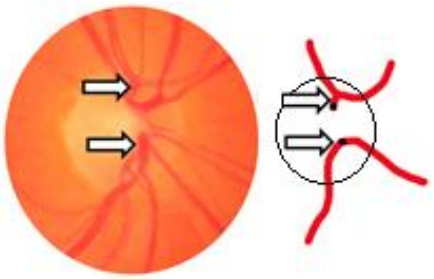

7

Fig. 5. Variants of the central retinal artery pattern on the optic disc (vascular pattern): 1 - X-shaped pattern of the I; 2 - II; 3 - III type; 4 - Y-shaped; 5 - ζ (dzeta)-shaped pattern I type; 6 - ζ (dzeta)-shaped pattern II type; 7 - V-shaped pattern.

Y (38 observations, or 9.4%). The "mirror" variant of the structure, which we defined as lambda (λ)-shaped (formation of the upper, lower temporal and lower nasal branches) is theoretically possible, but we have not met;

5) ζ (zeta)-shaped pattern of type I - the artery at the exit of the optic nerve branches into branches of the first order and forms an angle, the pattern resembles the symbol ">" or "<" (see Fig. 5.5). The apex of the acute angle can be directed both towards the macula (the temporal direction - 18 observations, or 4.5 %), and from it (nasally 17 observations, or 4.2 %);

6) ζ (zeta)-like pattern of type II - similar to the previous version, but in this case on the surface of the optic disc you can see the trunk of the CRA, which then branches into the upper and lower branches of the first order. In contrast to the previous version, the trunk and the top of the corner are directed to the macula (60 observations, or 15.0 %) (see Fig. 5.6);

7) double V-shaped pattern - occurs when the artery branches into branches of the first order outside the lamina cribrosa, outside the eyeball. The images show a CAS already branched into branches of the second order. The optic disc has the appearance of two inverted letters V (or short "Y") (31 observations, or 7.7 %) (see Fig. 5.7).

The difference between the variant of the structure of the ζ (zeta)-like pattern of type I and II can be explained as follows:

- if the artery reaches the surface of the optic disc at an angle of 900 to it, then its branching will not be visible its main trunk (ζ (zeta) similar figure of type I, see Fig. 5.5);

- if the artery comes out at a different angle (acute), then in many cases you can observe its entire course, starting from the main trunk (ζ (zeta) similar figure type II, see Fig. 5.6).

Its pattern depends on the level of branching. For example, the closer to the optic disc (after the passage of the lamina cribrosa) branching occurred, the smaller the distance between the exit points of the branches.

Discussion

The literature uses the term main trunk to describe the CRA until its branching [8, 20]. In one study [20] it is proposed to use such concepts as large and small arterial trunk. We also use the concept of the main trunk, but we suggest using such concepts. In the optic nerve or on the optic disc, the main trunk branches into two branches of the first order, or the main and additional branches of the first order, where the main branch has a larger diameter and branches further into a larger number of branches. After the next branching, they become second-order branches.

We have described three manifestations of individual anatomical variability of the CRA: variants of its branching within the optic disc on the branches of the first and second order; the beginning, or depth, branching of the CRA relative to the optic disc on next branches of the first order; the peculiarity of the division into branches of the second order and the pattern they form on the optic disc.

The literature describes the division of the CRA trunk on the optic disc into two (upper, lower) and three branches (upper, lower, macular and upper, lower, nasal) [6, 16]. We also identified the presence of two: upper and lower branches (264 observations, or 73.1 %) and three branches: upper, lower and nasal (72, or 20.0 % of observations) and upper, lower and macular (12, or 3.3 %). This division was also supplemented - division into four branches: upper, lower, macular, nasal (6, or 1.7 %).

In the literature [6, 8, 15] there are variants of CRA output to the optic disc in the form of one and two trunks. One study found the presence of two CRA trunks (in two images) branching from the ocular artery [8]. Another paper described the large and small trunks of the CRA, which extended to the optic disc. In various cases, small trunks located in the macular and upper nasal region have been described [6]. We also described one main trunk, which branches into next branches of the first order (355 observations, or 86.8 %), as well as a variant in which the CRA branches before the passage of the lamina cribrosa into two branches (53 observations, or 13.0 %). The option of having three CRA trunks protruding on the optic disc (1 observation, or 0.2 %) was also described.

The literature describes the variants of branching of the CRA and CRV on the optic disc together, where there are A-, O-, Y-, D- and X-shaped branching among relatives [2, 15]. We studied images of the ophthalmoscopies in greater numbers, and people who are not related to each other. It has been shown that A, O and Y-like branching are the most common. It should be noted that only 17.0 % were selected for analysis as appropriate, which confirms the existence of other types of branching options, which was not described. In turn, we proposed a classification of variants of branching only CRA on the optic disc without CRV.

Conclusion

1. Individual variability of CRA branching on the disc of optic nerve consist in the level of its branching, the number of branches of the first and second orders and the pattern that forms the CRA on the disc of optic nerve.

2. Classic (most common) option: CRA goes to the optic disc in the form of a single trunk; branches into two branches: upper and lower. The latter on the upper temporal, upper nasal, lower temporal and lower nasal. The most common variant of the pattern of arteries and veins on the optic disc - X-shaped pattern of the first type. In addition, an X-shaped pattern of the second and third types was described, depending on the length of the first-order branches; Y-shaped pattern, ζ (zeta)-like pattern of I and II type, as well as V-shaped pattern.

References

[1] Akay, F., Gündogan, F. C., Yolcu, U., Toyran, S., Tunç, E., & Uzun, S. (2016). Retinal structural changes in systemic arterial hypertension: an OCT study. *European journal of ophthalmology,* 26(5), 436-441. doi: 10.5301/ejo.5000740

[2] Bouthillier, A., Berthiaume, L. F., Nguyen, A. X., Zhai, S. Y., Lalla, S., Bédard, O., ... & Lachapelle, P. (2020). Distinguishing Familial from Acquired Traits in the Retinal Blood Vessel Arborization. *Translational vision science & technology,* 9(8), 27. doi: 10.1167/tvst.9.8.27

[3] Budai, A., Bock, R., Maier, A., Hornegger, J., & Michelson, G. (2013). Robust vessel segmentation in fundus images. *International journal of biomedical imaging,* 2013, 154860. doi: 10.1155/2013/154860

[4] Carmona, E. J., Rincón, M., Garcia-Feijoó, J., & Martinez-de-la-Casa, J. M. (2008). Identification of the optic nerve head with genetic algorithms. *Artificial intelligence in medicine,* 43(3), 243-259. doi: 10.1016/j.artmed.2008.04.005

[5] Decenciére, E., Zhang, X., Cazuguel, G., Lay, B., Cochener, B., Trone, C., ... & Klein, J. C. (2014) Feedback on a publicly distributed database: the Messidor database. *Image Analysis & Stereology,* 33(3), 231-234. doi: 10.5566/ias.1155

[6] Ewis, S. H., & Elsyedahmed, F.S. (2012). Anatomical variation of the central retinal artery at the optic disc. *AAMJ,* 10(2), 246-270.

[7] Fraz, M. M., Remagnino, P., Hoppe, A., Uyyanonvara, B., Rudnicka, A.R., Owen, C. G., & Barman, S. A. (2012). An ensemble classification-based approach applied to retinal blood vessel segmentation. *IEEE transactions on bio-medical engineering,* 59(9), 2538-2548. doi: 10.1109/TBME.2012.2205687

[8] Hayreh, S. S. (2011). Acute retinal arterial occlusive disorders. *Progress in retinal and eye research,* 30(5), 359-394. doi: 10.1016/j.preteyeres.2011.05.001

[9] Hayreh, S. S. (2014). Ocular vascular occlusive disorders: natural history of visual outcome. *Progress in retinal and eye research,* 41, 1-25. doi: 10.1016/j.preteyeres.2014.04.001

[10] Hendrix, P., Griessenauer, C. J., Foreman, P., Shoja, M. M., & Tubbs, R. S. (2015). Blood Supply of the Cranial Nerves. *Nerves and Nerve Injuries,* 427-438. doi: 10.1016/B978-0-12-410390-0.00031-7

[11] Hernandez-Matas, C., Zabulis, X., Triantafyllou, A., Anyfanti, P., & Douma, S. (2017) FIRE: Fundus Image Registration Dataset. *Journal for Modeling in Ophthalmology,* 1(4), 16-28.

[12] Hoover, A., & Goldbaum, M. (2003). Locating the optic nerve in a retinal image using the fuzzy convergence of the blood vessels. *IEEE transactions on medical imaging,* 22(8), 951-958. doi: 10.1109/TMI.2003.815900

[13] Hoover, A., Kouznetsova, V., & Goldbaum, M. (2000). Locating blood vessels in retinal images by piecewise threshold probing of a matched filter response. *IEEE transactions on medical imaging*, 19(3), 203-210. doi: 10.1109/42.845178

[14] Justice, J., & Lehmann, R. P. (1976). Cilioretinal arteries: a study based on review of stereo fundus photographs and fluorescein angiographic findings. *Archives of Ophthalmology,* 94(8), 1355-1358. doi: 10.1001/archopht.1976.03910040227015

[15] Niemeijer, M., Xu, X., Dumitrescu, A. V., Gupta, P., van Ginneken, B., Folk, J. C., & Abramoff, M. D. (2011). Automated measurement of the arteriolar-to-venular width ratio in digital color fundus photographs. *IEEE transactions on medical imaging,* 30(11), 1941-1950. doi: 10.1109/TMI.2011.2159619

[16] Orlova, T. V. (2021). Варіантна анатомія центральної артерії сітківки (огляд літератури) [Variant anatomy of the central retinal artery (review)]. *Медицина сьогодні і завтра - Medicine Today and Tomorrow,* 90(2), 7. In press. doi: 10.35339/msz.2021.90.2.otv

[17] Pournaras, C. J., Rungger-Brandle, E., Riva, C. E., Hardarson, S. H., & Stefansson, E. (2008). Regulation of retinal blood flow in health and disease. *Progress in retinal and eye research,* 27(3), 284-330. doi: 10.1016/j.preteyeres.2008.02.002

[18] Prokofyeva, E., & Zrenner, E. (2012). Epidemiology of major eye diseases leading to blindness in Europe: a literature review. *Ophthalmic research,* 47(4), 171-188. doi: 10.1159/000329603

[19] Rosenblatt, T., Vail, D., Saroj, N., Boucher, N., Moshfeghi, D., & Moshfeghi, A. A. (2020). Epidemiology of common retinal diseases in retina practices in the United States. *Invest. Ophthalmol. Vis. Sci.,* 61(7), 4186.

[20] Sobhy, H., Ewis, A., & Shatla, E. F. (2012). Anatomical variation of the central retinal artery at the optic disc. *AAMJ,* 10(2), 246-270.

[21] Staal, J., Abramoff, M. D., Niemeijer, M., Viergever, M. A., & van Ginneken, B. (2004). Ridge-based vessel segmentation in color images of the retina. *IEEE transactions on medical imaging,* 23(4), 501-509. doi: 10.1109/TMI.2004.825627

[22] Steinmetz, J. D., Bourne, R. R., Briant, P. S., Flaxman, S. R., Taylor, H. R., Jonas, J. B., ... & Morse, A. R. F. (2021). Causes of blindness and vision impairment in 2020 and trends over 30 years, and prevalence of avoidable blindness in relation to VISION 2020: the Right to Sight: an analysis for the Global Burden of Disease Study. *The Lancet Global Health*, 9(2), e144-e160. doi: 10.1016/S2214-109X(20)30489-7

[23] van Overbeeke, J., & Sekhar, L. (2003). Microanatomy of the blood supply to the optic nerve. *Orbit* (Amsterdam, Netherlands), 22(2), 81-88. doi: 10.1076/orbi.22.2.81.14316

ЦЕНТРАЛЬНА АРТЕРІЯ СІТКІВКИ: ЗАКОНОМІРНОСТІ РОЗГАЛУЖЕННЯ НА ДИСКУ ЗОРОВОГО НЕРВА

Орлова Т. В., Степаненко О. Ю.

Судинна патологія сітківки є поширеною проблемою серед хворих на цукровий діабет, гіпертонічну хворобу. Для дослідження сітківки існують неінвазивні методи діагностики, що надає перевагу над іншими методами дослідження. Патологічні процеси варто диференціювати від нормального стану судин без їх ураження, тому слід розуміти закономірність організації та варіантну анатомію судинного русла. Метою дослідження було дослідити характер мінливості розгалуження центральної артерії сітківки на диску зорового нерва. Нами було вивчено 402 знімків очного дна з 8 баз даних, які знаходяться у

відкритому доступі в мережі інтернет. Було визначено, що центральна артерія сітківки виходить на диск зорового нерва у вигляді одного стовбура (86,8 %) або двох (13,0 %) і трьох (0,2 %) гілок першого порядку. Одним із найбільш поширеніших варіантів було відгалуження двох гілок першого порядку - верхньої та нижньої (73,1 %). Далі виявлялись три гілки: верхня, нижня, носова гілка - 20,0 %; верхня, нижня, макулярна - 3,3 %. Також спостерігались інші варіанти, але в незначній мірі. В 1,7 % випадків від головного стовбура відгалужувалось чотири гілки: верхня, нижня, носова та макулярна. При описі варіантів виходу артерії та вени на ДЗН спостерігаються схожі варіанти рисунку, які було об'єднано в групи: Х-подібний рисунок I (41,3 %), II (7,7 %) та III типу (10,2 %), Y-подібний (9,4 %), ζ (дзета)-подібний рисунок I типу (8,7 %), ζ (дзета)-подібний рисунок II типу (15,0 %) та V-подібний рисунок (7,7 %). Класичний варіант можна представити таким чином. Найчастіше центральна артерія сітківки виходить на диск зорового нерва у вигляді одного стовбура. Одним із найбільш поширеніших варіантів було відгалуження двох гілок: верхньої та нижньої. Найбільш поширений варіант рисунку виходу артерії та вени на диску зорового нерва - Х-подібний рисунок I типу.

Ключові слова: *людина, око, сітківка, центральна артерія сітківки.*

DOI: 10.31393/morphology-journal-2022-28(2)-03 Reports of Morphology, Vol. 28, №2, Pages 20-24

ISSN 1818-1295 eISSN 2616-6194

REPORTS OF MORPHOLOGY

Official Journal of the Scientific Society of Anatomists, Histologists, Embryologists and Topographic Anatomists of Ukraine

journal homepage: https://morphology-journal.com

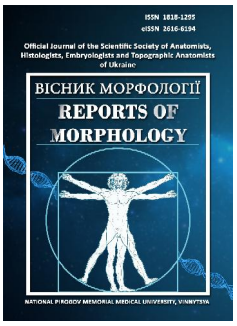

Skinfold thickness in men and women with seborrheic dermatitis of varying severity

Khasawneh A. R., Dmytrenko S. V., Serheta I. V., Bondar S. A., Anfilova M. R.
National Pirogov Memorial Medical University, Vinnytsya, Ukraine

ARTICLE INFO
Received: 17 January 2022
Accepted: 22 February 2022

UDC: 616.53-008.811.1:159.923.2

CORRESPONDING AUTHOR
e-mail: dr_ahmad_khasawneh@yahoo.com
Khasawneh A. R.

CONFLICT OF INTEREST
The authors have no conflicts of interest to declare.

FUNDING
Not applicable.

Significant progress has been made in the diagnosis of seborrheic dermatitis. It is based on the anamnesis and clinical picture of skin lesions. Carrying out a detailed analysis of the structure and size of the body in combination with clinical and instrumental studies allows us to further make a more reliable prognosis of complications of this disease and improve the results of treatment of such patients. The aim of the study was to establish and analyze the features of the skinfold thickness in Ukrainian men and women with seborrheic dermatitis of varying severity. Skinfold thickness (SFT) was determined in 40 men and 40 women (aged 25 to 44 years) with generalized fatty seborrheic dermatitis (mild and severe). The control group consisted of SFT values of practically healthy men (n=82) and women (n=154) of the same age group from the database of the research center National Pirogov Memorial Medical University, Vinnytsya. Statistical processing of SFT indicators was performed in the license package "Statistica 6.0" using non-parametric evaluation methods. Compared with practically healthy men, patients with mild and severe seborrheic dermatitis had lower SFT values on the posterior (by 49.7 % and 46.5 %) and anterior (by 41.9 % and 46.4 %) surfaces of the shoulder and chest (by 28.9 % and 27.9 %), on the thigh (47.3 % and 38.3 %), on the forearm (only compared to severe severity by 18.5 %), at the lower angle of the shoulder blade (only compared to mild severity by 3.5 %) and on the shin (only compared to severe severity by 15.9 %), as well as higher values of SFT on the side (by 36.7 % and 51.6 %); and in women patients of varying severity- also lower values of SFT on the posterior surface of the shoulder (by 51.0 % and 43.6 %), on the anterior surface of the shoulder (by 46.6 % and 31.0 %), on the chest (by 31.3 % and 18.9 %), on thighs (by 47.4 % and 38.9 %) and on the shin (only compared to the mild degree by 10.2 %), as well as higher values of SFT on the side (by 37.0 % and 44.6 %). Among men or women with seborrheic dermatitis of varying severity, only higher values were found in women with severe SFT on the anterior surface of the shoulder (by 22.6 %), and in men with severe severity - higher values of SFT on the thigh (by 14.6 %). Manifestations of sexual dimorphism of SFT among patients with seborrheic dermatitis of varying severity were found only between men and women with severe disease, namely, higher values of SFT in women on the front shoulder surface (by 28.6 %), forearm (by 16.0 %) and on the shin (by 26.3 %).

Keywords: *seborrheic dermatitis, constitutional features of skin diseases, Ukrainian men and women, anthropometry, skinfold thickness, sex differences.*

Introduction

Seborrheic dermatitis (SD) is a common disease and has great social significance, as it often leads to physical and psycho-emotional maladaptation of the patient and his family members. Clinical manifestations of dermatitis lead to psycho-emotional experiences, reduce social activity and quality of life, as well as cause the development of inferiority complex in patients. The disease is often resistant to therapy and occurs with frequent recurrences [6, 11, 18].

SD develops in the face and body with developed secretion of sebum [19]. The pathological process on the head is manifested by increased oiliness of the scalp, dandruff, constant itching and discomfort. SD of the scalp is accompanied by the appearance of plaques and thick scales, which can spread beyond hair growth and resemble

psoriasis. On the face, the pathological process is localized in the eyebrows, central part of the face, nasolabial folds and chin. If skin of a scalp is affected - thinning and thinning of hair which are often followed by formation of small white scales is observed. On the smooth skin of the back, face, chest appear macular-erythematous elements, papules, plaques appear [15, 16].

Significant progress has been made in the diagnosis of SD. It is based on the anamnesis and clinical picture of skin lesions. To date, many aspects of etiopathogenesis remain poorly understood. Genetic predisposition to certain metabolic features and the influence of the external environment on the development of the disease cannot be ruled out [13].

At the same time, a number of new emphases have emerged in the tactics of diagnosis, including the role of constitutional dermatology, aimed at a personalized approach to each patient [9]. This approach is essential both in terms of theoretical constitutional human biology and to address the problems of modern preventive medicine. For example, it is known that in the group of dolichomorphic somatotypes there is a tendency to reduce the incidence of severe skin lesions in the pathological process of pyoderma, atopic dermatitis with weight gain, while people with brachymorphic somatotype get an average of 42 % of all severe diseases [20]. In the group of patients with mesomorphic somatotype, the highest incidence of psoriasis was noted, as this type of somatotype most often occurs in the population [17].

Isolation of signs of diagnostic value (anthropometric, dermatoglyphic, etc.) and their further use in the clinic is another approach to the study of multifactorial diseases, including SD. The search for constitutional markers in connection with its resistance in the norm and in various pathological conditions is a necessary component of multifaceted comprehensive studies of the biological status of man [1, 8].

An important form of prevention of multifactorial nosologies is the formation of risk groups for primary prevention, genetic counseling and medical examination. In this regard, the practical work of doctors and geneticists is relevant to the use in low practice of low-cost and highly informative diagnostic methods [8, 9]. A good example is a more detailed analysis of the structure and size of the body in combination with clinical and instrumental studies, which will further obtain a reliable prognosis for the development of complications of dermatosis and improve the treatment of such patients [14].

The aim of the study was to establish and analyze the features of the skinfold thickness in Ukrainian men and women with seborrheic dermatitis of varying severity.

Materials and methods

Clinical and anthropological examination of 40 men and 40 young women with generalized oily form of SD of mild and severe severity (25-44 years according to the age periodization of the WHO, 2015) was conducted on the basis of the Department of Dermatology and Venereal Diseases with a postgraduate course in National Pirogov Memorial Medical University, Vinnytsya and the Central Military Medical Center.

The Bioethics Committee of the National Pirogov Memorial Medical University, Vinnytsya (Minutes № 10 of 26.11.2020) found that the studies did not contradict the basic bioethical standards of the Helsinki Declaration, the Council of Europe Convention on Human Rights and Biomedicine (1977), WHO regulations and Ukrainian law.

The diagnosis of SD was established on the basis of the subject's complaints, life history and illness, examination of the face, scalp, torso and extremities with the assessment of subjective and objective signs of the disease.

Anthropometric survey was conducted in accordance with the scheme of Bunak V. V. [4]. Measurements of skinfold thickness (SFT) were performed using a caliper (mm). Measured: SFT on the posterior (GZPL) and anterior (GPPL) surfaces of the shoulder, on the forearm (GPR), at the lower angle of the shoulder blade (GL), on the chest (GGR), abdomen (GG), sides (GB), thighs (GBD) and on the shin (GGL).

As a control group used SFT indicators of practically healthy men (n=82) and women (n=154) of the same age, which were selected from the database of the research center National Pirogov Memorial Medical University, Vinnytsya.

Statistical processing of the results was performed in the license package "Statistica 6.0" using non-parametric evaluation methods. The reliability of the difference between the values between the independent quantitative values was determined using the U-Mann-Whitney test.

Results

Table 1 presents the results of the comparison of SFT between healthy and patients with mild to severe SD men and/or women.

Table 1. Comparison of SFT between healthy and SD patients of varying severity in men and/or women (M±σ).

Indexes	Healthy men (n=82)	Men with SD		p_{h-ms}	p_{h-ss}	p_{ms-ss}
		MS (n=20)	SS (n=20)			
GZPL	7.848±2.914	3.950±1.146	4.200±1.609	**<0.001**	**<0.001**	>0.05
GPPL	5.592±2.132	3.250±1.070	3.000±1.214	**<0.001**	**<0.001**	>0.05
GPR	4.173±1.621	3.550±0.686	3.400±0.940	>0.05	**=0.088**	>0.05

Continuation of table 1.

Indexes	Healthy men (n=82)	Men with SD		p_{h-ms}	p_{h-ss}	p_{ms-ss}
		MS (n=20)	SS (n=20)			
GL	13.53±3.92t	13.05±6.50	13.30±6.31	**=0.071**	>0.05	>0.05
GGR	4.924±1.729	3.500±1.000	3.550±1.317	**<0.001**	**<0.001**	>0.05
GG	12.33±4.79	12.35±5.78	13.65±9.00	>0.05	>0.05	>0.05
GB	10.75±4.41	14.70±7.32	16.30±8.05	**<0.05**	**<0.001**	>0.05
GBD	12.80±3.85	6.750±1.618	7.900±2.125	**<0.001**	**<0.001**	**=0.058**
GGL	8.982±2.691	8.000±2.152	7.550±1.986	>0.05	**=0.052**	>0.05
Indexes	Healthy women (n=154)	Women with SD		p_{h-ms}	p_{h-ss}	p_{ms-ss}
		MS (n=20)	SS (n=20)			
GZPL	8.163±3.168	4.000±1.338	4.600±1.501	**<0.001**	**<0.001**	>0.05
GPPL	6.091±2.514	3.250±0.967	4.200±1.542*	**<0.001**	**<0.001**	**<0.05**
GPR	4.264±2.092	4.000±1.170	4.050±1.099t	>0.05	>0.05	>0.05
GL	12.70±4.13	14.55±6.57	12.60±4.28	>0.05	>0.05	>0.05
GGR	5.238±2.452	3.600±1.046	4.250±1.482	**<0.001**	**<0.05**	>0.05
GG	13.71±5.14*	14.60±4.69	15.80±6.15	>0.05	>0.05	>0.05
GB	11.93±4.99t	16.35±5.95	17.25±5.99	**<0.01**	**<0.001**	>0.05
GBD	14.74±4.38***	7.750±3.076	9.000±3.061	**<0.001**	**<0.001**	>0.05
GGL	10.80±3.09***	9.700±2.993t	10.25±2.47***	**<0.05**	>0.05	>0.05

Notes: MS - mild severity; SS - severe severity; p_{h-ms} - the significance of the difference in SFT values between healthy and patients with mild SD; p_{h-ss} - the significance of the difference in SFT values between healthy and patients with severe SD; p_{ms-ss} - the significance of the difference in SFT values between patients with mild to severe SD; * - the reliability of the difference in the values of the corresponding folds between men and women at the level p<0.05; ** - the reliability of the difference in the values of the corresponding folds between men and women at the level p<0.01; *** - the reliability of the difference in the values of the corresponding folds between men and women at the level p<0.001; t - trends in the difference between the values of the corresponding folds between men and women.

Discussion

It is a known fact that in solving the problem of identifying the peculiarities of the pathology depending on the physique, algorithms for taking into account the constitutional parameters of the body have long been actively used, which we consider necessary to use in groups of patients with SD. Establishing differences between healthy and patients with different dermatitis [2, 5, 7, 10] suggested the presence of such a pattern in SD.

Thus, Chaplyk-Chizho I. O. [5] found significantly higher values of SFT on the posterior, anterior surface of the shoulder and on the side in men with pyoderma compared to healthy men.

According to the results of Makarchuk I. M. [7] found that in healthy individuals of both sexes SFT on the front surface of the shoulder, forearm, lower angle of the shoulder blade, chest, abdomen, side, lower extremity recorded significantly higher values compared with patients with acne.

Al-Omary Ala'a Osama Ahmad et al. [2] found that in men with various forms and severity of eczema, most SFT (except fold on the side) are significantly lower than in healthy men.

Obadeh Bassam Abdel-Rahman Al-Qaraleh [10] found that in men with mild or severe psoriasis, compared to healthy men, significantly higher SFT at the lower angle of the shoulder blade, abdomen and side and lower - on the back and front of the shoulder, chest and thighs are observed.

In the analysis of *SFT between healthy and patients with mild to severe SD* Ukrainian men or women, we found the following significant or trends of differences (Table 2, see Table 1):

between healthy and sick men - in practically healthy men SFT values are higher on the posterior surface of the shoulder (49.7 % and 46.5 %, respectively), on the anterior surface of the shoulder (41.9 % and 46.4 %, respectively), on the chest (28.9 % and 27.9 %, respectively), on the thigh (by 47.3 % and 38.3 %, respectively), on the forearm (only compared to severe severity by 18.5 %), at the lower angle of the shoulder blade (only compared to mild severity by 3.5 %) and on the shin (only compared to with severe severity by 15.9 %), as well as lower values of SFT on the side (by 36.7 % and 51.6 %, respectively);

between healthy and sick women - in practically healthy women SFT values are higher on the posterior surface of the shoulder (by 51.0 % and 43.6 %, respectively), on the anterior surface of the shoulder (by 46.6 % and 31.0 %, respectively), on the chest (by 31.3 % and 18.9 %, respectively), on the thigh (by 47.4 % and 38.9 %,

Table 2. Differences in SFT between healthy and patients with seborrheic dermatitis of varying severity in men and/or women.

Indexes	Men			Women		
	H	SD/MS	SD/TC	H	SD/MS	SD/TC
GZPL	D	Ñ	Ñ	D	Ñ	Ñ
GPPL	D	Ñ	Ñ	D	Ñ▼	Ñ▲
GPR	-		¯			
GL	-	¯				
GGR	D	Ñ	Ñ	D	Ñ	Ñ
GG						
GB	Ñ	D	D	Ñ	D	D
GBD	D	Ñ ˅	Ñ ^	D	Ñ	
GGL	-		¯	D	Ñ	

Notes: H - healthy; SD/MS - SD of mild severity; SD/SS - SD of severe severity; D or Ñ - significant differences in SFT between healthy and sick men; - or ¯ - trends in SFT differences between healthy and sick men; ^ or ˅ - trends in differences in SFT between sick men of varying severity; D or Ñ - significant differences in SFT between healthy and sick women; ▲or ▼ - significant differences in SFT between sick women of varying severity; significantly higher SFT are highlighted in green when comparing the respective groups between men and women; trends in higher SFT values are highlighted in yellow when comparing the respective groups between men and women.

respectively) and on the shin (only compared to the mild severity by 10.2 %), as well as lower values of SFT on the side (by 37.0 % and 44.6 %, respectively).

Differences in the studied groups of patients are revealed in a comprehensive assessment of the patient's condition and features of the constitutional parameters of the body. Indeed, the role of the severity of the initial state of the patient remains a leading reflection of morphology, area, topography of the pathological process, the body's response and becomes a major factor in predicting adverse disease [3, 12].

For a long time, clinicians have drawn attention to the more severe course of dermatoses in overweight people [15]. The type of fat distribution is important.

When comparing *SFT between patients with SD of varying severity* in Ukrainian men or women, we found in men only a tendency to higher values in patients with severe SD of SFT on the thigh by 14.6 %; and in women - only significantly higher in patients with severe SD of SFT on the anterior surface of the shoulder by 22.6 % (see Tables 1, 2).

To date, many scientific and practical studies have been performed to study the characteristics of the thickness and distribution of subcutaneous fat in humans at different ages of ontogenesis. At the same time, it should be emphasized that the modern realities of human life dictate the need to develop subtler and practical research, also aimed at studying the sexual differences of this parameter in people with certain pathologies. This is especially true at a young age [8, 9].

In the analysis of *sex differences of SFT between patients with SD of varying severity* in Ukrainian women with severe severity found significantly higher or tendencies to higher values of SFT on the anterior surface of the shoulder by 28.6 %, forearm by 16.0 % and shin by 26.3 % (see Tables 1, 2). In contrast to SD patients with severe severity, practically healthy women had significantly higher or a tendency to have higher SFT values on the abdomen, side, thighs and shin, as well as a tendency to lower SFT values at the lower angle of the scapula (see Tables 1, 2).

The size and structure of the body as morphogenetic markers in the plane of the constitutional integrity of the organism are studied in connection with the adaptive potential of man during ontogenesis, taking into account the influence of the environment. The study of the patterns of intersystem connections makes it possible to further develop a set of criteria for prognostic assessment of the risk of SD on the basis of the phenotypology of anthropometric indicators.

Conclusion

1. Patients with SD of varying severity men and women, compared with healthy men and women, found significantly higher values of SFT on the shoulders, chest, thighs and shin (only in women with mild severity), as well as lower values of SFT on the side.

2. There is only a tendency to higher values of SFT on the thigh in patients with severe SD men, as well as significantly higher values of SFT on the posterior surface of the shoulder in patients with severe SD women, than in men or women with mild severity disease.

3. Among patients with SD of varying severity, minor manifestations of sexual dimorphism of SFT were found only in people with severe disease, namely - significantly higher or a tendency to higher values of SFT in the anterior surface of the shoulder, forearm and shin in women.

References

[1] Acharya, J., Shetty, B. S. K., Shrestha, R., & Kanchan, T. (2017). Approximation of height of an individual using somatometry of human male skull. *JNMA J Nepal Med Assoc,* 56(206), 238-242. PMID: 28746322

[2] Al-Omary Ala'a Osama Ahmad, Dmytrenko S. V., Chaika V. H., Isakova, N. M., & Gunas, I. V. (2021). Skinfold thickness in men with various forms of eczema. *World of Medicine and Biology,* 3(77), 11-15. doi: 10.26724/2079-8334-2021-3-77-11-15

[3] Augustin, M., Kirsten, N., Körber, A., Wilsmann-Theis, D., Itschert, G., Staubach-Renz, P., ... & Zander, N. (2019). Prevalence, predictors and comorbidity of dry skin in the general population. *Journal of the European Academy of Dermatology and Venereology,* 33(1), 147-150. doi: 10.1111/jdv.15157

[4] Bunak, V. V. (1941). *Антропометрия [Anthropometry]*. M.: Наркомпрос РСФСР - M.: People's Commissariat of the RSFSR.

[5] Chaplyk-Chyzho, I. O. (2016). Відмінності товщини шкірно-жирових складок між здоровими та хворими на піодермії чоловіками і жінками [Differences in the thickness of skin and fat folds between healthy and patients with pyoderma

men and women]. *Вісник проблем біології і медицини - Bulletin of problems of biology and medicine,* 1(2), 121-124.
[6] Dai, R. Y., & Gu, X. H. (2017). Study on health related quality of life and influencing factors in seborrheic dermatitis patients. *Chin J Gen Pract,* 15(02), 292-294.
[7] Makarchuk, I. M. (2015). Особливості товщини шкірно-жирових складок у хворих на вугрову хворобу юнаків та дівчат Поділля з урахуванням і без урахування соматотипу [Features of the thickness of skin and fat folds in patients with acne in boys and girls of Podillya, taking into account and without taking into account the somatotype]. *Мир медицины и биологии - World of Medicine and Biology,* 11(4-2 (54)), 47-50.
[8] Nikityuk, D. B. (2018). Anthroponutriciology as a New Scientific Direction. *Journal of Anatomy and Histopathology,* 7, 9-19. doi: 10.18499/2225-7357-2018-7-4-9-19
[9] Nikolenko, V. N., Nikityuk, D. B., & Klochkova, S. V. (2017). *Somatic constitution and clinical medicine.* Practical Medicine, Moscow.
[10] Obadeh Bassam Abdel-Rahman Al-Qaraleh. (2020). Skinfold thickness in men with mild and severe psoriasis without and taking into account the somatotype. *Biomedical and Biosocial Anthropology*, (40), 48-53. doi: 10.31393/bba40-2020-08
[11] Paerna, E., Aluoja, A., & Kingo, K. (2015). Quality of life and emotional state in chronic skin disease. *Acta Dermato-Venereologica,* 95(3), 312-316. doi: 10.2340/00015555-1920
[12] Park, S. Y., Kwon, H. H., Min, S., Yoon, J. Y., & Suh, D. H. (2016). Clinical manifestation and associated factors of seborrheic dermatitis in Korea. *European Journal of Dermatology*, 26(2), 173-176. doi: 10.1684/ejd.2015.2706
[13] Paulino, L. C. (2017). New perspectives on dandruff and seborrheic dermatitis: lessons we learned from bacterial and fungal skin microbiota. *European Journal of Dermatology,* 27(1), 4-7. doi: 10.1684/ejd.2017.3038
[14] Petukhov, A. B. (2015). *Medical anthropology: an analysis and development prospects in clinical practice* / A.B. Petukhov, D.B. Nikityuk, V.N. Sergeev/under the general editorship of the Prof. D.B. Nikitiuk. M.: Publishing House Medpraktika-M.
[15] Pouradier, F., Liu, C., Wares, J., Yokoyama, E., Collaudin, C., Panhard, S., ... & Loussouarn, G. (2017). The worldwide diversity of scalp seborrhoea, as daily experienced by seven human ethnic groups. *International Journal of Cosmetic Science,* 39(6), 629-636. doi: 10.1111/ics.12425
[16] Ramos-e-Silva, M., Sampaio, A. L., & Carneiro, S. (2014). Red face revisited: Endogenous dermatitis in the form of atopic dermatitis and seborrheic dermatitis. *Clinics in dermatology,* 32(1), 109-115. doi: 10.1016/j.clindermatol.2013.05.032
[17] Sakibaev, K., Kyzy, K. Z., Tashmatova, N., Klochkova, S., Atabaev, I., Nikityuk, D., ... & Satylganov, I. (2020). Somatotypological Features of the Skin Fat Fold Thickness in Ethnic Kyrgyz Women. *Forensic Medicine and Anatomy Research,* 9(01), 1. doi: 10.4236/fmar.2021.91001
[18] Sampogna, F., Linder, D., Piaserico, S., Altomare, G., Bortune, M., Calzavara-Pinton, P., ... & Abeni, D. (2014). Quality of life assessment of patients with scalp dermatitis using the Italian version of the Scalpdex. *Acta dermato-venereologica,* 94(4), 411-414. doi: 10.2340/00015555-1731
[19] Shi, V. Y., Leo, M., Hassoun, L., Chahal, D. S., Maibach, H. I., & Sivamani, R. K. (2015). Role of sebaceous glands in inflammatory dermatoses. *Journal of the American Academy of Dermatology,* 73(5), 856-863. doi: 10.1016/j.jaad.2015.08.015
[20] Silveira, E. A., Barbosa, L. S., Rodrigues, A. P. S., Noll, M., & De Oliveira, C. (2020). Body fat percentage assessment by skinfold equation, bioimpedance and densitometry in older adults. *Archives of Public Health,* 78(1), 1-9. doi: 10.1186/s13690-020-00449-4

ОСОБЛИВОСТІ ТОВЩИНИ ШКІРНО-ЖИРОВИХ СКЛАДОК У ЧОЛОВІКІВ І ЖІНОК ХВОРИХ НА СЕБОРЕЙНИЙ ДЕРМАТИТ РІЗНОГО СТУПЕНЯ ВАЖКОСТІ

Хасавнех А. Р., Дмитренко С. В., Сергета І. В., Бондар С. А., Анфілова М. Р.

У діагностиці себорейного дерматиту досягнуто значного прогресу. Вона ґрунтується на анамнезі та клінічній картині ураження шкіри. Проведення детального аналізу особливостей будови та розмірів тіла в комплексі з клініко-інструментальними дослідженнями дозволяє надалі проводити більш достовірний прогноз розвитку ускладнень цього захворювання та покращити результати лікування таких хворих. Мета дослідження - встановити та провести аналіз особливостей товщини шкірно-жирових складок в українських чоловіків і жінок хворих на себорейний дерматит різного ступеня важкості. Проведено визначення товщини шкірно-жирових складок (ТШЖС) у 40 чоловіків і 40 жінок (віком від 25 до 44 років) хворих на генералізовану жирну форму себорейного дерматиту (легкого та тяжкого ступеня важкості). Контрольну групу складали показники ТШЖС практично здорових чоловіків (n=82) і жінок (n=154) аналогічної вікової групи з банку даних науково-дослідного центру Вінницького національного медичного університету ім. М. І. Пирогова. Статистична обробка показників товщини шкірно-жирових складок проведена в ліцензійному пакеті "Statistica 6.0" із використанням непараметричних методів оцінки. У хворих на себорейний дерматит легкого та тяжкого ступеня важкості чоловіків, порівняно з практично здоровими чоловіками, встановлені менші значення ТШЖС на задній (на 49,7 % і 46,5 %) та передній (на 41,9 % і 46,4 %) поверхнях плеча, на грудях (на 28,9 % і 27,9 %), на стегні (на 47,3 % і 38,3 %), на передпліччі (лише порівняно з тяжким ступенем важкості на 18,5 %), під нижнім кутом лопатки (лише порівняно з легким ступенем важкості на 3,5 %) та на гомілці (лише порівняно з тяжким ступенем важкості на 15,9 %), а також більші значення ТШЖС на боці (на 36,7 % і 51,6 %); а у хворих різного ступеня важкості жінок - також менші значення ТШЖС на задній поверхні плеча (на 51,0 % і 43,6 %), на передній поверхні плеча (на 46,6 % і 31,0 %), на грудях (на 31,3 % і 18,9 %), на стегні (на 47,4 % і 38,9 %) та на гомілці (лише порівняно з легким ступенем важкості на 10,2 %), а також більші значення ТШЖС на боці (на 37,0 % і 44,6 %). Між хворими на себорейний дерматит різного ступеня важкості чоловіками або жінками встановлені лише більші значення у жінок із тяжким ступенем важкості ТШЖС на передній поверхні плеча (на 22,6 %), а у чоловіків із тяжким ступенем важкості - більше значення ТШЖС на стегні (на 14,6 %). Прояви статевого диморфізму ТШЖС між хворими на себорейний дерматит різного ступеня важкості встановлені лише між чоловіками та жінками з тяжким ступенем важкості захворювання, а саме - більші значення у жінок ТШЖС на передній поверхні плеча (на 28,6 %), на передпліччі (на 16,0 %) та на гомілці (на 26,3 %).

Ключові слова: *себорейний дерматит, конституціональні особливості захворювань шкіри, українськи чоловіки та жінки, антропометрія, товщина шкірно-жирових складок, статеві розбіжності.*

DOI: 10.31393/morphology-journal-2022-28(2)-04 Reports of Morphology, Vol. 28, №2, Pages 25-31

ISSN 1818-1295 eISSN 2616-6194

REPORTS OF MORPHOLOGY

Official Journal of the Scientific Society of Anatomists, Histologists, Embryologists and Topographic Anatomists of Ukraine

journal homepage: https://morphology-journal.com

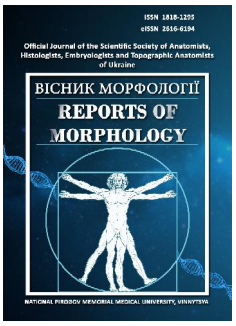

Influence of vitamin D on the histostructure of the testis and morphometric indications of spermatogenesis of intact rats

Marakhovskyi I. O., Laryanovska Yu. B., Korenieva Ye. M., Smolienko N. P., Chystiakova E. Ye., Belkina I. O., Velychko N. F., Misiura K. V., Bondarenko V. O.

S I "V. Danilevsky Institute for endocrine pathology problems of NAMS of Ukraine", Kharkiv, Ukraine

ARTICLE INFO

Received: 04 February 2022

Accepted: 11 March 2022

UDC: 612.616.3;591.147.8

CORRESPONDING AUTHOR

e-mail: ihor1marahovskiy@gmail.com

Marakhovskyi I. O.

CONFLICT OF INTEREST

The authors have no conflicts of interest to declare.

FUNDING

The work was financially supported by the S I "V. Danilevsky Institute for endocrine pathology problems of NAMS of Ukraine", Kharkiv, National Academy of Medical Sciences of Ukraine (No state registration: 0119U102387).

One of the current problems is the study of the effects of vitamin D on the body, and in men its action is closely related to the pathogenesis of androgen deficiency and hypofertility. Particular attention needs to be paid to determining whether cholecalciferol (D3) has a negative effect on the gonads and spermatogenesis of intact individuals, as vitamin D therapy is used in reproductive disorders with or without vitamin D deficiency. The aim of the study was to determine the effect of vitamin D on the histological structure of gonads and morphometric parameters of spermatogenesis of adult intact male rats. The studies were performed on adult sexually active male Wistar rats. Vitamin D3 was administered orally in doses of 1000 IU, 4000 IU and 10000 IU. The solutions were made on seed oil. The control was intact rats. Vitamin D and its solvent were administered throughout the period of spermatogenesis and the time of maturation of sperm in the epididymis, after which the structural organization of the testes was determined. Gonadal samples were fixed in 10 % formalin solution, leave in alcohols of increasing strength, and embedded in paraffin. In addition to survey microscopy, morphometric evaluation of the process of spermatogenesis was performed on sections of gonads stained with hematoxylin and eosin. Micropreparations were examined using a Granum L 30 (03) light microscope, and microscopic images were taken with a Granum DSM 310 digital video camera. Photographs were processed on a Pentium 2.4 GHz computer using Toup View. Statistical processing of data results was performed in the standard software package "Statistica 6.0" using Student's t-test and using a non-parametric analogue of one-way analysis of variance - Kruskal-Wallis criterion. In rat testicular sections, seminiferous tubules were located transversely or obliquely and were oval or round in shape. The diameter of the tubules is normal, the tubular membrane, as well as the protein and vascular membranes were normal. The basal department contains the youngest cells of the germinal epithelium - spermatogonia. Cells have a pronounced functional activity. Morphometric characteristics of spermatogenesis of intact rats corresponded to the physiological norm. The introduction of the solvent throughout the period of spermatogenesis and maturation of mature sperm in the epididymis did not affect the histoarchitectonics of the testicles. The testicular lobes are filled with concentric or flattened profiles of sections of the seminal tubules, which are close enough to each other. The diameter of the tubules is normal, the intrinsic membrane of the tubules, as well as the protein and vascular membranes corresponded to those in intact animals. 3-4 generations of spermatogenic cells, which were at different stages of development, can be seen in the tubules. However, few tubules with focal destruction of the germinal epithelium and exfoliation of germ cells in the lumen of the tubules have been observed. No significant changes in the microstructure of the seminal tubules were observed after administration of vitamin D at all doses studied. Not only spermatogenesis but also spermiogenesis is clearly traced in different tubules of rats - stages of cellular transformations from spermatid to sperm. Morphometric parameters of the process of spermatogenesis of rats receiving different doses of vitamin D3 do not differ from those of intact rats. Thus, the use of vitamin D in these doses revealed the safety of its effect on the number of spermatogonia and tubules with stage 12 meiosis. When cholecaciferol was used in male rats for 68 days, the

spermatogenesis index remained at the level of animals that did not receive the test substance. The use of vitamin D3 in intact adult male rats does not adversely affect the histological structure of the testes.
Keywords: *vitamin D, testicle, gonadotoxicity, testicular histostructure, morphometric parameters of spermatogenesis.*

Introduction

One of the current problems is the study of the effects of vitamin D on the body [11], and in men its action is closely related to the pathogenesis of androgen deficiency and hypofertility [17]. Seasonal fluctuations in vitamin D levels have been found, with high levels in summer and autumn and low levels in winter and spring, which are almost identical to similar annual cycles of testosterone levels, suggesting a strong association between androgen metabolism and vitamin D [22].

It has been shown that in men the level of vitamin D determines the qualitative and quantitative parameters of ejaculate [6, 16], including motility and morphology of sperm [1, 14]. There is growing evidence of the importance of vitamin D for sperm maturation. An association between low levels of vitamin D and decreased numbers of motile and morphologically normal sperm has been reported [10].

Vitamin D deficiency in animals leads to impaired maturation of the vas deferens, decreased testicular weight and sperm concentration [8]. The experiment showed that vitamin D saturation leads to a significant improvement in spermatogenesis in experimental reproductive diseases [12, 21]. Evidence from the literature on the use of vitamin D on the male body to demonstrate the wide variability in design, methodology, patient population, reference values and routes of administration of both vitamin D and its metabolites and requires further study.

Vitamin D belongs to the group of fat-soluble secosteroids. Secosteroid is a molecule that is very similar to steroids, but with a broken steroid ring. Vitamin D is naturally available in several forms, but only two forms are important for the human body (D2 and D3), which differ chemically in their side chains. These structural differences alter their binding to the carrier protein, ie vitamin D-binding protein, and their metabolism, but in general the biological activity of these active derivatives is close [7, 15].

Particular attention needs to be paid to determining whether cholecalciferol (D3), which is the most active metabolite of this vitamin and is often used in the clinic, has an adverse effect on gonads and spermatogenesis of intact individuals, as vitamin D therapy is used in reproductive disorders vitamin D deficiency, so without it [4].

The aim of the study was to determine the effect of vitamin D on the histological structure of gonads and morphometric parameters of spermatogenesis of adult intact male rats.

Materials and methods

The study was performed on adult sexually active male Wistar rats weighing 250-300 g, kept in standard vivarium conditions under natural light and drinking mode ad libitum in accordance with the national "General Ethical Principles of Animal Experiment" (Minutes № 2 meeting of the Bioethics Commission from January 29, 2021).

Vitamin D3 was administered orally in doses of 1000 IU, 4000 IU and 10000 IU. The solutions were made on seed oil from vitamin D3 (powder) (China, batch CHG20062009, which meets the quality standard GB 9840-2017). The control was intact rats. Vitamin D in various doses and its solvent were administered throughout the period of spermatogenesis and the time of maturation of sperm in the epididymis - only 68 days. At the end of the introduction of animals was removed from the experiment by decapitation under mild chloroform anesthesia.

After euthanasia, rats' gonads were removed and weighed, structural organization of the testes was further studied. Gonadal samples were fixed in 10 % formalin solution, in alcohols of increasing strength, and embedded in paraffin. In addition to survey microscopy, morphometric evaluation of the process of spermatogenesis was performed on sections of gonads stained with hematoxylin and eosin [2].

Micropreparations were examined using a Granum L 30 (03) light microscope, and microscopic images were taken with a Granum DCM 310 digital video camera. Photographs were processed on a 2.4 GHz Pentium computer using Toup View.

Statistical processing of data results was performed in the standard software package "Statistica 6.0" using Student's t-test and using a non-parametric analogue of one-way analysis of variance - Kruskal-Wallis criterion, followed by the Mann-Whitney test [13].

Results

The testicles of intact rats served as a general intact control in our study. Figure 1 and Table 1 show the histostructure of testicular tissue and morphometric parameters that characterize the process of spermatogenesis of these animals. Light microscopy showed that the testicles of rats, which did not receive any substances, convoluted seminal tubules were cut in the transverse or oblique direction and had an oval or round shape. The diameter of the tubules is normal, the tubule membrane, as well as the protein and vascular membranes were normal [9]. The wall of the seminal tubules is built of germ cells. The basal department contains the youngest cells of the germinal epithelium - spermatogonia. Among them are cells with chromatin in the nucleus of condensed (type B) and non-condensed

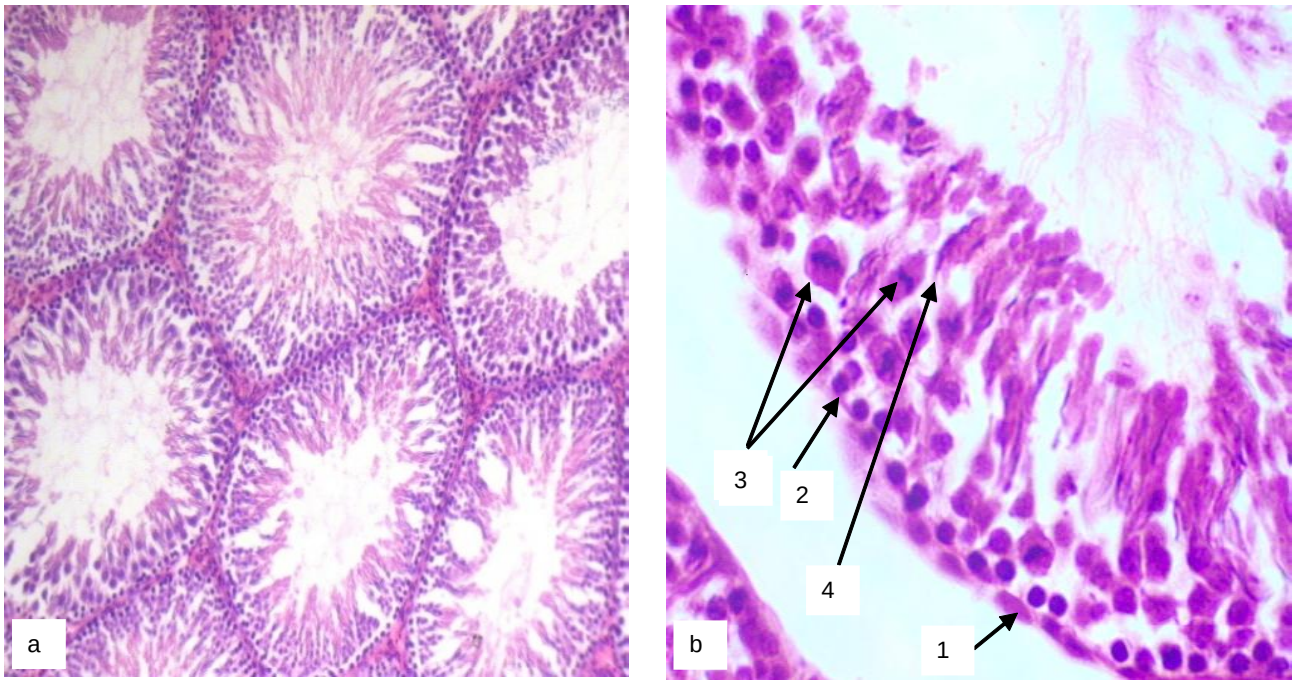

Fig. 1. Testicles of an intact rat: a - general view of seminiferous tubules. Hematoxylin-eosin. x100; b - in germinal epithelium in the tubule are visible Sertoli cells (1), spermatogonia (2), spermatocytes in the metaphase of the I and II divisions (3), spermatids (4). Hematoxylin-eosin. x250.

Table 1. The effect of vitamin D on the quantitative indicators of spermatogenesis process in rats.

Group of rats	Indicators			
	The amount of normal spermatogonia in the tubule, (M±m)	Number of tubules with stage 12 meiosis, %, Me (LQ; UQ)	The number of tubules with squamous epithelium, %, Me (LQ; UQ)	Index of spermatogenesis, points, Me (LQ; UQ)
Intact	61.07±0.5	4.0 (3.0; 5.0)	0 (0; 0)	3.33 (3.32; 3.34)
Solvent	61.23±0.66	2.5 (2.0; 4.0)	0.0 (0; 3.0)	3.30 (3.26; 3.30)
Vitamin D3, 1000 IU	60.89±13.0	4.0 (3.0; 5.0)	0.0 (0; 1.0)	3.34 (3.33; 3.34)
Vitamin D3, 4000 IU	61.23±0.77	3.0 (3.0; 4.0)	0 (0; 0)	3.33 (3.33; 3.34)
Vitamin D3, 10000 IU	61.41±0.34	3.00 (3.0; 4.0)	0 (0; 1.0)	3.33 (3.32; 3.34)

Notes: Me - median; LQ - lower quartile; UQ - upper quartile.

(type A) species. Spermatogonia type A is represented by both so-called light (renewable) and dark (reserve) cells.

Mitosis is sometimes seen in the spermatogonia of intact animals. Spermatocytes are located in the intermediate part of the wall of the seminiferous tubule. Most of the first-order spermatocytes were in the pachynema stage. Metaphases of the first and (much less often) second division and anaphases of these divisions were well observed in some tubules. Numerous spermatids and formed spermatozoa are observed in the adluminal compartment of the seminiferous tubules. Germ cells of different stages of development are arranged in a strict order, concentric layers according to the stages of the spermatogenic cycle. The associations of germ cells are clearly demarcated, in different parts of the same tubule can be seen only one typical combination of cells. Not only spermatogenesis (the process of successive germ cell rearrangements: spermatogonia ® sperm) is clearly traced in different tubules, but also spermiogenesis - stages of cellular transformations from spermatid to sperm. The germinal epithelium tape contained at least 4-6 rows of cells. Numerous Sertoli cells are located between the spermatogonia on the basement membrane. Their light pear-shaped nucleus with a nucleolus is clearly visible. Cytoplasmic processes of cells are masked by germ cells of the subsequent stages of development. Interstitial connective tissue is very limited. Clusters (up to 7-20) of Leydig cells and a few fibroblasts are visible near the blood vessels contained in the intertubular loci. The nuclei were mostly round-oval in shape, rather large in volume, well-contoured, normochromic, with a noticeable uniform "scattering" of chromatin granules, and contained mostly one nucleolus. The cytoplasm of cells is intensely eosinophilic, in single cells on the periphery is weakly vacuolated, cell boundaries are blurred. The described state of Leydig cells characterizes the normal functional

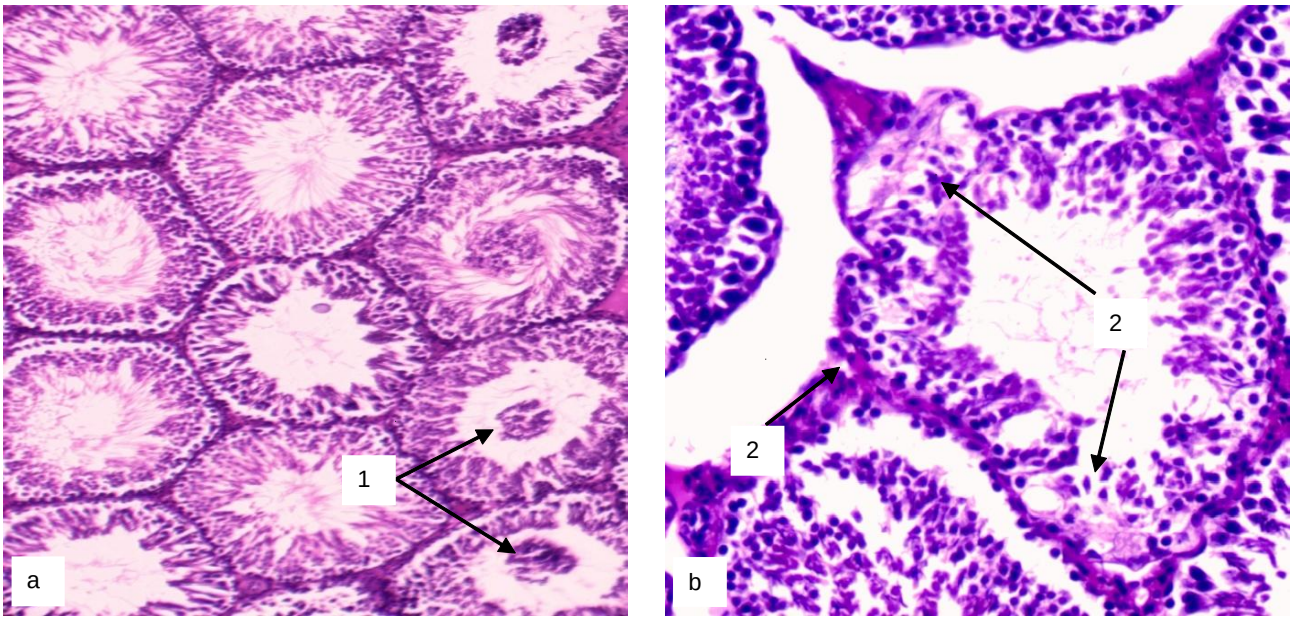

Fig. 2. Rat testis after the introduction of seed oil: a - in the germinal epithelium of the seminiferous tubules, germ cells of different stages of development, epithelial exfoliation (arrow, 1) in the part of the tubules are presented. Hematoxylin-eosin. x100; b - focal destruction (arrows, 2) of germinal epithelium in the seminiferous tubule. Hematoxylin-eosin. x250.

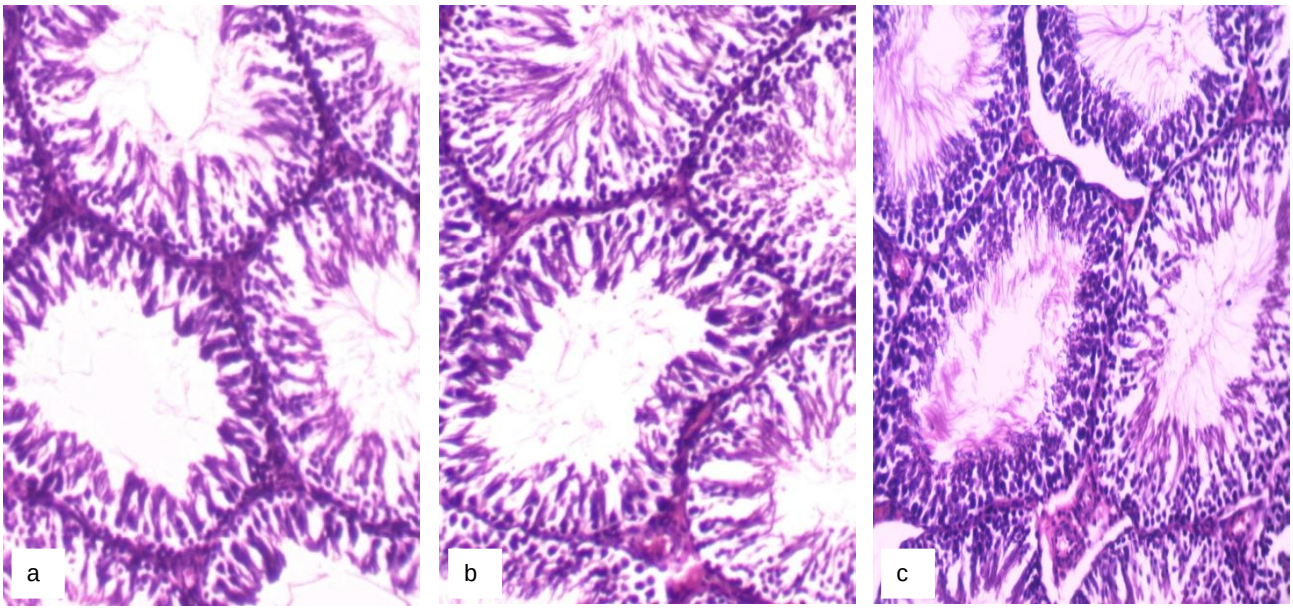

Fig. 3. Rat testis after vitamin D administration: a - in a dose 1000 IU; b - in a dose 4000 IU; c - in a dose 10000 IU. Normal condition of testicular tissue. Hematoxylin-eosin. x200.

activity of cells.

Morphometric characteristics of spermatogenesis of intact rats corresponded to the physiological norm for these animals (see Table 1).

The introduction of the solvent throughout the period of spermatogenesis and maturation of mature sperm in the epididymis did not affect the histoarchitectonics of the testicles. The testicular lobes are filled with concentric or flattened profiles of sections of the seminal tubules, which are close enough to each other. The diameter of the tubules is normal, the tubular membrane, as well as the protein and vascular membranes were normal. 3-4 generations of spermatogenic cells, which were at different stages of development, can be seen in the tubules. The cells are arranged in concentric layers according to the stages of the spermatogenic cycle. In all rats of this group, the cell population is presented in full number. However, in one animal, against the background of most unchanged seminal tubules, a few tubules were observed with focal destruction of the germinal epithelium, looseness of the rows, exfoliation of germ cells in the lumen of the tubules (Fig. 2).

Quantitative indicators characterizing the process of

spermatogenesis of rats injected with seed oil are given in the above table 1.

No significant changes in the microstructure of the seminal tubules were observed after administration of vitamin D at doses of 1000 IU, 4000 IU and 10000 IU. In different tubules in rats clearly traced not only spermatogenesis (the process of successive rearrangements of germ cells: spermatogonia - sperm), but also spermiogenesis - stages of cellular transformation from spermatids to sperm (Fig. 3).

Quantitative indicators of the process of spermatogenesis of rats receiving different doses of vitamin D3 are presented in table 1.

Discussion

Drugs can affect reproductive function, causing not only ugliness or death of embryos and fetuses, but also disrupting gametogenesis and preventing fertilization [19]. Therefore, when evaluating pharmacological substances in their safety studies, their effect on reproductive function should be investigated in animal studies [1], part of this study was the study of the safety of cholecalciferol (vitamin D3) on testicular histostructure and morphometric parameters of spermatogenesis of intact rats. Detection of gonadopathies in animals requires special experimental approaches, which is why we studied three doses and long-term intake of the substance to identify the effects of gonadal lesions, which may later manifest themselves in inability or reduced ability to conceive or in fetal development, and also in subsequent generations.

In the study of the testes of intact adult rats, we observed not only the normal structure of germinal epithelium cells, Sertoli cells, but also Leydig cells, which characterizes their functional activity [20], led to the normal course of spermatogenesis, was reflected in morphometric parameters and corresponded to the physiological norm for these animals.

The safety of long-term intake of cholecalciferol in relation to the histological picture of male gonads was studied at a dose of 1000 IU, which is ten times greater than it, and conditionally therapeutic. In the study of the effect of vitamin D not only in the minimum dose, therapeutic but also in high (10000 IU) morphological structure of testes and morphometric parameters of speratogenesis did not differ from that of intact animals, ie corresponded to the data obtained in rats of appropriate age [5, 19]. Considering that only quantitative assessments in the safety of drugs are evidence to establish the level of harmful gonadotoxic effects of drugs, pathomorphological morphometric methods are used to determine the degree of disorders that occurred in the gonads [1].

The number of normal spermatogonia in the tubule, the proportion of tubules with stage 12 meiosis and squamous epithelium probably did not differ between the studied groups with different dosage of the test substance and morphometric parameters of intact rats, which also indicates harmlessness to germinal epithelium. The relative number of different populations of seminiferous tubules - the index of spermatogenesis, which does not change with the studied doses of vitamin D, suggests the possibility of its use for a long time in individuals who did not have reproductive disorders, given that cholecalciferol is usually prescribed long courses, and recently in high doses [18].

Reproductive safety studies in males are studied after chronic administration, as different generations of the epithelial epithelium are equally sensitive to chemical agents. In this regard, only the repeated action of the test compound at all stages of spermatogenesis allows to detect pathology [1]. Animal administration of cholecalciferol in all three doses for almost seventy days did not lead to disruption of gonads and spermatogenesis, which may indicate its safety against gonads under these conditions. Under the action of solvent (seed oil) signs of focal destruction of germinal epithelium were observed in only one male rat, in general, they do not significantly affect both the histological picture of gonads and general morphometric parameters of spermatogenesis.

Thus, it can be stated that vitamin D3 when used in intact individuals in the studied doses does not have a negative effect on the youngest cells of the germinal epithelium - spermatogonia; does not reduce the number of tubules with stage 12 meiosis - ie does not reduce the reserve of spermatogenesis. As a result, the index of spermatogenesis does not change.

The data obtained for the first time show the safety of vitamin D3 in terms of testicular morphological structure and spermatogenesis, which was studied by morphometric studies of structural elements of the gonads, and are of great practical importance because they indicate the safety of cholecalciferol in both minimum and even maximum doses [18] under the conditions of modeling vitamin D deficiency.

Conclusion

1. When using cholecalciferol in doses of 1000 IU, 4000 IU and 10000 IU, the safety for both spermatogonia and tubules with stage 12 meiosis were confirmed.

2. When cholecalciferol was used in adult rats for 68 days, the spermatogenesis index remained at the level of animals that did not receive the test substance or diluent.

3. The use of vitamin D3 in intact mature male rats does not adversely affect the histological structure of the testes.

References

[1] Anagnostis, P., Karras, S., & Goulis, D. G. (2013). Vitamin D in human reproduction: a narrative review. *International journal of clinical practice,* 67(3), 225-235. doi: 10.1111/ijcp.12031

[2] Bahriy, M. M., Dibrova, V. A., Popadynets, O. H., & Hryshchuk, M. I. (2016). *Методики морфологічних досліджень: Монографія [Methods of morphological research: Monograph].*

Вінниця: Нова книга - Vinnytsya: A new book.

[3] Barylyak, I. R., Neumerzhyts'ka, L. V., Byshovets', T. F., & Danylenko, V. S. (2000). *Вивчення гонадотоксичної дії нових лікарських засобів та їх впливу на репродуктивну функцію тварин. Методичні рекомендації [Study of gonadotoxic effects of new drugs and their effects on reproductive function of animals. Guidelines].* Київ: Авіцена - Kyiv: Avicenna.

[4] Bondarenko, V. A., Minukhin, A. S., & Skorniakov, E. I. (2021). Levels of vitamin d, homocystein and incre asor function of testaments among males with idiopathic patosperm. *Problems of Endocrine Pathology,* 75(1), 21-25. doi: 10.21856/j-PEP.2021.1.03

[5] Brechka, N. M. (2019). The effect of long-term administration of chondroitin sulfate on the functioning of the reproductive system of male rats. *Problems of Endocrine Pathology,* 67(1), 74-78. doi: 10.21856/j-PEP.2019.1.09

[6] Ciccone, I. M., Costa, E. M., Pariz, J. R., Teixeira, T. A., Drevet, J. R., Gharagozloo, P., … & Hallak, J. (2021). Serum vitamin D content is associated with semen parameters and serum testosterone levels in men. *Asian journal of andrology,* 23(1), 52-58. doi: 10.4103/aja.aja_9_20

[7] Chekman, I. S., Horchakova, N. O., Berezhnyi, V. V., Davydiuk, A. V., & Roman'ko, M. R. (2017). Фармакология витамина D [Pharmacology of vitamin D]. *Современная педиатрия - Modern Pediatrics,* 82(2), 28-36. doi: 10.15574/SP.2017.82.28

[8] Chen, Y., & Zhi, X. (2020). Roles of Vitamin D in Reproductive Systems and Assisted Reproductive Technology. *Endocrinology,* 161(4), bqaa023. doi: 10.1210/endocr/bqaa023

[9] Jeremy, M., Gurusubramanian, G., & Roy, V. K. (2019). Vitamin D3 mediated regulation of steroidogenesis mitigates testicular activity in an aged rat model. *J Steroid Biochem Mol Biol,* 190, 64-75. doi: 10.1016/j.jsbmb.2019.03.016

[10] Jueraitetibaike, K., Ding, Z., Wang, D. D., Peng, L. P., Jing, J., Chen, L., … & Yao, B. (2019). The effect of vitamin D on sperm motility and the underlying mechanism. *Asian journal of andrology,* 21(4), 400-407. doi: 10.4103/aja.aja_105_18

[11] Karras, S., Anagnostis, P., Kotsa, K., & Goulis, D. G. (2016). Vitamin D and gonadal function in men: a potential inverse U-shaped association?. *Andrology,* 4(3), 542-544. doi: 10.1111/andr.12173

[12] Karim, D., Mustafa Mohammed, S., & Abdullah Azeez, H. (2021). Impact of vitamin D3 Nanoemulsion on spermatogenesis and antioxidant enzymes in Vitamin D deficient induced albino male rats. *Zanco Journal of Pure and Applied Sciences,* 33(1), 55-67. doi: 10.21271/ZJPAS.33.1.7

[13] Lapach, S. N., Gubenko, A. V., & Babich, P. N. (2000). *Статистические методы в медико-биологических исследованиях с использованием Excel [Statistical methods in biomedical research using Excel].* Киев: Морион - Kiev: Morion.

[14] Maghsoumi-Norouzabad, L., Zare Javid, A., Mansoori, A., Dadfar, M., & Serajian, A. (2021). Evaluation of the effect of vitamin D supplementation on spermatogram, seminal and serum levels of oxidative stress indices in asthenospermia infertile men: a study protocol for a triple-blind, randomized controlled trial. *Nutrition journal,* 20(1), 49. doi: 10.1186/s12937-021-00711-7

[15] Mazur, I. P, & Novoshytsky, V. Ye. (2014). Вітамін D: метаболізм, функції та важливість для організму людини. Роль у патогенезі генералізованого пародонтиту. Частина 1 [Vitamin D: metabolism, functions, and importance for the human body. Role in the pathogenesis of generalised periodontitis. Part 1]. *Современная стоматология - Modern dentistry*, 1, 40-45.

[16] Nasreen, K., Ishrat, S., Banu, J., Fatima, P., Ansary, S. A., Jahan, I., … & Islam, M. K. (2021). Comparison of vitamin D (25OHD) status between fertile and infertile men. International *Journal of Reproduction, Contraception, Obstetrics and Gynecology,* 10(4), 1303-1309. doi: 10.18203/2320-1770.ijrcog20211104

[17] Nimptsch, K., Platz, E. A., Willett, W. C., & Giovannucci, E. (2012). Association between plasma 25-OH vitamin D and testosterone levels in men. *Clinical endocrinology*, 77(1), 106-112. doi: 10.1111/j.1365-2265.2012.04332.x

[18] Pludowski, P., Holick, M. F., Grant, W. B., Konstantynowicz, J., Mascarenhas, M. R., Haq, A., … & Wimalawansa, S. J. (2018). Vitamin D supplementation guidelines. *The Journal of steroid biochemistry and molecular biology,* 175, 125-135. doi: 10.1016/j.jsbmb.2017.01.021

[19] Seluykova, N. Y., Sergiyenko, L. Y., Koreneva, E. M., Karpenko, N. A. & Brechka, N. M. (2015). Гістологічна структура сім'яників щурів-нащадків фітоестрогенізованих батьків [Histological structure of testes rats offspring father's who received an excess consumption of phytoestrogens]. *Клінічна та експериментальна патологія - Clinical and experimental pathology,* 14(3), 117-121.

[20] Sharapova, O. M. (2019). *Морфофункціональні зміни в статевих органах щурів-самців після дії електромагнітного поля та їх медикаментозна корекція [Morphofunctional changes in the genitals of male rats after electromagnetic field and their drug correction].* Дніпро: Літограф - Dnipro: Litohraf.

[21] Smolienko, N. P., Chystiakova, E. Ye., Marakhovskiy, I. O., Korenieva, Ye. M., Bielkina, I. O., Velichko, N. F., … & Bondarenko, V. A. (2021). Effect of introduction of prostatilene and vitamin D3 in different ways on the state of spermatogenesis of rats with prostatitis. *Polish Jounal of Science*, 45, 25-27.

[22] Wehr, E., Pilz, S., Boehm, B. O., März, W., & Obermayer-Pietsch, B. (2010). Association of vitamin D status with serum androgen levels in men. *Clinical endocrinology,* 73(2), 243-248. doi: 10.1111/j.1365-2265.2009.03777.x

ВПЛИВ ВІТАМІНУ D НА ГІСТОСТРУКТУРУ СІМ'ЯНИКІВ І МОРФОМЕТРИЧНІ ПОКАЗНИКИ СПЕРМАТОГЕНЕЗУ ІНТАКТНИХ ЩУРІВ

Мараховський І. О., Ларьяновська Ю. Б., Коренєва Є. М., Смолєнко Н. П., Чистякова Е. Є., Бєлкіна І. О., Величко Н. Ф., Місюра К. В., Бондаренко В. О.

Однією з актуальних проблем сьогодення є вивчення впливу вітаміну D на організм, при цьому у чоловіків його дія тісно пов'язана з патогенезом андрогенного дефіциту та гіпофертильністю. Особливої уваги потребує визначення відповіді на питання, чи не має введення холекальциферолу (D3) негативної дії на гонади та сперматогенез інтактних особин, так як терапію вітаміном D застосовують при репродуктопатіях як із дефіцитом вітаміну D, так і без нього. Метою дослідження було визначення дії вітаміну D на гістологічну картину гонад і морфометричні параметри сперматогенезу дорослих інтактних щурів самців. Дослідження проводились на дорослих статевоактивних самцях щурів популяції Вістар. Вітамін D3 застосовували перорально у дозах 1000 МО, 4000 МО і 10000 МО. Розчини виготовляли на кісточковій олії. Контролем

слугували інтактні щури. Вітамін D та його розчинник вводили впродовж всього періоду сперматогенезу і часу дозрівання сперматозоїдів у придатку сім'яника, після чого визначали структурну організацію сім'яників. Зразки статевих залоз фіксували у 10 % розчині формаліну, проводили по спиртах міцності, що зростає, та заливали у парафін. На зрізах гонад, які забарвлювали гематоксиліном та еозином, окрім оглядової мікроскопії проводили морфометричну оцінку процесу сперматогенезу. Перегляд мікропрепаратів проводили за допомогою світлового мікроскопу Granum L 30 (03), фотографування мікроскопічних зображень здійснювали цифровою відеокамерою Granum DCM 310. Фотознімки обробляли на комп'ютері Pentium 2,4 GHz за допомогою програми Toup View. Статистичну обробку результатів даних проводили в стандартному пакеті програм "Statistica 6.0" з використанням t-критерію Стьюдента та застосовуючи непараметричний аналог однофакторного дисперсійного аналізу - критерій Краскела-Уоліса. На зрізах сім'яників інтактних щурів звивисті сім'яні канальці були розташовані у поперечному або косому напрямку і мали овальну чи округлу форму. Діаметр канальців звичайний, власна оболонка канальців, а також білкова та судинна оболонки відповідали нормі. В базальному відділі містяться найбільш молоді клітини сперматогенного епітелію - сперматогонії. Клітини мають виражену функціональну активність. Морфометрична характеристика сперматогенезу інтактних щурів відповідала фізіологічній нормі. Введення розчинника протягом всього періоду сперматогенезу та дозрівання зрілих спермій у придатку сім'яника не вплинуло на гістоархітектоніку тестикул. Часточки сім'яника заповнені концентричними або сплощеними профілями зрізів сім'яних канальців, які достатньо щільно прилягали один до одного. Діаметр канальців звичайний, власна оболонка канальців, а також білкова та судинна оболонки відповідали таким у інтактних тварин. В канальцях видно 3-4 генерації сперматогенних клітин, що знаходилися на різних стадіях розвитку. Однак простежені нечисленні канальці з вогнищевою деструкцією епітеліосперматогенного пласта та злущенням статевих клітин у просвіт канальців. Після введення вітаміну D у всіх вивчених дозах ніяких помітних змін у мікроструктурі сім'яних канальців не виявлено. У різних канальцях у щурів чітко простежено не тільки сперматогенез, а і сперміогенез - етапи клітинних перетворень від сперматиди до сперматозоїда. Морфометричні показники процесу сперматогенезу щурів, що отримували у різних дозах вітамін D3 не відрізняються від показників інтактних щурів. Таким чином при використанні вітаміну D у зазначених дозах виявлено нешкідливість його дії як на кількість сперматогоній, так і канальців із 12 стадією мейозу. При застосуванні холекацифероlу у самців щурів протягом 68 діб індекс сперматогенезу залишався на рівні тварин, які не отримували досліджувану речовину. Застосування вітаміну D3 у інтактних статевозрілих самців щурів не має негативного впливу на гістологічну картину сім'яників.

Ключові слова: *вітамін D, сім'яник, гонадотоксичність, гістоструктура сім'яників, морфометричні показники сперматогенезу.*

DOI: 10.31393/morphology-journal-2022-28(2)-05 Reports of Morphology, Vol. 28, №2, Pages 32-39

ISSN 1818-1295 eISSN 2616-6194

REPORTS OF MORPHOLOGY

Official Journal of the Scientific Society of Anatomists, Histologists, Embryologists and Topographic Anatomists of Ukraine

journal homepage: https://morphology-journal.com

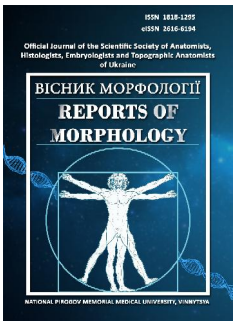

Ultrastructural changes in the myocardium of animals under conditions of simulated hyperhomocysteinemia, hyper- and hypothyroidism and their combination

Nechiporuk V. M.[1], Pentyuk L. O.[1], Kovalchuk O. V.[1], Mazur O. I.[1], Korda M. M.[2]

[1]National Pirogov Memorial Medical University, Vinnytsya, Ukraine
[2]I. Horbachevsky Ternopil National Medical University, Ternopil, Ukraine

ARTICLE INFO
Received: 07 February 2022
Accepted: 14 March 2022

UDC: 616.127-018.2-02:616.253.478.6-06:616.441-008.64-092.9

CORRESPONDING AUTHOR
e-mail: nechiporuk@vnmu.edu.ua
Nechiporuk V. M.

CONFLICT OF INTEREST
The authors have no conflicts of interest to declare.

FUNDING
Not applicable.

Thyroid hormones have a significant impact on heart function through both genomic and non-genomic effects. Deficiency or excess of thyroid hormones leads to profound changes in the regulation of cardiac function and cardiovascular hemodynamics. The heart is the main target organ for the action of thyroid hormones and in patients with hypo- or hyperthyroidism there are marked changes in the work of the heart. The aim of the work was to establish ultrastructural changes in myocardial components in experimental hyperhomocysteinemia (HHCy) against the background of hyper- and hypothyroidism. Thiolactone HHCy was modelized by administering to animals an exogenous HCy in the form of thiolactone at a dose of 100 mg/kg body weight once a day for 28 days. Hyperthyroidism was modelized by daily administration of L-thyroxine at a dose of 200 μg/kg for the 21 days, hypothyroidism - daily administration of thiamazole at a dose of 10 mg/kg for the 21 days. Individual groups of animals were administered L-thyroxine and thiamazole in parallel with HCy. High levels of HCy adversely affected the walls of myocardial blood vessels. The lumens of hemocapillaries were plethoric, filled with erythrocytes. Changes in endotheliocytes were revealed, and cardiomyocytes contained deformed nuclei. In laboratory animals with hyperthyroidism, an increase in ultrastructural changes in the walls of blood vessels (edema of the walls of hemocapillaries, damaged cristae in mitochondria) were established. In animals that were modeled for hyperthyroidism and HHCy, more significant changes in endotheliocytes were revealed, most of the mitochondria were destroyed. More pronounced alterative changes were revealed in cardiomyocytes. An electron microscopic examination of the myocardium of animals with hypothyroidism showed significant degenerative changes in the ultrastructure of the walls of blood vessels, and hypertrophied mitochondria were also found. The combined influence of hypothyroidism and HHCy caused the most profound disturbances in the ultrastructure of cardiomyocytes and hemocapillaries in comparison with other groups of animals. The integrity of intercellular contacts was impaired, most of the mitochondria of myocytes had destroyed cristae and the outer membrane.

Keywords: *hyperthyroidism, hypothyroidism, hyperhomocysteinemia, myocardium.*

Introduction

Thyroid hormones are known to affect the cardiovascular system [18]. Clinically, both excess and deficiency of thyroid hormones may cause or exacerbate cardiovascular disorders, including atrial and ventricular arrhythmias, atherosclerotic vascular disease, dyslipidemia, and heart failure, thereby increasing the risk of premature death and disease. Thyroid hormones are an important regulator of cardiac function and cardiovascular hemodynamics. Triiodothyronine (T_3) binds to nuclear receptor proteins and mediates the expression of several important cardiac genes, causing transcription of positively regulated genes, including β-myosin heavy chain and sarcoplasmic reticulum calcium ATPase. Negatively regulated β-myosin and phospholamban genes are reduced in the presence of normal levels of thyroid hormone in the serum [16]. T_3-mediated effects on the cardiovascular system include relaxation of vascular smooth muscle, leading to decreased arterial resistance

and diastolic blood pressure. With hyperthyroidism, heart rate and cardiac output increase, and systemic vascular resistance decreases, whereas with hypothyroidism, the opposite is true.

Changes in plasma or tissue levels of thyroid hormones are associated with significant changes in cardiovascular function. A significant proportion of patients with heart failure have some form of thyroid dysfunction, including hypothyroidism, hyperthyroidism and low T_3 syndrome [8]. Several clinical and experimental studies have shown the beneficial effects of thyroid hormones in cardiac pathology [2, 6, 19]. Epidemiological data confirm a higher risk of heart failure and a worse prognosis in patients with low thyroid hormone heart failure.

The aim of the study was to establish ultrastructural changes in myocardial components under the conditions of simulated HHCy, hyper- and hypothyroidism and their combined effects.

Materials and methods

The experiments were performed on 50 outbred white male rats weighing 180-200 g. Rats were kept at standard light day on a normal diet. All studies were conducted in compliance with the requirements of humane treatment of experimental animals, regulated by the Law of Ukraine "On Protection of Animals from Cruelty" (№ 3447-IV of 21.02.2006) and the European Convention for the Protection of Vertebrate Animals Used for Research and Other Scientific Purposes (Strasbourg, March 18, 1986). The Committee on Bioethics of National Pirogov Memorial Medical University, Vinnytsya found that the study does not contradict the basic bioethical standards (Minutes № 7 of 7.04.2022).

All animals were divided into 5 groups: 1 - intact rats. This group of animals was injected intragastrically with 1 % starch solution; 2 - animals with thiolactone HHCy, which was caused by intragastric administration of HCy in the form of thiolactone at a dose of 100 mg/kg body weight in 1 % starch solution once a day for 28 days. The dose, route and duration of thiolactone administration of HCy are borrowed from the literature and did not cause animal death [14]; 3 - animals with hyperthyroidism, which were administered intragastrically daily for 21 days L-thyroxine at a dose of 200 μg/kg in 1 % starch solution [11]; 4 - animals with thiolactone HHCy, which were daily administered intragastrically daily for 21 days L-thyroxine at a dose of 200 μg/kg in 1 % starch solution; 5 - animals with hypothyroidism, which were daily administered intragastrically on the 21st day mercazolyl in 1 % starch solution at a dose of 10 mg/kg body weight [11]; 6 - animals with thiolactone HHCy, which were administered intragastrically mercazolyl at a dose of 10 mg/kg per 1 % starch solution daily for 21 days. Animals were removed from the experiment 24 hours after the last administration of the selected substances.

Collection of material for electron microscopic examination of the myocardium was performed according to generally accepted rules [4]. The material was fixed in 2.5 % glutaraldehyde solution with active reaction medium pH 7.2-7.4, prepared on phosphate buffer. Postfixation was performed with 1 % osmium tetroxide solution, followed by dehydration in alcohols and propylene oxide and poured into a mixture of epoxy resins. Ultrathin sections made on an ultramicrotome LKB-3 (Sweden) were stained with 1 % aqueous uranyl acetate solution, contrasted with lead citrate according to the Reynolds method and studied under an electron microscope PEM-125K.

Results

Ultrastructural studies of the heart wall of intact animals have shown that cardiomyocytes have an elongated shape and are interconnected by desmosomal and slit contacts. Externally, cardiomyocytes are surrounded by sarcolemma. In the central part of the cells is an oval nucleus with one or two nucleoli. Euchromatin predominates in the karyoplasm. The karyolemma contains a uniform perinuclear space and numerous nuclear pores. In the cytoplasm of cells there are organelles of general and special purpose (myofibrils). There is a large number of mitochondria, which are located between myofibrils in the form of chains and groups near the nucleus. These organelles contain densely packed cristae and electron-dense matrix. In the perinuclear part of the cytoplasm there are tanks of the Golgi complex, free ribosomes and polyribosomes. The smooth endoplasmic reticulum forms a system of anastomotic tubules and contacts the T-tubes. A significant amount of cytoplasm is occupied by myofibrils. In the longitudinal section of the cell, they have a well-defined sequential alternation of actin and myosin microfilaments in the sarcomeres (Fig. 1). Between the myocardial muscle fibers is a stromal loose connective tissue that contains blood vessels and nerves.

The myocardium contains a significant number of

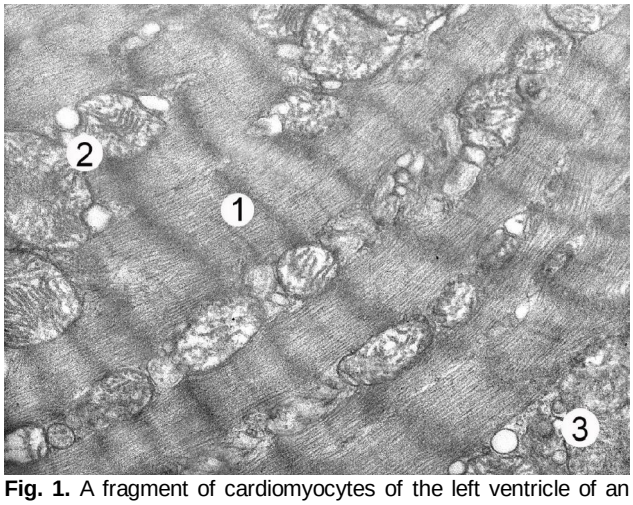

Fig. 1. A fragment of cardiomyocytes of the left ventricle of an intact animal in a state of contraction. Sarcomeres in the composition of myofibrils (1), mitochondria (2), layers of interstitial connective tissue (3). x17 000.

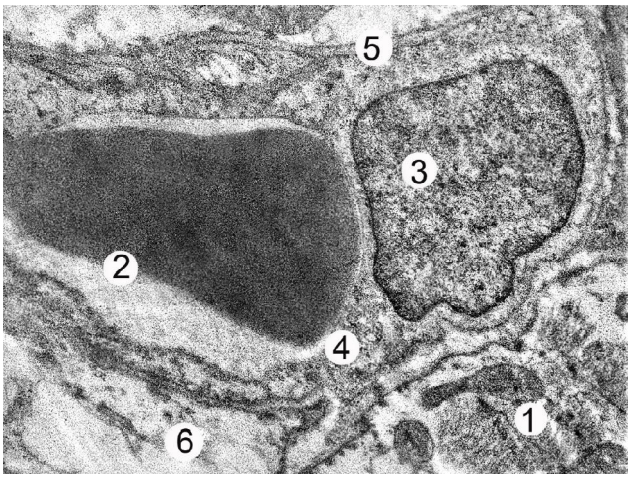

Fig. 2. Ultrastructural state of the hemocapillary of an intact group animal. Cardiomyocyte fragment (1), capillary lumen (2) with erythrocyte, nucleus (3) and endothelial cell cytoplasm (4), basement membrane (5), perivascular space (6). x14 000.

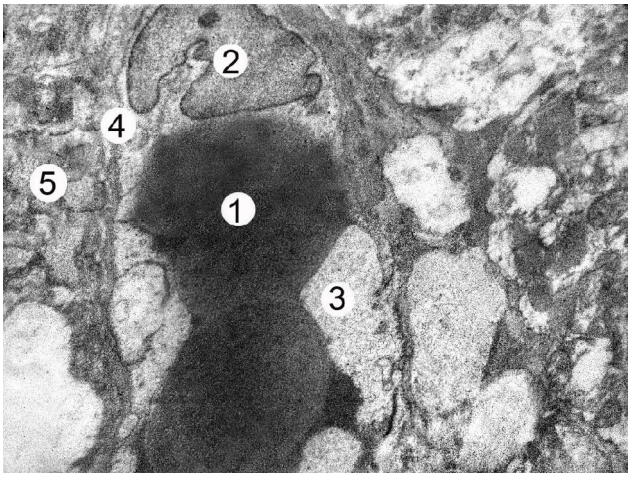

Fig. 3. Ultrastructural changes in the hemocapillar of the left ventricular myocardium of the animal under conditions of simulated HHCy. Capillary lumen with erythrocytes (1), deformed nucleus (2), swollen cytoplasmic area of endothelial cell (3), basement membrane (4), fragment of cardiomyocyte (5). x14 000.

hemocapillaries. The capillary wall is formed by endothelial cells that include the oval nucleus. Karyoplasm contains mainly euchromatin, heterochromatin forms small lumps, nucleoli are rare. The cytoplasm of endothelial cells has a moderate electron density, organelles are moderately developed and localized near the nucleus. Micropinocytic vesicles are found in peripheral, cytoplasmic areas. Endothelial cells lie on a clearly contoured solid basement membrane, in its cleavage or outside localized pericytes and adventitial cells, which are rare. The lumen of hemocapillaries is moderate (Fig. 2).

Submicroscopic studies of the heart of laboratory animals of the second experimental group, which simulated HHCy, showed the presence of alternative changes in the walls of blood vessels. The lumens of the hemocapillaries were mostly full-blooded, mostly filled with erythrocytes. Changes in endothelial cells were revealed, which were manifested by edema of the peripheral part of the cell, a decrease in the number of pinocytic vesicles and caveolae, an increase in heterochromatin in the nucleus and local expansion of the perinuclear space. Contacts between endothelial cells were partially disrupted. The basement membrane is compacted or locally swollen (Fig. 3).

Impaired microcirculation of the organ provoked changes in cardiomyocytes. In the deformed nuclei of cardiomyocytes the growth of intussusception of a karyolemma is revealed, in their karyoplasm heterochromatin prevails, nucleoli are not defined. Hypertrophied mitochondria with electron-dense matrix and reduced cristae were observed in electron-dense sarcoplasm. In some cells, myofibrils were shortened, compacted, homogenized, and sarcomere structure was

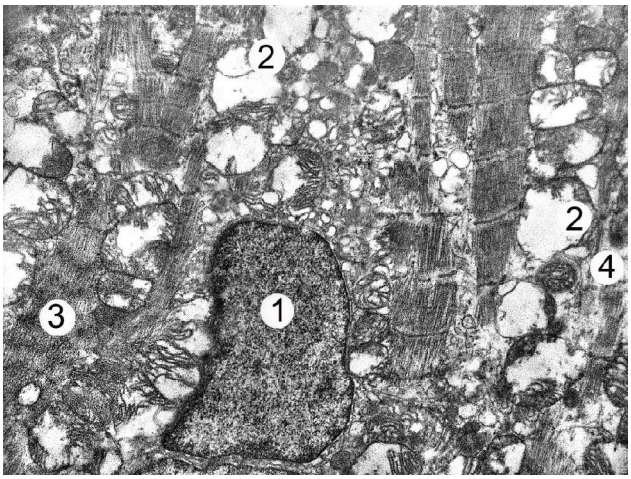

Fig. 4. Ultrastructural changes of the cardiomyocyte of the left ventricle of the animal under the conditions of simulated hyperhomocysteinemia. Deformed nucleus (1), destructively altered mitochondria with fragmented cristae (2), myofibril overgrowth zone (3), myofibril lysis sites (4). x15 000.

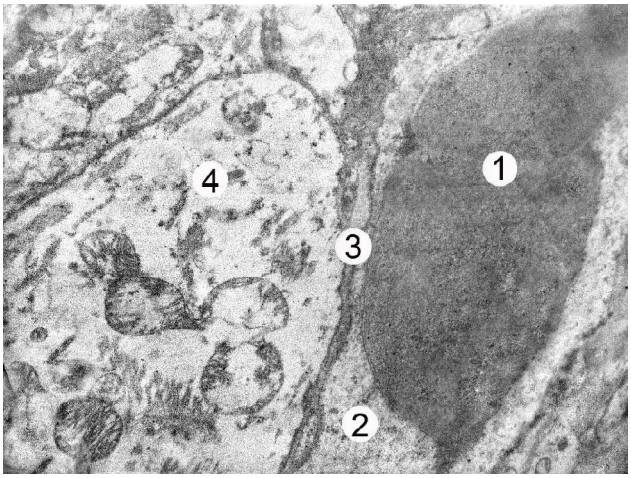

Fig. 5. Ultrastructural changes of the left ventricular myocardium in simulated hyperthyroidism. Capillary lumen with erythrocytes (1), endothelial cell cytoplasm (2), basement membrane (3), cardiomyocyte fragment (4). x14 000.

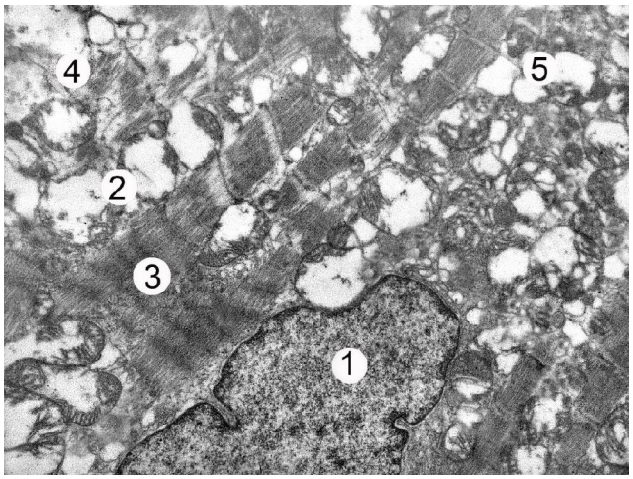

Fig. 6. Submicroscopic changes of the cardiomyocyte of the left ventricle in white rat under the conditions of simulated hyperthyroidism. Nucleus (1), altered mitochondria (2), zones of myofibril rupture (3) and lysis (4), dilated tubules of the endoplasmic reticulum (5). x14 000.

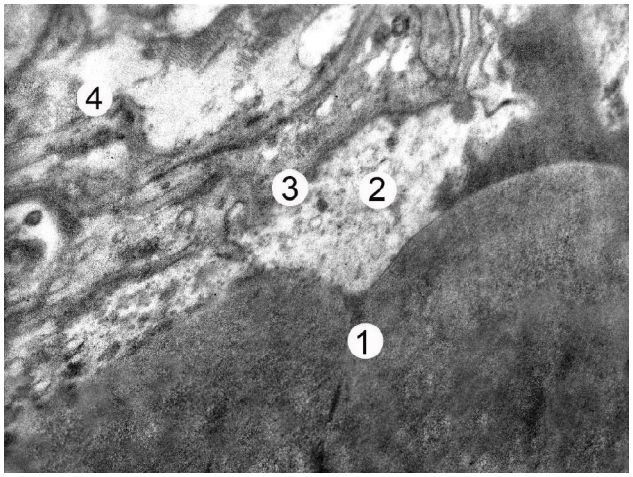

Fig. 7. Submicroscopic changes in the hemocapillar of the left ventricular myocardium of the animal under conditions of simulated hyperthyroidism and HHCy. Capillary lumen with erythrocytes (1), swollen cytoplasmic area of endothelial cell (2), basement membrane (3), fragment of cardiomyocyte (4). x20 000.

disturbed (Fig. 4).

Submicroscopic studies of the heart of laboratory animals of the third experimental group, which simulated hyperthyroidism, revealed edema of the walls of hemocapillaries, while the basement membrane was thickened, the cytoplasm of endothelial cells was enlightened. The lumenal surface of endothelial cells formed single cytoplasmic outgrowths and microvilli, and a decrease in micropinocytic vesicles in the cytoplasm was determined. In some mitochondria the cristae and the locally enlightened matrix were damaged, the tubules of the endoplasmic reticulum were partially dilated (Fig. 5).

Changes in the ultrastructural organization of cardiomyocytes were manifested by increased intussusception of the karyolemma and expansion of the perinuclear space. An increase in changes in the structural components of the sarcoplasm of some myocytes was revealed. Myofibrils were thinned with partial lysis, in some areas sarcomeres were located in a disorderly manner, areas of myofibril overshortening were determined. Enlightenment of the matrix and damage to the cristae were found in the mitochondria. The tubules of the sarcoplasmic reticulum are dilated (Fig. 6).

Studies of ultrastructural reorganization of the heart of laboratory animals of group IV, which simulated hypothyroidism and HHCy, revealed hemocapillaries with narrowed lumens filled with platelets and erythrocytes. Endothelial cells underwent significant changes. Their nuclei were reduced, there were no nucleoli in the karyoplasm, the karyolemma formed deep

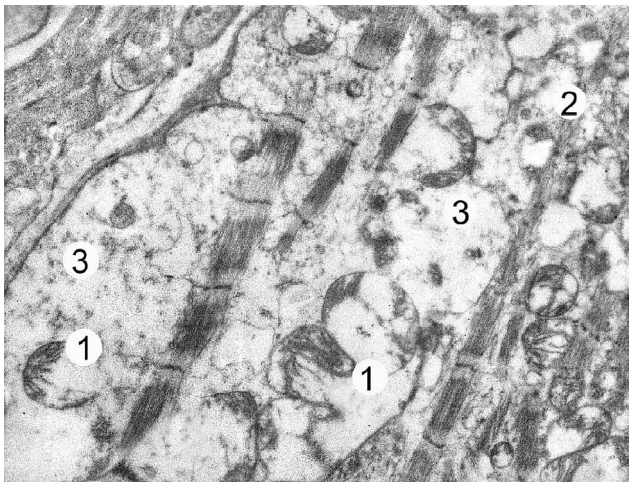

Fig. 8. Submicroscopic changes of myocardial cardiomyocyte of the left ventricle of white rat heart under conditions of simulated hyperthyroidism and HHCy. Damaged mitochondrial membranes (1), myofibril lysis zones (2), optically bright areas of the cell, devoid of organelles (3). x18 000.

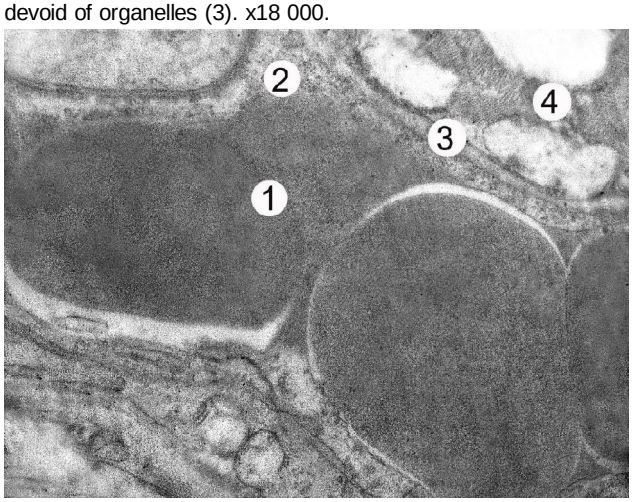

Fig. 9. Ultrastructural changes of the left ventricular myocardial hemocapillar of a white rat heart under the conditions of simulated hypothyroidism. Erythrocyte stasis in the capillary lumen (1) endothelial cell cytoplasm (2), thickened basement membrane (3), cardiomyocyte fragment (4). x14 000.

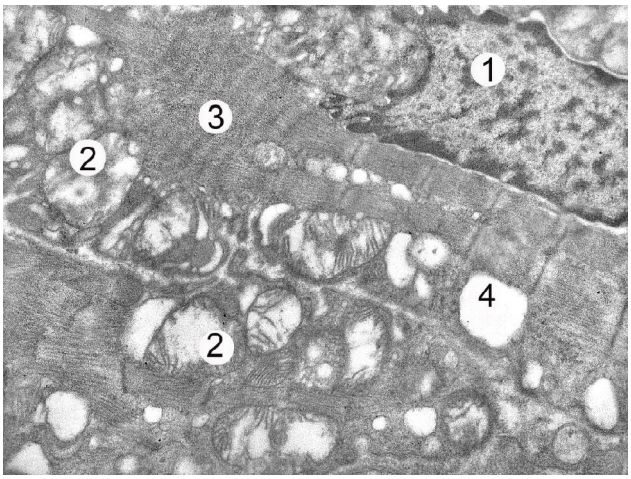

Fig. 10. Submicroscopic changes of the left ventricle cardiomyocyte in white rat under the conditions of simulated hypothyroidism. Deformed nucleus (1) with intussusception of the karyolemma, destruction of mitochondria (2), zones of myofibril overgrowth (3), enlarged endoplasmic reticulum vacuole (4). x15 000.

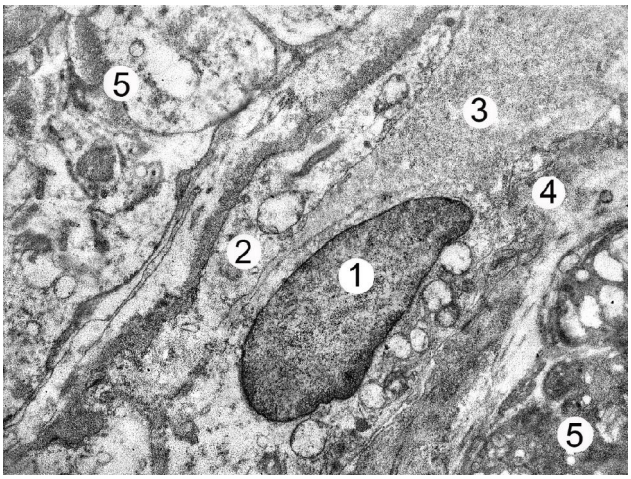

Fig. 11. Ultrastructural changes in the left ventricular myocardial hemocapillar of a white rat heart under conditions of simulated hypothyroidism and HHCy. The nucleus (1) and cytoplasm of the endothelial cell (2), the lumen of the capillary (3), the homogeneous basement membrane (4), a fragment of the cardiomyocyte (5). x13 000.

intussusception. The cytoplasm of endothelial cells is enlightened and swollen. The tubules of the endoplasmic reticulum are dilated and partially fragmented. In most mitochondria, cristae and the matrix were significantly enlightened. Few pinocytic vesicles were found in the cytoplasm. The basement membrane of hemocapillaries is thickened and poorly contoured (Fig. 7).

Cardiomyocytes showed more pronounced alternative changes compared to previous observation groups. A decrease in the area of the nucleus, an increase in the number and depth of karyolemma intussusception was found. Karyoplasm was filled with homogeneous chromatin, nucleoli were not detected. Disturbances in myofibrils were manifested by their thinning, fragmentation and lysis. In most mitochondria the cristae were destroyed, in some of these organelles the outer membrane was damaged. Sarcoplasm of cells is swollen, enlightened, electron-bright areas devoid of organelles are determined (Fig. 8).

Electron microscopic examination of the myocardium of laboratory animals of group V, which simulated hypothyroidism, found that hemocapililary endothelial cells contained few microbubbles and caveolae, their cytoplasm was swollen. It revealed dilatation of the endoplasmic reticulum tubules, hypertrophied mitochondria with an enlightened matrix and partially reduced cristae. The karyolemma of the nuclei formed deep intussusception, the perinuclear space was unevenly expanded. Thickening and swelling of the basement membrane of blood vessels were detected (Fig. 9).

Decreased levels of thyroid hormones caused a violation of the ultrastructure of contractile cardiomyocytes. Euchromatin predominated in the nuclei, heterochromatin formed osmophilic lumps, nucleoli were rare. Karyolemma formed deep intussusception. Sarcoplasm revealed damage to the contractile apparatus of the cell, which was manifested by stratification of myofibrils and their partial fragmentation or compaction, homogenization, areas of overshortening were detected. Sarcomeres were of different sizes, actin and myosin microfilaments were located unevenly. Most mitochondria were hypertrophied, their matrix was enlightened, cristae were partially destroyed, not clearly contoured. The expansion of the tubules and vacuoles of the endoplasmic reticulum was determined (Fig. 10).

Submicroscopic studies of laboratory animals heart of the VI experimental group revealed profound violations of the ultrastructure of endothelial cells. The nuclei of endothelial cells were compacted, pyknotically altered in some cells. The cytoplasm was clear and swollen,

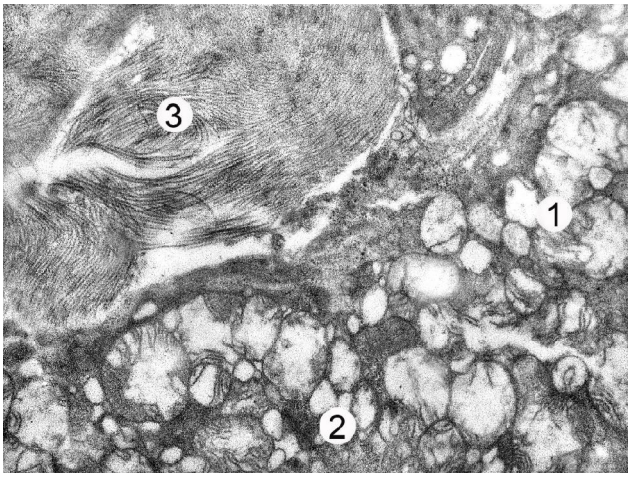

Fig. 12. Ultrastructural changes in the left ventricular myocardium of a white rat under conditions of simulated hypothyroidism and HHCy. Damaged mitochondria (1), endoplasmic reticulum tubules (2), collagen fibers in the interstitium (3). x14 000.

micropinocytic vesicles were rare. The lumenal part of the plasmalemma is indistinctly blurred or destroyed. The integrity of intercellular contacts is violated. The tubules of the endoplasmic reticulum were dilated and partially fragmented. In many mitochondria, cristae and outer membranes were destroyed. The mitochondrial matrix is enlightened. The integrity of intercellular contacts is violated. The basement membrane of the blood vessel wall is significantly thickened and poorly contoured, damaged (Fig. 11).

An increase in ultrastructural changes was also found in cardiomyocytes. The cell nuclei were compacted and pyknotically altered, the perinuclear space was weakly expressed. Mitochondria were hypertrophied, they revealed violations of the integrity of the outer and inner membranes. Myofibrils have undergone profound changes. Thinning, fragmentation, and lysis were observed in most cells, and sarcomeres were unevenly distributed. Activation of fibroblasts is accompanied by the growth of collagen fibers in the interstitium (Fig. 12).

Discussion

The results of submicroscopic examination of the myocardium in HHCy are consistent with the available data from the literature. We found a negative effect of HCy on the walls of myocardial blood vessels. The lumens of the hemocapillaries were mostly full-blooded, mostly filled with erythrocytes. Changes in endothelial cells were detected, myocytes contained deformed nuclei. There are several theories that can explain our data. HCy is thought to cause degradation and block the synthesis of "long-lived" peptides such as collagen, elastin and protein glycans. It is able to destroy disulfide bridges in proteins, which leads to their gross structural and functional disorders and causes vascular pathology [1, 5].

We found ultrastructural changes in the walls of blood vessels in laboratory animals with hyperthyroidism. Edema of the walls of hemocapillaries was detected, the basement membrane was thickened, the cytoplasm of endothelial cells was enlightened. Cristae were damaged in some mitochondria. Changes in the ultrastructural organization of cardiomyocytes were manifested by increased intussusception of the karyolemma and expansion of the perinuclear space. An increase in changes in the structural components of the sarcoplasm was revealed. Gopinathannair R., Sullivan R. and Olshansky B. [3] found that increased levels of thyroid hormones cause tachycardia and rapid oxygen consumption, increased production of end products of metabolism and relaxation of smooth muscle fibers of arteries, peripheral vasodilation, leading to reduce peripheral vascular resistance and further increase heart rate [7]. It has been shown that the autoimmune process associated with endothelial damage or dysfunction in hyperthyroidism is accompanied by increased cardiac output and increased metabolism of vasodilators [12].

Studies of ultrastructural reorganization of the heart of laboratory animals, which simulated hypothyroidism and HHCy, revealed significant changes in endothelial cells, most mitochondria were destroyed. Cardiomyocytes showed more pronounced alternative changes compared to previous observation groups. This can be explained, in particular, by decreased regulation of the potassium channel (IK1), which is a characteristic feature of cardiac hypertrophy and insufficiency in hyperthyroidism. Q. H. Liu et al. [10] investigated the major cardioprotective mechanisms of zacopride (selective agonist IK1) in cardiac remodeling induced by L-thyroxine (T_4) or triiodothyronine (T_3) in vivo in adult Sprague-Dawley rats. Zacopride treatment reduced cardiac hypertrophy and collagen deposition, ventricular dilatation, decreased ejection fraction, increased cardiomyocytes apoptosis, hyperactivation of CaMKIAkt and PI3K/signal to reduce cardiac autophagy, and increased integrin β_3 expression, ie symptoms of cardiac remodeling and dysfunction. Cardioprotection of zacopride is closely associated with increased homeostasis of IK1, SAP97 and [Ca^{2+}] in cardiomyocytes. In a study by Song E. et al. [13] similar results were found. The authors found that high levels of thyroid hormones cause so-called "thyrotoxic cardiomyopathy" - damage to the myocardium caused by toxic effects, which leads to changes in myocyte energy production (oxidative phosphorylation, glycolysis), intracellular synthesis (protein synthesis) and contractile function of myofibrils.

Our electron microscopic examination of the myocardium of animals with hypothyroidism showed significant degenerative changes in the ultrastructure of blood vessel walls. Hemocapillary endothelial cells contained few microbubbles and caveolae, and their cytoplasm was swollen. Hypertrophied mitochondria with an enlightened matrix and partially reduced cristae were detected. Thickening and swelling of the basement membrane of blood vessels, hypothyroidism caused a violation of the ultrastructure of contractile cardiomyocytes. Work of Udovcic M. and others [15] have shown that hypothyroidism is associated with decreased cardiac output due to impaired vascular smooth muscle relaxation and decreased endothelial nitric oxide availability. This causes a cascading effect of increasing the stiffness of the arteries, which leads to increased systemic vascular resistance. At the molecular level, these changes are the result of decreased Ca^{2+}-ATPase expression of the sarcoplasmic reticulum and increased expression of phospholamban, which inhibits ATPase. Thyroid hormones also affect the renin-angiotensin-aldosterone system. Under the action of T_3, renin substrates are synthesized in the liver. Thus, in the hypothyroid state, diastolic blood pressure increases, pulse pressure decreases, and renin levels decrease. This leads to diastolic hypertension, which is often sensitive to sodium. Thyroid hormones also regulate pacing genes through transcription, as well as

the beta-adrenergic system in cardiomyocytes. As a result of these mechanisms, heart rate increases in the presence of thyroid hormones and decreases in hypothyroidism [17].

Under the conditions of the combined influence of hypothyroidism and HHCy, we found the deepest violations of the ultrastructure of endothelial cells. Integrity of intercellular contacts is broken, in many mitochondria cristae and an external membrane were destroyed. The basement membrane of the blood vessel wall is significantly thickened and poorly contoured, damaged. An increase in ultrastructural changes was also found in cardiomyocytes (hypertrophied mitochondria). Thinning, fragmentation, and lysis were observed in most cells, sarcomeres were unevenly distributed. Activation of fibroblasts is accompanied by the growth of collagen fibers in the interstitium. Thyroid hormones affect endothelial functions mediated by the thyroid hormone receptor (THR)-α1 and THR-β. Activation of THR-α1 increases coronary blood flow, reduces coronary resistance in mouse models, and increases nitric oxide production in endothelial and vascular smooth muscle cells. Activation of THR-β by thyroid hormones induces angiogenesis by initiating a mitogen-activated protein kinase pathway. Severe hypothyroidism can also cause pericardial effusion due to increased capillary permeability and reduced lymphatic drainage from the pericardial space [17]. Hypothyroidism can affect the contractility of the heart and disrupt the relaxation of the heart muscle [9].

Conclusion

1. Under conditions of HHCy, hyper- and hypothyroidism in the myocardium of laboratory rats there are ultrastructural changes in the nuclear, contractile and energy apparatus of cardiomyocytes with the development of adaptive-compensatory and destructive changes.

2. Under the combined effects of hyperthyroidism and HHCy, hypothyroidism and HHCy, deeper remodeling of the hemocapililary wall with damage to the ultrastructure of endothelial cells and basement membrane was found. Against the background of insufficient microhemocirculation in cardiomyocytes revealed profound degenerative changes in the nuclei, components of the contractile and energy apparatus of the sarcoplasm, manifested by contractile zones, defibering and lysis of myofilaments, mitochondrial hypertrophy and lysis of their cristae.

References

[1] Afshin, A., Micha, R., Khatibzadeh, S., & Mozaffarian, D. (2014). Consumption of nuts and legumes and risk of incident ischemic heart disease, stroke, and diabetes: a systematic review and meta-analysis. *The American journal of clinical nutrition,* 100(1), 278-288. doi: 10.3945/ajcn.113.076901]

[2] Gerdes, A. M. (2015). Restoration of thyroid hormone balance: a game changer in the treatment of heart failure?. *American journal of physiology. Heart and circulatory physiology,* 308(1), H1-H10. doi: 10.1152/ajpheart.00704.2014

[3] Gopinathannair, R., Sullivan, R., & Olshansky, B. (2009). Tachycardia-mediated cardiomyopathy: recognition and management. *Current heart failure reports,* 6(4), 257-264. doi: 10.1007/s11897-009-0035-3

[4] Goralskiy, L. P., Homich, V. T., & Kononskiy, O. I. (2011). *Fundamentals of histological technique and morphofunctional methods of research in norm and in pathology.* Zhitomir: Polissya.

[5] Gözüküçük, M., Gürsoy, A. Y., Destegül, E., Taskin, S., & Şatiroglu, H. (2021). Homocysteine and C-reactive Protein Levels in Women with Polycystic Ovary Syndrome. *Gynecology and minimally invasive therapy,* 10(4), 210-214. doi: 10.4103/GMIT.GMIT_30_20

[6] Holmager, P., Schmidt, U., Mark, P., Andersen, U., Dominguez, H., Raymond, I., ... Faber, J. (2015). Long-term L-Triiodothyronine (T3) treatment in stable systolic heart failure patients: a randomised, double-blind, cross-over, placebo-controlled intervention study. *Clinical endocrinology*, 83(6), 931-937. doi: 10.1111/cen.12648

[7] Kazama, I., Mori, Y., Baba, A., & Nakajima, T. (2014). Pitting type of pretibial edema in a patient with silent thyroiditis successfully treated by angiotensin ii receptor blockade. *The American journal of case reports*, 15, 111-114. doi: 10.12659/AJCR.889854

[8] Kerp, H., Hönes, G. S., Tolstik, E., Hönes-Wendland, J., Gassen, J., Moeller, L. C., … & Führer, D. (2021). Protective Effects of Thyroid Hormone Deprivation on Progression of Maladaptive Cardiac Hypertrophy and Heart Failure. *Frontiers in cardiovascular medicine,* 8, 683522. doi: 10.3389/fcvm.2021.683522

[9] Lisco, G., Giagulli, V. A., Iovino, M., Zupo, R., Guastamacchia, E., De Pergola, G., … & Triggiani, V. (2021). Endocrine system dysfunction and chronic heart failure: a clinical perspective. *Endocrine,* 1-17. Advance online publication. doi: 10.1007/s12020-021-02912-w]

[10] Liu, Q. H., Zhang, L. J., Wang, J., Wu, B. W., & Cao, J. M. (2021). Cardioprotection of an IK1 channel agonist on L-thyroxine induced rat ventricular remodeling. *American journal of translational research*, 13(8), 8683-8696.

[11] Nechiporuk, V. & Korda, M. (2017). Metabolism of cysteine in experimental hyper- and hypothyroidism in rats. *Medical and Clinical Chemistry,* 19(4), 32-40. doi: 10.11603/mcch.2410-681X.2017.v0.i4.8433

[12] Paschou, S. A., Bletsa, E., Stampouloglou, P. K., Tsigkou, V., Valatsou, A., Stefanaki, K., … & Siasos, G. (2022). Thyroid disorders and cardiovascular manifestations: an update. *Endocrine,* 10.1007/s12020-022-02982-4. Advance online publication. doi: 10.1007/s12020-022-02982-4]

[13] Song, E., Kim, M., Park, S., Park, M. J., Kim, J. A., Roh, E., … & Yoo, H. J. (2021). Treatment Modality and Risk of Heart Failure in Patients With Long-Standing Graves' Disease: A Nationwide Population-Based Cohort Study. *Frontiers in endocrinology,* 12, 761782. doi: 10.3389/fendo.2021.761782

[14] Stangl, G. I. (2007) Homocysteine thiolactone-induced hyperhomocysteinemia does not alter concentrations of cholesterol and SREBP-2 target gene mRNAS in rats. *Exp. Biol. Med.,* 232(1), 81-87.

[15] Udovcic, M., Pena, R. H., Patham, B., Tabatabai, L., & Kansara, A. (2017). Hypothyroidism and the Heart. *Methodist DeBakey cardiovascular journal,* 13(2), 55-59. doi: 10.14797/mdcj-13-2-55

[16] Vale, C., Neves, J. S., von Hafe, M., Borges-Canha, M., & Leite-Moreira, A. (2019). The Role of Thyroid Hormones in Heart Failure. *Cardiovascular drugs and therapy,* 33(2), 179-188. doi: 10.1007/s10557-019-06870-4

[17] Vargas-Uricoechea, H., Bonelo-Perdomo, A., & Sierra-Torres, C. H. (2014). Effects of thyroid hormones on the heart. *Clinica e investigacion en arteriosclerosis: publicacion oficial de la Sociedad Espanola de Arteriosclerosis,* 26(6), 296-309. doi: 10.1016/j.arteri.2014.07.003]

[18] Yamakawa, H., Kato, T. S., Noh, J. Y., Yuasa, S., Kawamura, A., Fukuda, K., & Aizawa, Y. (2021). Thyroid Hormone Plays an Important Role in Cardiac Function: From Bench to Bedside. *Frontiers in physiology,* 12, 606931. doi: 10.3389/fphys.2021.606931

[19] Zhang, Y., Dedkov, E. I., Lee, B., Li, Y., Pun, K., & Gerdes, A. M. (2014). Thyroid hormone replacement therapy attenuates atrial remodeling and reduces atrial fibrillation inducibility in a rat myocardial infarction-heart failure model. *Journal of cardiac failure*, 20(12), 1012-1019. doi: 10.1016/j.cardfail.2014.10.003]

УЛЬТРАСТРУКТУРНІ ЗМІНИ МІОКАРДА ТВАРИН ЗА УМОВ ЗМОДЕЛЬОВАНИХ ГІПЕРГОМОЦИСТЕЇНЕМІЇ, ГІПЕР- ТА ГІПОТИРЕОЗУ ТА ЇХ ПОЄДНАНІЙ ДІЇ

Нечипорук В. М., Пентюк Л. О., Ковальчук О. В., Мазур О. І., Корда М. М.

Гормони щитоподібної залози мають значний вплив на функцію серця як за допомогою геномних, так і негеномних ефектів. Дефіцит чи надлишок тиреоїдних гормонів призводить до глибоких змін у регуляції серцевої функції та серцево-судинної гемодинаміки. Серце є основним органом-мішенню для дії гормонів щитоподібної залози і у пацієнтів з гіпо- або гіпертиреозом відбуваються помітні зміни в роботі серця. Метою роботи було встановити ультраструктурні зміни компонентів міокарда за умов експериментальної гіпергомоцистеїнемії (ГГЦ) на фоні гіпер- та гіпотиреозу. Тіолактонову ГГЦ моделювали введенням тваринам екзогенного гомоцистеїну (ГЦ) у формі тіолактону в дозі 100 мг/кг маси тіла один раз на добу впродовж 28 діб. Гіпертиреоз моделювали шляхом щоденного введення L-тироксину в дозі 200 мкг/кг впродовж 21 доби, гіпотиреоз - щоденного введення мерказолілу в дозі 10 мг/кг маси впродовж 21 дня. Окремим групам тварин вводили L-тироксин і мерказоліл паралельно з ГЦ. Високі рівні ГЦ негативно впливали на стінки кровоносних судин міокарду. Просвіти гемокапілярів були повнокровними, заповнені еритроцитами. Виявлено зміни в ендотеліоцитах, а кардіоцити містили деформовані ядра. У лабораторних тварин з гіпертиреозом встановлено наростання ультраструктурних змін в стінках кровоносних судин (набряк стінок гемокапілярів, пошкоджені кристи у мітохондріях). У тварин, яким моделювали гіпертиреоз та ГГЦ, виявлені більш значні зміни у ендотеліоцитах, більшість мітохондрій були зруйновані. У кардіоміоцитах виявлено більш виражені альтеративні зміни. Електронномікроскопічне дослідження міокарда тварин при гіпотиреозі показало значні дегенеративні зміни в ультраструктурі стінок кровоносних судин, виявлені також гіпертрофовані мітохондрії. Поєднаний вплив гіпотиреозу та ГГЦ викликав найбільш глибокі порушення ультраструктури кардіоміоцитів і гемокапілярів порівняно з іншими групами тварин. Цілісність міжклітинних контактів була порушена, більшість мітохондрій міоцитів мали зруйновані кристи та зовнішню мембрану.

Ключові слова: *гіпертиреоз, гіпотиреоз, гіпергомоцистеїнемія, міокард.*

DOI: 10.31393/morphology-journal-2022-28(2)-06 Reports of Morphology, Vol. 28, №2, Pages 40-47

ISSN 1818-1295 eISSN 2616-6194

REPORTS OF MORPHOLOGY

Official Journal of the Scientific Society of Anatomists, Histologists, Embryologists and Topographic Anatomists of Ukraine

journal homepage: https://morphology-journal.com

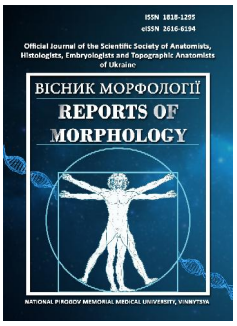

Fractal dimension of skeletonized MR images as a measure of cerebral hemispheres spatial complexity

Maryenko N. I., Stepanenko O. Yu.
Kharkiv National Medical University, Kharkiv, Ukraine

ARTICLE INFO
Received: 11 February 2022
Accepted: 17 March 2022

UDC: 611.813:57.086:517:530.191

CORRESPONDING AUTHOR
e-mail: maryenko.n@gmail.com
Maryenko N. I.

CONFLICT OF INTEREST
The authors have no conflicts of interest to declare.

FUNDING
Not applicable.

In recent decades, fractal analysis has been increasingly used in various scientific fields, including neuroscience; this method of mathematical analysis allows you to quantify the space filling degree of the studied object and the degree of its spatial configuration complexity. The aim of the study was to determine the values of the fractal dimension of the cerebral hemispheres using fractal analysis of skeletonized magnetic resonance brain images. The present study used magnetic resonance brain images of 100 relatively healthy individuals (who had no structural changes in the brain) of both sexes (56 women, 44 men) aged 18-86 years (mean age 41.72±1.58 years). 5 tomographic sections of each brain were studied. The 1st coronal tomographic section was located at the level of the most anterior points of the temporal lobes, the 2nd - at the level of the mammillary bodies, the 3rd - at the level of the quadrigeminal plate, the 4th - at the level of the splenium of corpus callosum. The axial tomographic section was located at the level of the thalamus. Fractal analysis of skeletonized images was performed using box counting method. The obtained data were processed using generally accepted statistical methods. The average, minimum and maximum values of the fractal dimension of different tomographic sections were the following: 1st coronal section - 1.207±0.003 (1.147÷1.277), 2nd coronal section - 1.162±0.003 (1.077÷1.243), 3rd coronal section - 1.156±0.003 (1.094÷1.224), 4th coronal section - 1.158±0.003 (1.109÷1.218), axial section - 1.138±0.002 (1.079÷1.194). The average value of the fractal dimension of the five tomographic sections was 1.164±0.002 (1.126÷1.209), and the average value of the fractal dimension of the four coronal sections was 1.171±0.002 (1.122÷1.219). Fractal analysis of skeletonized images of the cerebral hemispheres allows to quantify the features of the topology and complexity of the spatial configuration of the cerebral hemispheres. The value of the fractal dimension can be influenced by the anatomical features of the studied areas of the brain, individual anatomical features, as well as atrophic and other pathological changes that lead to changes in the shape of the cerebral hemispheres. The values of the fractal dimension of skeletonized brain images tend to decrease with age. Coronal tomographic sections are the most representative for characterizing age-related atrophic changes. Fractal analysis of skeletonized images of the cerebral hemispheres can be used to diagnose diseases of the nervous system, and the results of the present study can be used as norm criteria.

Keywords: *fractal analysis, fractal dimension, brain, cerebral hemispheres, morphometry.*

Introduction

The brain is one of the most complex structures of the human body, and the study of its morphology is devoted to a huge number of scientific papers: from classical anatomical research to innovative research in modern neuroscience. In recent decades, diagnostic methods of neuroimaging, including magnetic resonance imaging, have become increasingly common. These methods allow us to study the lifelong morphology of brain structures, which is important not only for classical morphological studies, but also for the diagnosis of many diseases of the nervous system.

Various morphometric methods are often used in neuromorphological research (including the use of neuroimaging methods) to objectify them and increase information. Most often, morphometry involves measuring

the linear size, area, volume of different structures and pathological foci and the calculation of various indices and indicators based on these parameters [19]. Most methods of morphometry are based on Euclidean geometry and are quite informative in the study of structures with geometrically simple shapes. However, the spatial configuration of brain hemispheres is not geometrically correct, so it is difficult to characterize using traditional methods of morphometry.

In recent decades, many natural sciences, including neuroscience, are increasingly using methods of fractal geometry, namely fractal analysis [2, 3, 14]. This method of mathematical analysis allows you to quantify the degree of filling of space by the object and the degree of complexity of its spatial configuration [10, 14]. Given this, the use of fractal analysis for morphometric study of the cerebral hemispheres is appropriate and informative, as quantitative characterization of the shape will assess both individual anatomical features that affect the configuration of the hemispheres and the presence of age or pathological changes in the brain [2].

To characterize the spatial configuration of different biological structures using fractal analysis, three types of images are most often used - silhouette (corresponding to the silhouette of the structure as a whole), outlined (to characterize the configuration of the contour, boundary or surface of the structure) and skeletonized [10]. The last type of images involves the procedure of skeletonization, which allows to obtain a digital skeleton of the studied structure by eroding the silhouette image [8, 10, 16, 17].

Skeletonization is most often used as a pre-treatment method for quantitative analysis (including fractal analysis) of dendritic tree neurons and other tree-like branched and reticulate structures [8, 10, 16, 17]. In these cases, skeletonization allows to level the thickness of the branches of branched structures and to characterize the degree of their branching. In our previous studies [15] and in the studies of other authors [13], fractal analysis of skeletal images of arbor vitae cerebelli was performed.

Other irregular structures that do not have a clear tree-like configuration can also be skeletonized. Such structures include brain hemispheres. In these cases, the skeletonization procedure detects the vertices of a certain figure (for example, the vertices of the convolutions of the cerebral hemispheres) and builds a network that connects all the detected vertices in the shortest segments and fills the space inside the silhouette. Despite the fact that brain hemispheres do not have the classical tree-like configuration, skeletalization of brain images has been useful for both fractal analysis and other methods of image analysis. Skeletonization is currently used as a pre-processing method to analyze magnetic resonance imaging of the cerebral hemispheres using the method of "Peak Width of Skeletonized Mean Diffusivity" [1], which in recent years has been used to detect diffuse pathological changes in vascular diseases of the brain, including diseases of small vessels [1, 7]. Skeletonization is also used for fractal analysis of the structures of the cerebral hemispheres as a method of image pre-processing. The vast majority of such studies used the construction of a digital skeleton of white matter [4, 6, 20, 21, 24-26]. Skeletonization and fractal analysis can be used not only to study white matter, but also to study brain hemispheres as a whole. But studies of skeletal images of brain hemispheres in general have not yet been conducted (according to the available scientific literature). Given the lack of such studies and the great clinical significance of neuromorphological studies, we decided to choose the brain hemispheres as a whole as the object of study.

The aim of the study is to determine the value of the fractal dimension of the cerebral hemispheres using fractal analysis of skeletonized magnetic resonance imaging of the brain.

Materials and methods

The study was conducted in compliance with the basic bioethical provisions of the Council of Europe Convention on Human Rights and Biomedicine (04.04.1997), the Helsinki Declaration of the World Medical Association on ethical principles of scientific medical research with human participation (1964-2008), and the Ministry of Health of Ukraine № 690 from 23.09.2009. The conclusion of the Commission on Ethics and Bioethics of Kharkiv National Medical University confirms that the study was conducted in compliance with human rights, in accordance with current legislation in Ukraine, meets international ethical requirements and does not violate ethical norms in science and standards of biomedical research (Minutes of the meeting of the Commission on Ethics and Bioethics of Kharkiv National Medical University № 10 dated November 7, 2018).

Magnetic resonance (MR) tomograms of 100 relatively healthy individuals brain (who did not have structural changes in the brain) of both sexes (women 56, men 44) aged 18-86 years (mean age 41.72±1.58 years) were used for the study. MR images were obtained using a Siemens Magnetom Symphony magnetic resonance imaging scanner with a magnetic induction value of 1.5 T. T2 and FLAIR modes with the following parameters were used: T2 mode - TE (echo time) 130 ms, TR (repetition time) 4440 ms, slice thickness - 5 mm; mode FLAIR - TE (echo time) 114 ms, TR (repetition time) 9000 ms, TI (inversion time) - 2500 ms; the thickness of the cut - 5 mm.

To examine each brain, 5 tomographic sections were selected, including four sections in coronal (frontal) projection and one section in axial (horizontal) projection. We chose tomographic sections that correspond to different parts of the cerebral hemispheres and are easily identifiable by anatomical landmarks, these sections correspond to areas of the brain where pathological lesions of the brain are most common in some neurodegenerative diseases, including Alzheimer's disease [11]. The 1st coronal tomographic section was located at the level of the anterior points of the

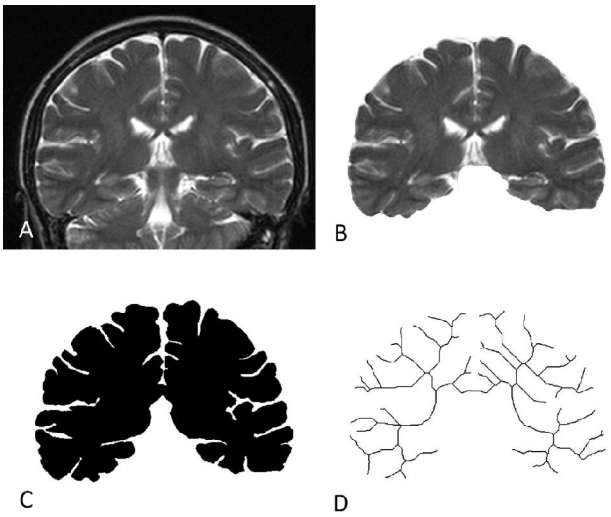

Fig. 1. Pre-processing of magnetic resonance imaging of the brain: A - original T-2 weighted MR image, B - removal of background structures, C - image segmentation with conversion to binary format, D - skeletalization of the image.

temporal lobes, the 2nd - at the level of corpus mamillare, the 3rd - at the level of lamina quadrigemina, the 4th - at the level of splenium corpori callosi. The axial tomographic section was located at the level of the thalamus.

After selecting the images, they were pre-processed (Fig. 1). The Adobe Photoshop CS5 graphics editor created images with a resolution of 128 pixels per inch and the following dimensions: 512x400 pixels for coronal sections and 512x800 pixels for axial sections. A fragment of the digital tomographic image corresponding to the study area was inserted into the previously created image, and this fragment was placed so that the tomographic section of the cerebral hemispheres was completely placed in the created image and did not go beyond it (see Fig. 1A).

The next stage of preliminary preparation was the segmentation of images with their conversion into binary format. Initially, the background structures were removed from the image (see Figure 1B). For this purpose, pixels that do not correspond to the studied structure (tomographic section of the hemispheres) were colored white (for T2-weighted images) or black (for images obtained in FLAIR mode). Next, Adobe Photoshop CS5's "threshold" tool was used for preliminary ("rough") segmentation. Pixel brightness threshold processing was performed: all pixels with a brightness value less than the specified threshold value were colored black, the remaining pixels were colored white. For images obtained in T2 mode, a median threshold value of 128 was used, with the pixels corresponding to the brain tissue stained black and the rest white. For images obtained in FLAIR mode, an empirical brightness threshold of 65 was used, with the pixels corresponding to the brain tissue stained white and the rest black. After the previous "rough" segmentation with the help of manual correction, precise segmentation was performed to improve the anatomical accuracy of the obtained images, using the tools of the program "Adobe Photoshop CS5". Thus, as a result of MR image segmentation, we obtained binary silhouette images of the cerebral hemispheres (see Fig. 1C).

For further stages of image processing and analysis, the Image J program was used [23]. Binary silhouette images were skeletonized using the "skeletonize" tool (see Figure 1D). The line thickness of the digital skeleton formed with this tool was 1 pixel. This tool was used to process each of the five selected tomographic sections of the cerebral hemispheres (Fig. 2).

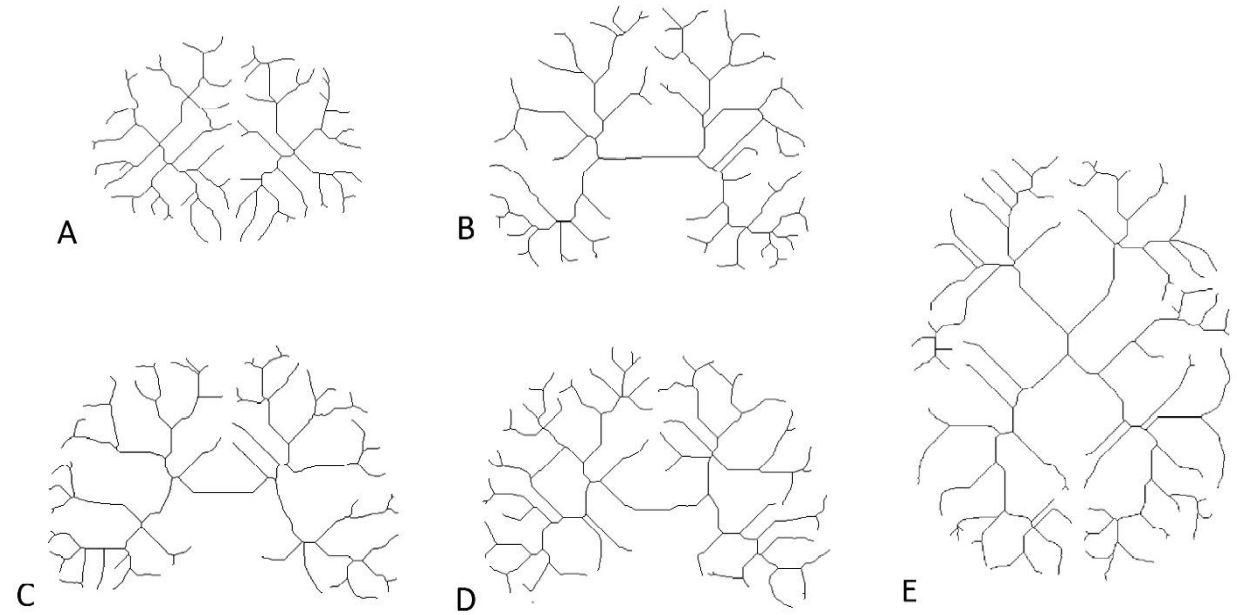

Fig. 2. Skeletonized images of the cerebral hemispheres: A - 1st coronal section, B - 2nd coronal section, C - 3rd coronal section, D - 4th coronal section, E - axial section.

Table 1. Statistical parameters of the distribution of fractal dimension (FD) values of cerebral hemispheres skeletonized images.

Tomographic section	M	m	s	CV, %	Min	Percentile 25	Me (percentile 50)	Percentile 75	Max
Coronal 1	1.207	0.003	0.027	2.27	1.147	1.186	1.210	1.227	1.277
Coronal 2	1.162	0.003	0.031	2.70	1.077	1.136	1.162	1.184	1.243
Coronal 3	1.156	0.003	0.029	2.47	1.094	1.137	1.152	1.177	1.224
Coronal 4	1.158	0.003	0.026	2.26	1.109	1.139	1.155	1.176	1.218
Axial	1.138	0.002	0.023	2.04	1.079	1.122	1.139	1.152	1.194
Average (all sections)	1.164	0.002	0.018	1.56	1.126	1.150	1.163	1.179	1.209
Average (1-4 coronal)	1.171	0.002	0.021	1.79	1.122	1.157	1.168	1.185	1.219

After skeletalization, fractal analysis of images was performed using the box counting method, using the "fractal box count" tool of the Image J. program. Fractal dimension (FD) values of skeletonized tomographic images of five different locations were determined in the MR tomogram of each brain (see Fig. 2). The mean FD values of all five sections and the average FD values of four coronal sections were also calculated for each brain.

Statistical data processing was performed using Microsoft Excel 2016. Data were processed using variation statistics. The following statistical parameters were calculated for each variation series: arithmetic mean (M), its error (mM), standard deviation (σ) and coefficient of variation (CV). To determine the peculiarities of the distribution of fractal dimension values, the median (Me), the values of the 25th and 75th percentiles, the minimum (min) and maximum (max) values were determined. The distribution of values for normality was checked using the Shaporo-Wilk W test. The significance of statistical differences between the fractal dimensions of tomographic sections of different localization was assessed using the Kruskal-Wallis KW test with Bonferroni correction and the post-hoc Dunn test for multiple comparisons. To determine the relationship between the values obtained, the Pearson correlation coefficient (r) was calculated, the significance of which was assessed using the Student's t test.

Results

The distribution of fractal dimensional (FD) values of skeletal images of tomographic sections of five localizations, as well as average FD values of five tomographic sections and average FD values of four coronal sections are shown in Table 1 and Figure 3. When checking the distribution of FD values for normality was it was found that the distributions of FD values of the 1st coronal section (p=0.674), 2nd coronal section (p=0.331), 3rd coronal section (p=0.166) and axial section (p=0.823) did not differ statistically significantly from the normal distribution. The difference in the distribution of FD values of the 4th coronal section from the normal distribution was questionable (p=0.084). The distributions of the mean FD values of the five sections and the mean FD values of the four coronal sections also did not differ statistically significantly from the normal distribution (p=0.451 and p=0.283, respectively).

The nonparametric Kruskal-Wallis test was chosen to compare the FD values of five tomographic sections. The calculated value of p was less than the specified threshold level of significance α (α=0.050, p»0), therefore, the null hypothesis (H_0 hypothesis) about the lack of differences between the studied samples can be refuted.

To find out which samples were statistically significantly different, we made pairwise comparisons using the Dunn post-hoc test. We chose the level of statistical significance α=0.050, which with the Bonferroni correction for multiple comparisons was α=0.005. It was found that the FD values of the 1st coronal section were statistically significantly different from the FD values of all other tomographic sections (p<0.001), as well as the FD values of the axial section (p<0.001). However, no statistically significant differences were found between the FD values of the following pairs of coronal sections: 2nd and 3rd (p=0.202), 2nd and

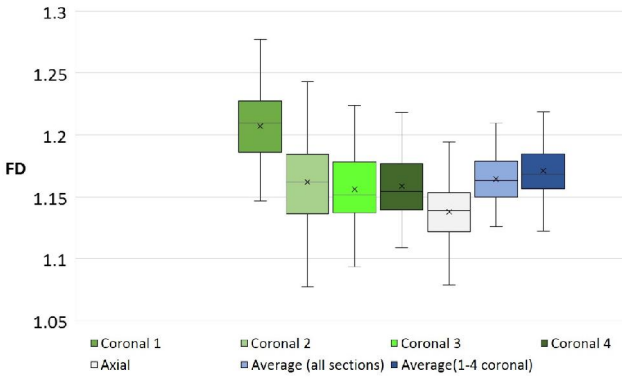

Fig. 3. Distribution of fractal dimensional (FD) values of skeletonized images of the cerebral hemispheres.

Table 2. Correlation relationships of fractal dimension values of skeletonized images of cerebral hemispheres.

	Coronal 1	Coronal 2	Coronal 3	Coronal 4	Axial
Coronal 1	-	0.40#	0.25*	0.29*	0.01
Coronal 2	0.40#	-	0.46#	0.43#	0.14
Coronal 3	0.25*	0.46#	-	0.51#	0.25*
Coronal 4	0.29*	0.43#	0.51#	-	0.10
Axial	0.01	0.14	0.25*	0.10	-

Note: the table shows the values of the Pearson correlation coefficients (r); * - p<0.01; # - p<0.001.

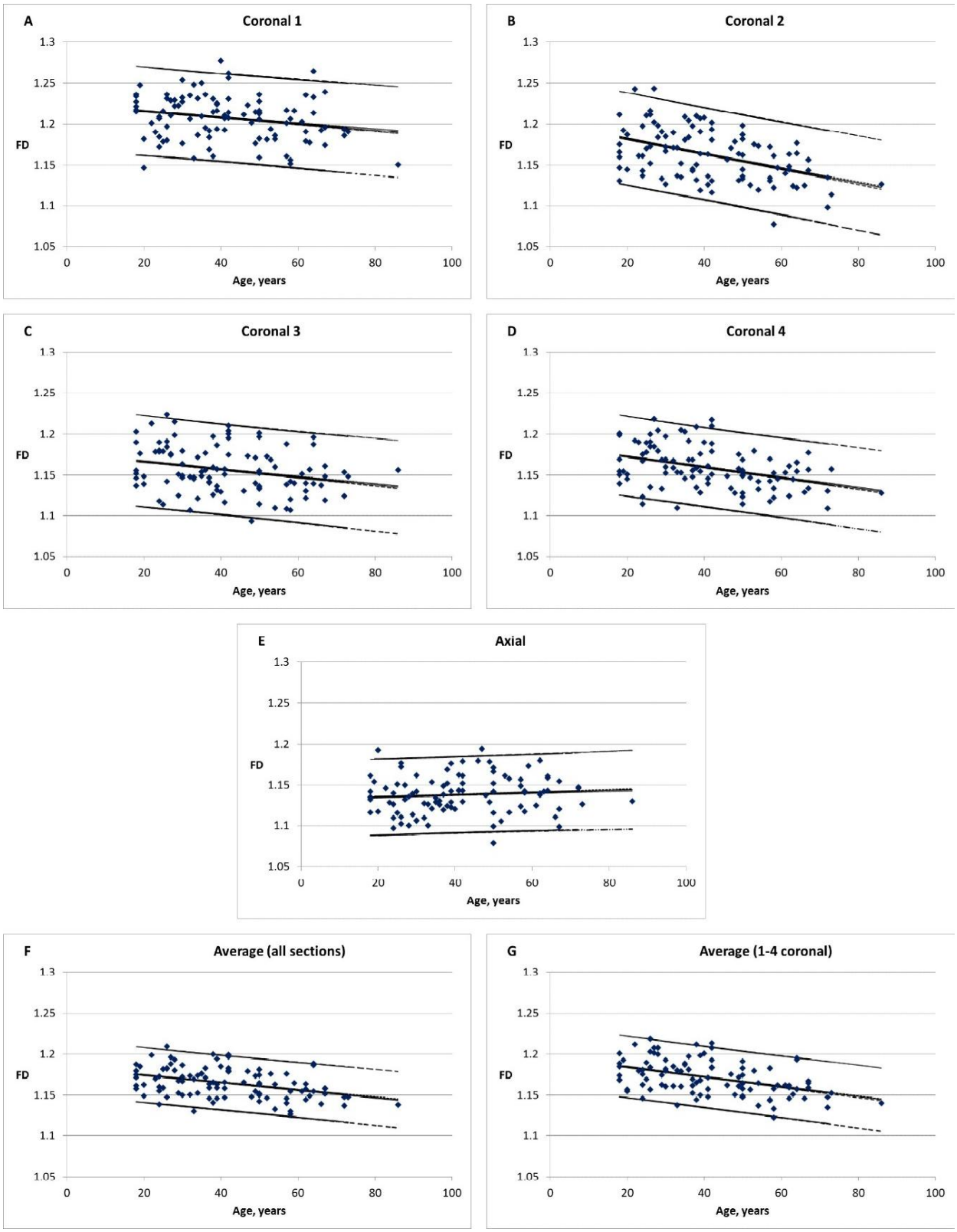

Fig. 4. Distribution of fractal dimensional (FD) values of different parts of the brain and confidence intervals of FD values; A - 1st coronal section, B - 2nd coronal section, C - 3rd coronal section, D - 4th coronal section, E - axial section, F - mean FD of all five sections, G - average value of 4 coronal sections FD; the level of significance selected for the calculation of confidence intervals of values - 95 %, $p<0.05$.

4th (p=0.477), 3rd and 4th (p=0.572).

Correlation analysis of FD values of five tomographic sections was also performed (Table 2). It was found that the FD values of coronal sections were associated with a statistically significant positive correlation between medium and low strength. A stronger correlation was found between the FD values of adjacent coronal sections: 3rd and 4th, 2nd and 3rd, 1st and 2nd. Axial section FD values were not strongly correlated with coronal section FD values. A statistically significant positive correlation of axial section FD values was found only with FD values of the 3rd coronal section; with FD values of the rest of the coronal sections statistically significant correlation was not detected ($p>0.05$).

Because the age range of the subjects was quite wide, ranging from 18 to 86 years, we investigated whether the values of the fractal dimension of skeletal images of the cerebral hemispheres change with age. As can be seen from the data in Figure 4, the FD values of different sections had a general tendency to decrease with age. The FD values of the coronal sections had a statistically significant negative correlation with age, while the FD values of the 1st and 3rd coronal sections had a weak correlation with age (respectively $r=-0.22$, $p<0.05$ and $r=-0.26$, $p<0.01$), and the 2nd and 4th sections - correlation of medium strength (respectively $r=-0.45$, $p<0.001$ and $r=-0.39$, $p<0.001$). In contrast to coronal sections, the FD values of the axial section did not have a statistically significant correlation with age ($r=0.09$, $p>0.05$). The mean FD values of all five tomographic sections and the mean FD values of the four coronal sections had a statistically significant negative correlation with age of medium strength (respectively $r=-0.40$, $p<0.001$ and $r=-0.46$, $p<0.001$).

Discussion

Brain hemispheres are the subject of a number of different studies using fractal analysis due to the irregularity of their shape, as well as the clinical significance of quantitative characterization of the complexity of the spatial configuration of brain structures [2]. For fractal analysis of cerebral hemispheres structures, various techniques are used, which involve the analysis of different types of images (silhouette, outlined and skeletonized). Different authors studied different structures and parts of large hemispheres. In the vast majority of works to characterize atrophic changes of the brain fractal analysis of the cortex as a whole [5, 11, 22] and the surface of the brain [9, 12], including - analysis of the skeletal surface of hemispheres [12]. A number of studies have performed fractal analysis of the white matter of the cerebral hemispheres, including their silhouettes or tissue as a whole [6, 18, 26], contours or surfaces (linear boundary between the cortex and white matter) [6, 26] and skeletonized images [4, 6, 20, 21, 24-26]. Studies using fractal analysis of skeletal images of the white matter of the cerebral hemispheres are closest to our study. But the skeletalization of the white matter of the cerebral hemispheres used in these studies involves the use of complex image segmentation algorithms, as it requires anatomically accurate separation of white matter and cortex. Therefore, the use of silhouette images of the cerebral hemispheres as a whole (including gray matter, white matter and cerebrospinal fluid inside the ventricles) with their subsequent skeletalization helps to simplify segmentation algorithms, and also allows to assess the spatial configuration of not only white matter but also the cerebral hemispheres in general.

Fractal analysis of skeletal images of both white matter and hemispheres of the brain as a whole provides a quantitative assessment of the topology of brain hemispheres. The digital skeleton repeats the configuration of the structure as a whole and has the same topology as the silhouette image. Therefore, the analysis of the digital skeleton makes it possible to assess how white matter and large hemispheres of the brain as a whole fill the space, eliminating the influence of the area of the silhouette image.

Fractal analysis of skeletal images also provides a quantitative characterization of the degree of spatial complexity and anatomical features of brain hemispheres. The number and density of convolutions visualized on tomographic sections may differ in different individuals and in different parts of the brain. The more vertices (convolutions) the silhouette image has, the more complex the configuration of its digital skeleton will be and the greater will be the value of its fractal dimension. The values of the fractal dimension determined by us as a result of this study may differ significantly in different individuals with close or the same age in the study of tomographic sections of the same localization (see Fig. 4). It can be assumed that the difference in FD values in these cases is significantly influenced by the peculiarities of individual anatomical variability. In addition, FD values may differ depending on the location and orientation of the tomographic section (including differences in FD values in the same person). This may indicate that the value of FD is also influenced by the anatomy of different parts of the brain (see Fig. 2). Thus, the FD values of skeletal images can reflect both individual and regional anatomical features of the cerebral hemispheres.

In addition to characterizing the anatomical features, fractal analysis of the digital skeleton of the white matter of brain hemispheres can detect changes in some diseases and pathological conditions. This method of research revealed changes after acute cerebrovascular disorders [24], after traumatic brain injury [20], multiple sclerosis [4] and amyotrophic lateral sclerosis [21]. This indicates the possibility of using this method of research to diagnose some diseases of the nervous system.

Age-related changes in the brain are of great importance for the development of normative criteria, which, in turn, can affect the value of the fractal dimension of skeletal images. Traditional morphometric methods based on Euclidean geometry have revealed a decrease in the gray and white matter of the brain; these features reflect the dynamics of

atrophic changes in the brain as a whole [19]. Using fractal methods, a statistically significant decrease in the values of the fractal dimension of the digital skeleton of white matter during normal aging was found [6, 25, 26], which is consistent with our data. Atrophic changes in the cortex and white matter of the cerebral hemispheres can change their spatial configuration, which in turn can affect the configuration of the digital skeleton - reducing the number and shortening of branches, reducing the number of connections, and so on. This simplification of the spatial configuration is reflected in the reduction of the fractal dimension of skeletal images.

According to our data, the FD values of coronal tomographic sections were more representative for characterizing age-related changes than the FD values of the axial section. In the work of King R. D. et al. [11] to study pathological atrophic changes in Alzheimer's disease, a fractal analysis of the cerebral cortex was performed; coronal sections of the same localization as in our study were studied; axial sections of three different localizations were also investigated. It was found that the difference between the FD values of the cerebral cortex of the control group and patients with Alzheimer's disease was greater in the study of coronal sections than in the study of axial sections. This data is consistent with the data we have received.

Given that the average FD value of the four coronal sections has a stronger correlation with age than the average FD value of all five tomographic sections, and given the lack of a statistically significant correlation between the FD values of the axial section and age, it is possible to consider that the most representative indicator for characterization of age changes is the average value of FD of four coronal sections. This value has the strength of the correlation with age, comparable to the greatest strength of the correlation of a separate (2nd) tomographic section with age (respectively r=-0.46 and r=-0.45) and exceeds the strength of the correlation with age other coronal sections (1st, 3rd and 4th). Thus, averaging the values of coronal sections allows to obtain a supertotal effect, as it reduces the impact of errors, artifacts of tomography and processing of tomographic sections, as well as individual anatomical features. We calculated 95 % confidence intervals of FD values, which can then be used as age criteria (see Fig. 4).

A promising area of further research is the quantitative analysis of digital skeletons of the cerebral hemispheres and traditional morphometry to determine the factors influencing the value of the fractal dimension and, consequently, the complexity of the spatial configuration of the cerebral hemispheres.

Conclusion

1. Fractal analysis of cerebral hemispheres skeletonized images allows to quantify the features of the topology and complexity of cerebral hemispheres spatial configuration.

2. The value of the fractal dimension can be influenced by the anatomical features of the studied areas of the brain, individual anatomical features, as well as atrophic and other pathological changes that lead to changes in the shape of the cerebral hemispheres. The values of the fractal dimension of skeletal images of the brain tend to decrease with age.

3. Coronal tomographic sections are the most representative for the characterization of age-related atrophic changes.

4. The obtained data can be used as normative criteria for the diagnosis of diseases of the nervous system using diagnostic methods of neuroimaging.

References

[1] Baykara, E., Gesierich, B., Adam, R., Tuladhar, A. M., Biesbroek, J. M., Koek, H. L., … & Duering, M. (2016). A Novel Imaging Marker for Small Vessel Disease Based on Skeletonization of White Matter Tracts and Diffusion Histograms. *Annals of neurology,* 80(4), 581-592. doi: 10.1002/ana.24758

[2] Di Ieva, A., Esteban, F. J., Grizzi, F., Klonowski, W., & Martin-Landrove, M. (2015). Fractals in the neurosciences, part II: clinical applications and future perspectives. *The Neuroscientist*, 21(1), 30-43. doi: 10.1177/1073858413513928

[3] Di Ieva, A., Grizzi, F., Jelinek, H., Pellionisz, A. J., & Losa, G. A. (2014). Fractals in the neurosciences, part I: general principles and basic neurosciences. *The Neuroscientist,* 20(4), 403-417. doi: 10.1177/1073858413513927

[4] Esteban, F. J., Sepulcre, J., de Mendizabal, N. V., Goñi, J., Navas, J., de Miras, J. R., … & Villoslada, P. (2007). Fractal dimension and white matter changes in multiple sclerosis. *NeuroImage,* 36(3), 543-549. doi: 10.1016/j.neuroimage.2007.03.057

[5] Esteban, F. J., Sepulcre, J., de Miras, J. R., Navas, J., de Mendizabal, N. V., Goñi, J., … & Villoslada, P. (2009). Fractal dimension analysis of grey matter in multiple sclerosis. *Journal of the neurological sciences,* 282(1-2), 67-71. doi: 10.1016/j.jns.2008.12.023

[6] Farahibozorg, S., Hashemi-Golpayegani, S. M., & Ashburner, J. (2015). Age- and sex-related variations in the brain white matter fractal dimension throughout adulthood: an MRI study. *Clinical neuroradiology,* 25(1), 19-32. doi: 10.1007/s00062-013-0273-3

[7] Frey, B. M., Petersen, M., Schlemm, E., Mayer, C., Hanning, U., Engelke, K., … & Cheng, B. (2021). White matter integrity and structural brain network topology in cerebral small vessel disease: The Hamburg city health study. *Human brain mapping,* 42(5), 1406-1415. doi: 10.1002/hbm.25301

[8] Greenblum, A., Sznitman, R., Fua, P., Arratia, P. E., Oren, M., Podbilewicz, B., & Sznitman, J. (2014). Dendritic tree extraction from noisy maximum intensity projection images in C. elegans. *Biomedical engineering online,* 13, 74. doi: 10.1186/1475-925X-13-74

[9] Ha, T. H., Yoon, U., Lee, K. J., Shin, Y. W., Lee, J. M., Kim, I. Y., … & Kwon, J. S. (2005). Fractal dimension of cerebral cortical surface in schizophrenia and obsessive-compulsive disorder. *Neuroscience letters,* 384(1-2), 172-176. doi: 10.1016/j.neulet.2005.04.078

[10] Jelinek, H. F., & Fernandez, E. (1998). Neurons and fractals: how reliable and useful are calculations of fractal dimensions?. *Journal of neuroscience methods,* 81(1-2), 9-

18. doi: 10.1016/s0165-0270(98)00021-1
[11] King, R. D., George, A. T., Jeon, T., Hynan, L. S., Youn, T. S., Kennedy, D. N., … & the Alzheimer's Disease Neuroimaging Initiative (2009). Characterization of Atrophic Changes in the Cerebral Cortex Using Fractal Dimensional Analysis. *Brain imaging and behavior,* 3(2), 154-166. doi: 10.1007/s11682-008-9057-9
[12] Lee, J. M., Yoon, U., Kim, J. J., Kim, I. Y., Lee, D. S., Kwon, J. S., & Kim, S. I. (2004). Analysis of the hemispheric asymmetry using fractal dimension of a skeletonized cerebral surface. *IEEE transactions on bio-medical engineering,* 51(8), 1494-1498. doi: 10.1109/TBME.2004.831543
[13] Liu, J. Z., Zhang, L. D., & Yue, G. H. (2003). Fractal dimension in human cerebellum measured by magnetic resonance imaging. *Biophysical journal,* 85(6), 4041-4046. doi: 10.1016/S0006-3495(03)74817-6
[14] Mandelbrot, B. B. (1983). *The fractal geometry of nature.* N.Y.: W. H. Freeman&Co.
[15] Maryenko, N., & Stepanenko, O. (2021). Characterization of white matter branching in human cerebella: quantitative morphological assessment and fractal analysis of skeletonized MR images. *Biomedical Research and Therapy,* 8(5), 4345-4357. doi: 10.15419/bmrat.v8i5.673
[16] Milosević, N. T., & Ristanović, D. (2006). Fractality of dendritic arborization of spinal cord neurons. *Neurosci Lett,* 396(3), 172-176. doi: 10.1016/j.neulet.2005.11.031
[17] Orlowski, D., & Bjarkam, C. R. (2012). A simple reproducible and time saving method of semi-automatic dendrite spine density estimation compared to manual spine counting. J *Neurosci Methods,* 208(2), 128-133. doi: 10.1016/j.jneumeth.2012.05.009
[18] Pantoni, L., Marzi, C., Poggesi, A., Giorgio, A., De Stefano, N., Mascalchi, M., … & Diciotti, S. (2019). Fractal dimension of cerebral white matter: A consistent feature for prediction of the cognitive performance in patients with small vessel disease and mild cognitive impairment. *NeuroImage Clinical,* 24, 101990. doi: 10.1016/j.nicl.2019.101990
[19] Podgórski, P., Bladowska, J., Sasiadek, M., & Zimny, A. (2021). Novel Volumetric and Surface-Based Magnetic Resonance Indices of the Aging Brain - Does Male and Female Brain Age in the Same Way?. *Frontiers in neurology,* 12, 645729. doi: 10.3389/fneur.2021.645729
[20] Rajagopalan, V., Das, A., Zhang, L., Hillary, F., Wylie, G. R., & Yue, G. H. (2019). Fractal dimension brain morphometry: a novel approach to quantify white matter in traumatic brain injury. *Brain imaging and behavior,* 13(4), 914-924. doi: 10.1007/s11682-018-9892-2
[21] Rajagopalan, V., Liu, Z., Allexandre, D., Zhang, L., Wang, X. F., Pioro, E. P., & Yue, G. H. (2013). Brain white matter shape changes in amyotrophic lateral sclerosis (ALS): a fractal dimension study. *PloS one,* 8(9), e73614. doi: 10.1371/journal.pone.0073614
[22] Roura, E., Maclair, G., Andorra, M., Juanals, F., Pulido-Valdeolivas, I., Saiz, A., … & Villoslada, P. (2021). Cortical fractal dimension predicts disability worsening in Multiple Sclerosis patients. *NeuroImage. Clinical,* 30, 102653. doi: 10.1016/j.nicl.2021.102653
[23] Schneider, C. A., Rasband, W. S., & Eliceiri, K. W. (2012). NIH Image to ImageJ: 25 years of image analysis. *Nature methods,* 9(7), 671-675. doi: 10.1038/nmeth.2089
[24] Zhang, L., Butler, A. J., Sun, C. K., Sahgal, V., Wittenberg, G. F., & Yue, G. H. (2008). Fractal dimension assessment of brain white matter structural complexity post stroke in relation to upper-extremity motor function. *Brain research,* 1228, 229-240. doi: 10.1016/j.brainres.2008.06.008
[25] Zhang, L., Dean, D., Liu, J. Z., Sahgal, V., Wang, X., & Yue, G. H. (2007). Quantifying degeneration of white matter in normal aging using fractal dimension. *Neurobiology of aging,* 28(10), 1543-1555. doi: 10.1016/j.neurobiolaging.2006.06.020
[26] Zhang, L., Liu, J. Z., Dean, D., Sahgal, V., & Yue, G. H. (2006). A three-dimensional fractal analysis method for quantifying white matter structure in human brain. *Journal of neuroscience methods,* 150(2), 242-253. doi: 10.1016/j.jneumeth.2005.06.021

ФРАКТАЛЬНА РОЗМІРНІСТЬ СКЕЛЕТОНОВАНИХ МАГНІТНО-РЕЗОНАНСНИХ ЗОБРАЖЕНЬ ЯК МІРА ПРОСТОРОВОЇ СКЛАДНОСТІ ВЕЛИКИХ ПІВКУЛЬ ГОЛОВНОГО МОЗКУ

Мар'єнко Н. І., Степаненко О. Ю.

Фрактальний аналіз в останні десятиліття дедалі ширше використовується у різних наукових сферах, у тому числі нейронауках. Цей спосіб математичного аналізу дозволяє кількісно визначати ступінь заповнення простору об'єктом та ступінь складності його просторової конфігурації. Мета дослідження - визначити значення фрактальної розмірності великих півкуль головного мозку за допомогою фрактального аналізу скелетонованих магнітно-резонансних зображень головного мозку. Для дослідження було використано магнітно-резонансні томограми головного мозку 100 умовно здорових осіб (які не мали структурних змін головного мозку) обох статей (жінок 56, чоловіків 44) віком 18-86 років (середній вік 41,72±1,58 років). У кожному мозку були досліджені 5 томографічних зрізів. 1-й корональний томографічний зріз був розташований на рівні найбільш передніх точок скроневих часток, 2-й - на рівні сосочкових тіл, 3-й - на рівні чотиригорбкової пластинки, 4-й - на рівні валка мозолистого тіла. Аксіальний томографічний зріз був розташований на рівні таламуса. Проводився фрактальний аналіз скелетонованих зображень за допомогою способу підрахунку квадратів. Отримані дані оброблялися за допомогою загальноприйнятих статистичних методів. Середні, мінімальне та максимальне значення фрактальної розмірності різних томографічних зрізів були наступними: 1-й корональний зріз - 1,207±0,003 (1,147÷1,277), 2-й корональний зріз - 1,162±0,003 (1,077÷1,243), 3-й корональний зріз - 1,156±0,003 (1,094÷1,224), 4-й корональний зріз - 1,158±0,003 (1,109÷1,218), аксіальний зріз - 1,138±0,002 (1,079÷1,194). Середнє значення фрактальної розмірності п'яти зрізів складало 1,164±0,002 (1,126÷1,209), середнє значення фрактальної розмірності чотирьох корональних зрізів складало 1,171±0,002 (1,122÷1,219). Фрактальний аналіз скелетонованих зображень великих півкуль головного мозку дозволяє кількісно характеризувати особливості топології та складності просторової конфігурації великих півкуль головного мозку. На значення фрактальної розмірності можуть впливати анатомічні особливості досліджуваних ділянок головного мозку, індивідуальні анатомічні особливості, а також атрофічні та інші патологічні зміни, що призводять до змін форми великих півкуль головного мозку. Значення фрактальної розмірності скелетонованих зображень головного мозку мають тенденцію до зниження з віком. Найбільш репрезентативними для характеризування вікових атрофічних змін є корональні томографічні зрізи. Фрактальний аналіз скелетонованих зображень великих півкуль головного мозку може бути використаний для діагностики захворювань нервової системи, а результати даного дослідження можуть бути використані у якості критеріїв норми.

Ключові слова: *фрактальний аналіз, фрактальна розмірність, головний мозок, великі півкулі головного мозку, морфометрія.*

DOI: 10.31393/morphology-journal-2022-28(2)-07 Reports of Morphology, Vol. 28, №2, Pages 48-56

ISSN 1818-1295 eISSN 2616-6194

REPORTS OF MORPHOLOGY

Official Journal of the Scientific Society of Anatomists, Histologists, Embryologists and Topographic Anatomists of Ukraine

journal homepage: https://morphology-journal.com

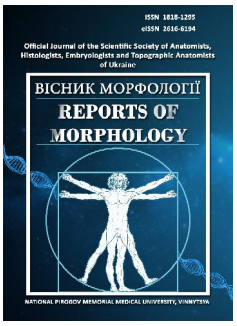

The role of myofibroblasts in the healing of chronic wounds

Slobodianyk S. V., Vernygorodskyi S. V., Khimich S. D., Shkolnikov V. S.
National Pirogov Memorial Medical University, Vinnytsya, Ukraine

ARTICLE INFO
Received: 15 February 2022
Accepted: 21 March 2022

UDC: 616-001.4-08:611.018.21

CORRESPONDING AUTHOR
e-mail: s3000000003@gmail.com
Slobodianyk S. V.

CONFLICT OF INTEREST
The authors have no conflicts of interest to declare.

FUNDING
Not applicable.

Surgical infection is one of the most important and important problems of modern medicine. The lack of a universal remedy and method of wound treatment, the difficulty of choosing universal tactics of management of patients with chronic wounds determines the need for further search for new treatments that stimulate reparative processes in chronic wounds, including morphological research methods. The role of cellular regulation in the pathogenesis of the restoration of the morphofunctional state of a chronic wound in the conditions of its damage remains undisclosed. Therefore, the aim of our study was to evaluate the role of myofibroblasts in the healing of chronic purulent-necrotic wounds in the treatment of mesenchymal stem cells using immunohistochemistry. In the experiment we obtained a model of chronic purulent-necrotic wound, which meets all the requirements for quality indicators in the study of morphological changes in chronic wounds and can then be used as a basis for preclinical research. The condition of chronic purulent-necrotic wounds in 120 rats was studied by histological and immunohistochemical methods. Chronic wound was modeled according to the original method of the author: during the formation of a standard skin defect in the interscapular area of the rat with a diameter of 1 cm, the surrounding tissue was superimposed ischemic metal structure to reduce blood flow in the wound area, which significantly slowed the delay. Treatment was started from 28 days from the beginning of wounding, which clinically and histologically corresponded to the chronicity of the wound process. Statistical processing of morphometric parameters was performed using the standard software package "Statistica 6.1". It was found that the positive dynamics of healing of chronic wounds, using 0.025 % decasan solution, was observed mainly in the early stages (3-7 days), while mesenchymal stem cells (MSC) and MSC cloned in inert gases (MSC-IG) were effective at all stages of the study. The use of MSC and MSC-IG creates favorable conditions for the normal course of regenerative processes and epithelialization of wounds, providing anti-edema and anti-inflammatory effects with activation of myofibroblasts, which increases the healing efficiency of chronic purulent-necrotic wounds. Prospects for the use of MSC in the treatment of chronic wounds are shown.

Keywords: *chronic wounds, treatment, mesenchymal stem cells, myofibroblasts, morphological changes, immunohistochemistry.*

Introduction

In recent years, there has been an increase in the number of patients with chronic purulent-necrotic wounds, due to the formation of antibiotic-resistant strains of microorganisms and the preservation of a significant number of wound complications [7, 15]. The treatment of chronic wounds is a significant burden on the health care system - both in the intensity of treatment and in its cost [6]. A significant amount of work has been devoted to the study of the mechanisms of regenerative processes in chronic wounds [1, 2, 3]. However, the role of cellular regulation in the pathogenesis of the restoration of the morphofunctional state of a chronic wound in terms of its damage remains undisclosed [2, 3]. Today, the therapeutic potential of different types of stem cells is being discussed, but in terms of therapy, the most effective cell population has not yet been determined. In recent years, experimental material has been accumulating that shows the ability of mesenchymal stem cells (MSC) to produce anti-inflammatory factors, growth factors that increase the proliferative activity of epitheliocytes and fibroblasts [7]. The role of myofibroblasts in the healing of chronic purulent-necrotic wounds has not been fully elucidated.

The aim of the study was to evaluate the role of myofibroblasts in the healing of chronic purulent-necrotic wounds in the treatment of mesenchymal stem cells using the immunohistochemical method.

Materials and methods

On the basis of the veterinary clinic (vivarium) National Pirogov Memorial Medical University, Vinnytsya performed an experimental study on 120 rats. All animals were divided into the following groups: I - control (without treatment); II - the use of classical wound healing (decasan); III - the use of clones of mesenchymal stem cells (from the umbilical cord); IV - the use of mesenchymal stem cell clones (cloned in inert gases). The study was performed in accordance with international conventions on the protection of animals used for experimental and other scientific purposes (Strasbourg, 1985), as well as in accordance with the provisions of the Bioethics Committee of the National Pirogov Memorial Medical University, Vinnytsya (Minutes № 6 of 20.06.2019).

To assess morphological changes in chronic wounds, fragments measuring 0.5 cm?1.0 cm?1.0 cm were excised from the wound edges, followed by fixation in 10 % neutral formalin solution. The samples were prepared according to standard methods. Histological sections 5-7 ?m thick were stained with hematoxylin and eosin, Mason's trichrome [5, 16]. Microscopy and photographing of histological specimens were performed using a light microscope OLIMPUS BX 41 at magnifications of 40, 100, 200 and 400 times. Microscopy assessed the condition and cell composition of chronic wounds, the presence and nature of reparative changes. Images were obtained and processed, morphometry and statistical processing were performed using the program "Quick PHOTO MICRO 2.3".

Immunohistochemical study was performed using paraffin blocks and DAKO reagents with monoclonal antibodies markers of intermediate filaments, mesenchymal cells and myofibroblasts - vimentin (Clone V9) and smooth muscle actin (αSMA, Clone 1A4), transmembrane protein of endothelial cells, stem and embryonic fibroblasts - CD34 (Clone QBEnd 10) with visualization system En VisionTMFLEX. The results of the study were evaluated taking into account the distribution of expression of vimentin, αSMA and CD34 in cells, the intensity of the reaction and the nature of the interaction with other structural elements. Evaluation of the immunohistochemical response was performed in 10 fields of view at 200 and 400-fold magnification. The intensity of expression was assessed by a semi-quantitative method based on the severity and integrity of the color of the cytoplasm according to the following scheme: low, moderate and strong, given the localization of pathological changes. Pieces of wounds obtained from experimental animals without corrective therapy were used as controls. To quantify vimentin, smooth muscle actin and endothelial cell marker CD34, a semi-quantitative method was used, according to which 4 categories were distinguished: 0 (-) - negative reaction (staining <5 % of cells), 1 (+) - weak staining (positively stained 10-30 % of cells), 2 (++) - moderate reaction (most positively stained cells - 31-60 %) and 3 (+++) - intense staining (>60 % of cells or almost all cells are positively stained). The expression coefficient (EX) was calculated for each observation according to the formula: KE=Σ(i x v)/100, where i is the intensity of staining in points (0 to 3), v is the percentage of stained cells (0 to 100% of the most expressed by the reaction in 10 fields of view at ?400) for each value [9].

Statistical processing of morphometric parameters was performed using the standard software package "Statistica 6.1" from StatSoft (SRC National Pirogov Memorial Medical University, Vinnytsya, licensed № BXXR901E246022FA) and Excel. Differences between samples were determined using Student's t-test, and the mean values for each trait and their standard deviations were determined. The level of $p<0.05$ was determined as probable in all tests.

Results

On the 28th day of the experiment we received chronic purulent-necrotic wounds in 97.0 % of experimental animals, which were characterized by classic signs of chronic progressive inflammation: the presence of a large area of fibrinoid necrosis with admixtures of polymorphonuclear leukocytes, macrophages, lymphocytes, lymphocytes and lymphocytes. At the same time both in the central departments (bottom of a wound), and in edges the multilayered flat keratinized epithelium was practically not defined due to considerable necrotic changes of epitheliocytes.

In the groups using decasan, MSC and MSC-IG on the third day of treatment (31 day of observation) around the wound edges and in the bottom recorded the appearance of a narrow layer of poorly differentiated cells (Fig. 1), the number of which differed significantly from the control group

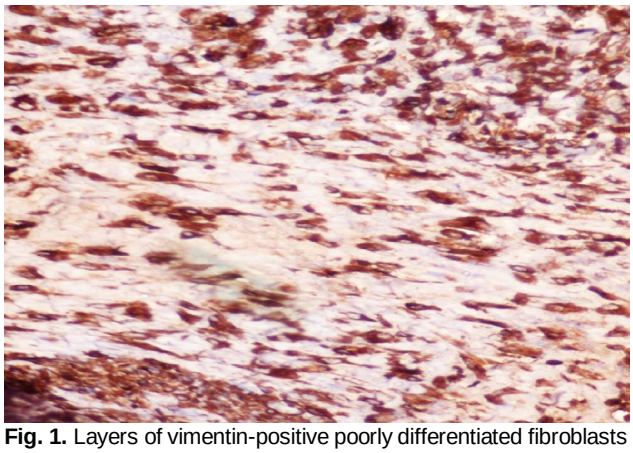

Fig. 1. Layers of vimentin-positive poorly differentiated fibroblasts at the bottom of a chronic wound. MSC-IG, 3 day of treatment (31 day of observation). Immunohistochemical (IHC) reaction with vimentin, x200.

Table 1. Intensity of αSMA, CD34 and vimentin expression in the treatment of chronic purulent-necrotic wounds (at the rate of 0.1 mm^2) on the 3 day of the experiment.

Cellular composition	Experimental groups			
	Control	Decasan	MSC	MSC-IG
aSMA	0.680±0.023	0.737±0.026^	0.852±0.036†	0.936±0.036*
CD34	0.090±0.010	0.110±0.012^	0.130±0.015†	0.140±0.007*
Vimentin	1.210±0.112	1.280±0.131^	1.640±0.126†	1.783±0.116*†

Notes: here and in the following tables, MSC - mesenchymal stem cells; MSC-IG - mesenchymal stem cells cloned in inert gases; * - p<0.001 compared to control; † - p<0.05 compared to Decasan; ^ - p>0.05 when comparing observation groups.

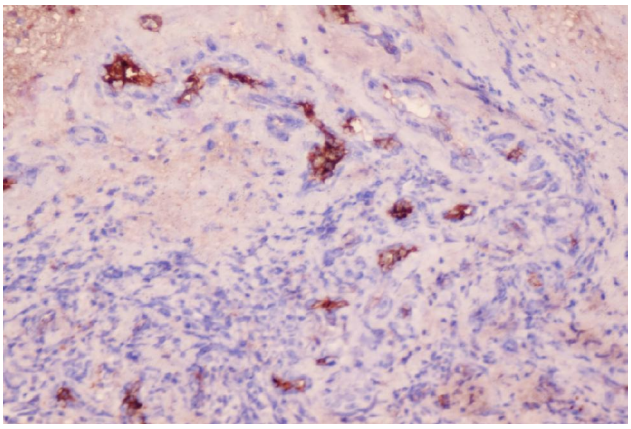

Fig. 2. Endothelial cells that form the walls of newly formed blood vessels. MSC-IG, 3 days after treatment (31 day of observation). IHC reaction with CD34, x200.

confirmed by immunohistochemical research (Table 1).

As can be seen from Table 1, in decasan, MSC, and MSC-IG groups significantly increased the number of αSMA-positive myofibroblasts, CD34-expressing endothelial cells, and mesenchymal cells (vimentin-positive fibroblasts), especially in the MSC-IG group (p<0.001).

The bottom of the wound at this observation period consisted in all experimental groups of three distinct layers: leukocyte-necrotic layer, a narrow surface layer containing vascular loops, and a deeper layer containing vertical vessels with surrounding cell clusters in the form of horizontally located and an amorphous intermediate. In longitudinal sections, the layer of horizontal fibroblasts was manifested by the concentration of cellular elements of the fibroblastic series: immature fibroblasts, myofibroblasts, fibroblasts that had an approximate course perpendicular to the wound edge. Cross sections of cell nuclei were oval and rod-shaped. Among the latter, slit-like lumens were identified, so they can be defined as endothelial cells that formed the walls of newly formed vessels in the immediate vicinity of the wound and gave a positive reaction on immunohistochemical labeling on CD34 (Fig. 2).

On day 7 of the experiment, morphological changes in chronic purulent-necrotic wounds of the control group corresponded to previously established, with a slight decrease in the thickness of the purulent-necrotic layer and a large number of randomly arranged fibroblasts, mast cells, macrophages, lymphocytes and plasma cells. A feature of this observation period in the groups with corrective treatment of MSC and MSC-IG was a significant decrease in mononuclear cells despite an increase in the number of cells of mesenchymal origin with active vasculogenesis, which was confirmed by immunohistochemical analysis (Fig. 3, Table 2), in which probable values were obtained (p<0.001) compared with the control and other groups, but the expression of αSMA and CD34 in animals treated with decasan and MSC was not significant (p>0.05) compared with the untreated group.

In the control group at this time of the experiment in micropreparations revealed severe edema, accumulation of lymphocytes, leukocytes, macrophages in the superficial departments and in immature granulation tissue. Histological examination revealed cellular detritus surrounded by a well-defined pyogenic membrane, abundantly infiltrated with leukocytes. At coloring on collagen fibers loosening of fibrous structures with their infiltration by neutrophilic leukocytes, a large number of lymphocytes, macrophages were defined. The fullness of the vessels was preserved with the expansion and thickening of their walls due to edema.

In the groups of decasan, MSC and MSC-IG on the 7th day of the experiment (35 day of observation) edema and vascular hyperemia, compared with the 3rd day, were significantly reduced. Coagulation necrosis in the center of the wound becomes homogeneous, eosinophilic, homogeneous, as a result of fluid loss and drying, cracks

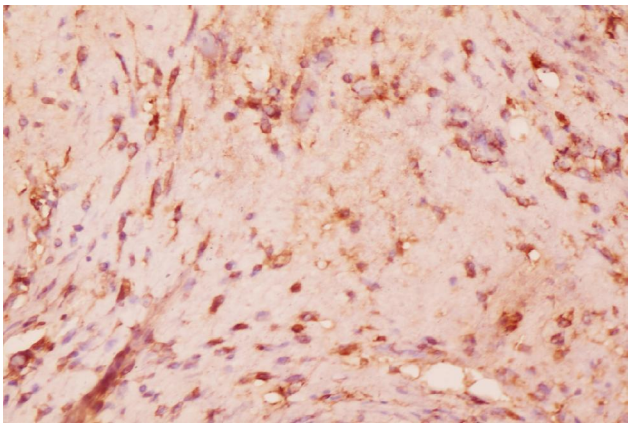

Fig. 3. Proliferation of myofibroblasts. MSC-IG, 7 days after treatment (35 day of observation). IHC reaction with smooth muscle actin (αSMA), x200.

Table 2. Intensity of αSMA, CD34 and vimentin expression in the treatment of chronic purulent-necrotic wounds (at the rate of 0.1 mm^2) on the 7 day of the experiment.

Cellular composition	Experimental groups			
	Control	Decasan	MSC	MSC-IG
a SMA	0.750±0.040	0.815±0.054^	0.794±0.027^	1.114±0.126*†
CD34	0.220±0.010	0.282±0.030^	0.290±0.040^	0.730±0.074*
Vimentin	1.500±0.143	1.610±0.120^	2.047±0.038*	2.346±0.074*

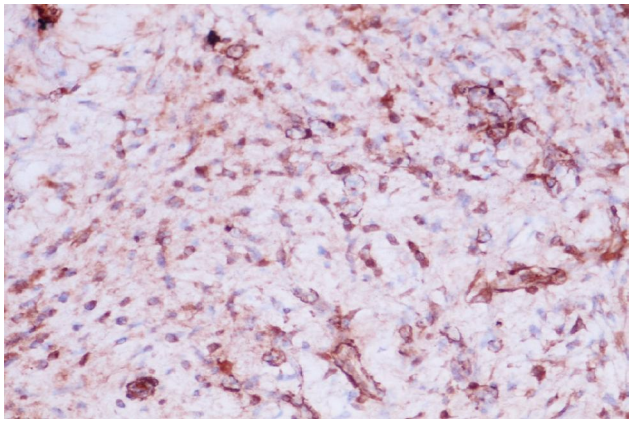

Fig. 4. Increased number of myofibroblasts around blood vessels. 14 days after treatment (MSC-IG, 42 day of observation). IHC reaction with smooth muscle actin (αSMA), x200.

appear in it, sometimes covered with endothelium. In a zone of a necrosis vessels with segmentally destroyed walls and agglutinin erythrocytes and thrombi with signs of the initial organization are found. On the periphery of the necrotized areas there are a large number of macrophages in the form of "granular balls", in the area of resorption of foci of hemorrhage - many siderophages and newly formed vessels of the microcirculatory tract. On the seventh day of the experiment (35 day of observation) according to our data in the control group with chronic progressive purulent-necrotic wounds in comparison with animals receiving decasan, MSC and MSC-IG there was no replacement of granulation tissue (vascular loops) with fibrous (horizontal fibrosis), in addition, we recorded a large number of plasma cells, which together, in our opinion, supports the chronicity of the inflammatory process.

On the 14th day of the experiment, histological analysis of the skin in the wound area showed that the first experimental group retained the same signs of exacerbation of chronic inflammation, such as infiltration of neutrophils and necrosis. The cell composition has undergone significant changes. In the groups MSC-IG and MSC on day 14 in 80 % and 70 % of experimental animals was almost complete cleansing of wounds from purulent-necrotic detritus and the formation of connective tissue scar with epithelialization, with similar changes in these terms were found in the control group only 10 % of rats and 60 % with decasan.

After treatment with decasan, MSC and MSC-IG observed attenuation of dystrophic changes in collagen fibers. However, in the MSC-IG group, a significant decrease in both dystrophic changes in smooth myocytes and an increase in the number of smooth muscle elements was observed at this observation period, which was confirmed by immunohistochemical data using SMA (Fig. 4).

In addition, at this time, the expression markers of myofibroblasts, endothelial and mesenchymal cells were significantly higher in the MSC and MSC-IG groups compared to the control ($p<0.001$), except for CD34 in the decasan group, whose enhancement of labeling was insignificant. The most effective immunohistochemical parameters were found in experimental animals treated with MSC-IG (Table 3).

Thus, for 2 weeks in the chronic wounds studied by us, further replacement of granulations with fibrous tissue continues, which is as follows: 1) by gradually replacing from the depth to the surface of the deep layers of granulations a strong layer of horizontal fibroblasts with the simultaneous development of collagen fibers, 2) by the development in the granulation tissue of thin vertical collagen strands (in the layer of vertical vessels), 3) by forming a superficial, weakly expressed horizontal layer of collagen fibers on the border with the leukocyte-necrotic layer. These processes are simultaneous, but the main role in the replacement of granulations and wound healing belongs to the first of them.

Thus, on the 14th day of the experiment in the group of MSC and MSC-IG animals, the process of vascular formation actively took place in the immediate vicinity of the

Table 3. Intensity of αSMA, CD34 and vimentin expression in the treatment of chronic purulent-necrotic wounds (at the rate of 0.1 mm^2) on the 14 day of the experiment.

Cellular composition	Experimental groups			
	Control	Decasan	MSC	MSC-IG
a SMA	0.760±0.020	0.842±0.052*	0.862±0.033*	0.983±0.098*
CD34	0.276±0.037	0.332±0.054^	0.380±0.054*	0.664±0.061*†
Vimentin	1.410±0.116	1.550±0.120*	1.872±0.026*	1.924±0.052*†

Table 4. Intensity of αSMA, CD34 and vimentin expression in the treatment of chronic purulent-necrotic wounds (at the rate of 0.1 mm^2) on the 30 day of the experiment.

Cellular composition	Experimental groups			
	Control	Decasan	MSC	MSC-IG
aSMA	0.614±0.050	0.768±0.023†	0.782±0.064†	0.910±0.031*
CD34	0.231±0.012	0.412±0.060†	0.370±0.050†	0.408±0.056†
Vimentin	1.364±0.105	1.515±0.110^	1.790±0.071†	1.850±0.092*†

wound bottom by forming microvessels with narrow lumen, maturation and differentiation of endothelial cells and fibroblastic cells.

On the 30 day of the experiment (58 day of observation) in the control group in 70 % of rats, the epithelium that grew on the edge of the chronic wound often necrotized and was permeated with leukocytes. However, epithelial growths in the granulation tissue, sometimes quite deep, persisted and, apparently, could be a source of new, re-growth of epithelium on the wound surface. In some wounds, the epithelium covers the granulation tissue and at the same time grows into it in the form of "tongues" in the shape of a wedge. Usually such pictures were observed at sharply expressed inflammatory process - in superficial layers of granulation fabric. Dystrophic changes and formation of an insignificant polymorphic capillary network were determined in the surrounding tissue.

Thus, on the 30th day of the experiment in 70 % of experimental animals in the control group there was no epithelialization of the wound, replacement of granulation tissue with fibrous, which indicated the progression of purulent inflammation and prolongation of the first phase of wound healing. In the days and edges of the chronic wound of rats of the control group was determined young connective tissue, which contained numerous cellular elements: macrophages, fibroblasts, lympho- and plasma cells, a small number of neutrophilic granulocytes. Some of the blood vessels found here were dilated. Stasis was often observed in the venules.

In contrast to the first group in experimental animals with the use of decasan, MSC and MSC-IG, the inflammatory cellular response was virtually absent, which was confirmed by quantitative analysis of cellular elements in the area of chronic wound. When comparing the activity of fibrillogenesis, it should be noted that in the group with MSC-IG fibroblastic reaction was stabilized for 30 days compared to previous dates. In the control group, delayed maturation of connective tissue was noted, as evidenced by the remnants of granulation tissue in the wound area. Compared with the control group with the use of decasan, MSC and MSC-IG granulation tissue at this time of observation was almost non-existent, which indicates an earlier period of recovery and stabilization of the wound process.

The results of immunohistochemical analysis (Table 4) confirmed the morphological data and showed a significant predominance of αSMA- and CD34-positive cells in the groups of decasan, MSC and MSC-IG ($p<0.05$ and $p<0.001$, respectively), despite insignificant increase in vimentin-positive cells in the decasan group ($p<0.05$), it should be noted that the animals injected with MSC-IG obtained the best results.

Therefore, in the dynamics in the groups with corrective treatment with decasan, MSC and MSC-IG with the progressive thickening of the deep layer of horizontal fibroblasts and the fibrous layer, the relationship between the layers of granulation tissue gradually changes. At the end of the 2nd month, in some wounds, the layer of horizontal fibroblasts and the actual fibrous layer is several times thicker than the layer of vertical vessels, which gradually thinned. These changes in the thickness of individual layers of granulation are more pronounced at the edges of the wound, where the layer of horizontal fibroblasts, gradually increasing, reaches in places the surface of the wound; here the growing epithelium lies not on the layer of loose granulation tissue, as observed in earlier terms, but on the layer of fibroblasts horizontally located to the epithelium, where the formation of the papillary layer of the skin is already visible.

Thus, at a later term of wound healing (from the 1st month and later) in the granulation tissue the following changes occur: the layer of vertical vessels gradually thins; the amount of amorphous intermediate in it decreases; at the same time the number of fibroblasts increases not only near the vessels, but also in between. Accelerating the development of the fibroblastic stage with the introduction of MSC and MSC+IG into the wound is important both for earlier restoration of the structure and function of damaged tissues and to prevent late wound complications, as failure to regenerate or fibrosis prolongs inflammation or causes its chronic course. In addition, the use of MSC and MSC+IG in the treatment of chronic wounds promotes accelerated epithelialization, according to our data, it has already begun on day 3 and was quite intense on day 7 (35 day of observation).

Discussion

Our research results are comparable with the literature on the stages of changes in the cells involved in the inflammatory process. According to modern ideas, the wound process is divided into 3 phases: inflammation, regeneration and reorganization of the scar with epithelialization [8, 12]. In the inflammatory phase, vascular reactions that characterize the mechanism of inflammation

predominate, and then the wound is cleaned of dead tissue. The second phase involves the formation of granulation tissue. Scar reorganization and epithelialization are the main components of the final stage of the wound process [13]. Regarding the formation of connective tissue in wound healing, we observe certain general patterns of its development, so first in response to damage there is an inflammatory reaction with cytokine synthesis and stimulation of fibroblasts to proliferate with secretion of collagen, glycosaminoglycans and extracellular fibrillogenesis. Then two important processes occur simultaneously: wound contraction and connective tissue remodeling with resorption of excess fibrils. The final stage can be characterized by three main processes: 1) complete involution of connective tissue; 2) stabilization of the scar; 3) chronicity of the process and progression of fibrosis. Undoubtedly, the leading role in all the above processes belongs to the fibroblast, as the main cellular element of connective tissue. Fibroblast produces proteoglycans, fibronectin, participates in the metabolism and structural stability of collagen, reticular and elastic fibers, their interaction with epithelial diferon. Immature (stem cells, poorly differentiated and young) fibroblasts and mature forms (myofibroblast, actively synthesizing fibroblast, fibroclast and fibrocyte) are usually distinguished. Mature fibroblasts maintain homeostasis between the extracellular matrix and cells, performing synthetic, resorbing and regulatory functions in connective tissue remodeling. Myofibroblasts are stellate cells with an active nucleus. The granular endoplasmic reticulum and the Golgi complex are developed in the cytoplasm. A unique feature is the degree of development and organization of the cytoskeleton, represented by bundles of parallel microfilaments. In their composition, along with cytoplasmic β-actin, there is also α-SMA, the amount of which is directly proportional to the local level of transforming growth factor beta (TGFβ) [4, 13]. In response to transforming growth factor β (TGFβ), Wnt ligands, biomechanical and profibrotic signals, fibroblasts can acquire a myofibroblast phenotype with marked expression of smooth muscle α-actin fibers (α-SMA). Myofibroblasts can also arise from bone marrow progenitor cells or through epithelial-mesenchymal junction (EMT) and endothelial-mesenchymal junction (endoMT) [13].

Prolonged inflammatory process, which we observed in the first group of observations, led to changes in the maturation of granulation tissue with inhibition of wound epithelialization, indicating a violation of epithelial-mesenchymal interactions. Also in our study, myofibroblasts were less common in the control group at a later date, which slowed wound contraction. However, in the decasan, MSC, and MSC-IG groups, there was a significant increase in αSMA-positive myofibroblasts, CD34-expressing endothelial cells, and mesenchymal cells (vimentin-positive fibroblasts), especially in the MSC-1 group ($p<0.001$). In the control group, the fibroblastic response was inhibited by prolongation and exacerbation of chronic inflammation with a significant decrease in the number of myofibroblasts in contrast to the groups using decasan, MSC and MSC-IG where the development of fibroblastic stage of the wound process was observed in most animals. The reduction of the purulent component established by us on the 3rd day of observation was more pronounced with the use of decasan. We found on the 7th day a significant increase in the number of fibroblasts after treatment of MSC-IG in the chronic wound indicates that the introduction of MSC-IG, provides a faster transition to the fibroblastic stage of wound inflammation. In the control group it was found that on the seventh day of the experiment the number of neutrophils was 2 times ($p<0.05$) higher than with decasan, MSC and MSC-IG, while the number of fibroblasts was significantly higher when using MSC-IG (208.0±3.9). At the same time, in the early observation period (3-7 days) the fibroblastic response was significantly ($p<0.05$) more active in the group with MSC and MSC-IG, which is consistent with the data of other authors [10, 11].

One of the essential signs of restoration of organ function is the formation of a vascular bed in the damaged area, so the rate of vascular formation in granulation tissue is one of the criteria for assessing the positive properties of the drug [17]. As is known [17, 18], vasculogenesis is associated with progenitor endothelial cells, which are precursors of endothelial cells, and which are well identified by the CD34 marker in the form of single cells, their small clusters and chains. In the groups with corrective therapy with decasan, MSC and MSC-IG, we were able to see the positive dynamics of vascular formation from progenitor endotheliocytes (vasculogenesis) from the proliferation of these cells to the formation of small spaces among them, which lengthen, forming a network of future vessels. Endothelial cells with membrane-cytoplasmic staining CD34 with the formation of capillary-type vessels were well visualized in the stromal component of the wound bottom, where they found chaotically located vessels of small caliber with a significant predominance of capillaries. We obtained reliable data on the predominance of CD34-positive cells in the group with MSC-IG (0.730±0.074, $p<0.001$) compared with the control group, which is consistent with the results of other researchers [4, 6, 18].

According to the literature [12], the growth of epithelium on the wound surface begins in the first stage of healing, but in our study it should be noted that it occurred very slowly in the control group. New collagen fibers appear in chronic wounds on day 7, their number increases rapidly, reaching a maximum of 7-14 days, and then the intensity of synthesis decreases to 30 days. Collagen, after its synthesis by fibroblasts, binds in the intercellular substance into bundles of fibrils and bundles of fibers, gradually filling the entire space between cells. The involution of the connective tissue begins and the wound process passes into the third phase - the phase of scarring and reorganization of the scar, which in the uncomplicated

course of the wound process usually takes 10-12 to 20 days. Fibroblasts in the conditions of physiological and pathological involution of connective tissue can function as fibroclasts, participating in the resorption of collagen fibers [8, 12]. The changing balance between collagen synthesis and its destruction underlies the mechanism of wound healing [12]. In the remodeling phase, collagen degradation increases and synthesis decreases, which was confirmed by our data with the use of MSC-IG and is consistent with other authors [7, 8, 12]. By synthesizing collagen, elastin, glycoproteins and proteoglycans, fibroblasts provide the support-mechanical function of the skin, producing signaling molecules that affect vascular permeability and metabolism, perform trophic function [4, 12, 14]. According to the results of our study on the 14th day of the experiment in the granulation tissue with the use of MSC and MSC-IG was less coarse connective tissue fibers, stained according to Mason in blue than in the group using only decasan. Microscopic examination of the wound canal of the dermis with the use of MSC showed faster dynamics of purification from the purulent process. The fibroblastic reaction with the use of decasan and MSC in the process of wound healing is quite pronounced, but with the use of decasan there was a tendency to form a coarser connective tissue scar. The tissue sections obtained for the study were usually well-developed granulation tissue with an increased number of microvessels compared to the first group and a decrease in the number of neutrophils, macrophages, lymphocytes, plasma cells and mast cells. The ability of MSC to stimulate fibroblast proliferation has been repeatedly confirmed experimentally [10, 12, 14]. Macrophage-fibroblastic interaction leads to migration and accelerated proliferation of fibroblasts, their differentiation, synthesis and secretion of collagen and other components of the matrix, active fibrillogenesis. In our study, we also observed stimulation of decasan, MSC and MSC-IG fibroblast activity and vascular formation in young connective tissue, which improved wound oxygenation and accelerated connective tissue maturation followed by remodeling and epithelialization of chronic purulent necrotic necrosis. In the control group there was a delay in the inflammatory response in the monocyte-macrophage stage, which not only increases the risk of purulent complications, but also prevents the completion of fibrosis and, consequently, the restoration of wound scar strength.

Morphometric studies showed that on the 30th day of the experiment (58 days of observation) the number of neutrophils, plasma cells, lymphocytes and macrophages in the control group numerically exceeds similar rates of inflammatory response in the groups of decasan, MSC and MSC-IG. A similar tissue reaction was also characteristic of degranulating mast cells involved in the release of inflammatory mediators, which indicated the progression of the chronic process in the wound. In the control group, the young connective tissue between the stratified fragments of capillaries contained mainly amorphous substance and cellular elements. The number of fibers was small, they had a different direction. While in the groups with corrective treatment, they were already oriented parallel to the wound surface. From the second month of the experiment, the number of collagen fibers around the fibroblasts forming vertical compact bundles in the intermediate substance increased. Thus, in the late stages of wound healing in the granulation tissue creates a fairly correct arrangement of fibrous structures, vertical and horizontal, intersecting in mutually perpendicular directions. However, special importance in wound healing (contraction), of course, belongs to the more developed deep layers of horizontal fibroblasts and fibrous fibers. It is these elements that replace the disappearing granulation tissue and in the late stages of healing perform and tighten to a greater or lesser extent the wound defect. The importance of horizontal structures and their role in wound healing is also recognized by other researchers [10, 12]. In the chronic wounds of the control group studied by us, despite the long time, after simulation of chronic purulent-necrotic wound (up to 2 months or more), complete closure and epithelialization was not observed, despite the growth of fibrous fibers.

Thus, pathomorphological studies indicate that the use of decasan, MSC and MSC-IG in the treatment of wounds leads to rapid suppression of purulent inflammation, edema and accelerates the processes of reparative regeneration. Granular tissue remodeling is faster with MSC and MSC-IG, and myofibroblasts, which in our study were positively labeled with αSMA, are a key link in wound healing, they not only maintain the homeostasis of the intercellular matrix of the dermis, providing its remodeling and renewal, but also play a significant role in maintaining the physiological state of other layers of the skin. Accelerating the development of fibroblastic stage with the introduction of MSC and MSC-IG into the wound is important for earlier restoration of the structure and function of damaged tissues and to prevent late wound complications, as failure to regenerate or fibrosis prolongs inflammation or causes its chronic course. In addition, the use of MSC and MSC-IG in the treatment of chronic wounds promotes accelerated epithelialization, according to our data it has already begun on day 3 and was quite intense on day 7 (35 days of observation), due to the synthesis of MSC of various growth factors that stimulate proliferation mesenchymal and epithelial differon of skin.

Further studies of the involvement of myofibroblasts in the restructuring of chronic wounds using the latest molecular biological markers in the use of MSC and MSC-IG will allow differentiated pharmacocorrection and increase the effectiveness of treatment of chronic wounds.

Conclusion

1. According to our data, in 97.0 % of experimental animals on the 28th day of the experiment morphological changes corresponded to chronic purulent-necrotic

inflammation with the presence of three main phases of the wound process: alteration, exudation and proliferation.

2. The results of the study proved the positive effect of 0.025 % decasan solution in the treatment of experimental wounds and the high efficiency of MSC and MSC-IG, which was confirmed by the dynamics of morphological changes in chronic wounds. The use of decasan showed positive dynamics of morphological parameters in the early stages (3-7 days), while MSC and MSC with IG were effective at all stages of the study.

3. Mesenchymal stem cells and MSC-IG accelerated the healing process of experimental chronic purulent-necrotic wounds after 3 days of treatment (31 day of observation). At this time there was a faster cleaning of the wound surface from purulent-necrotic tissues, accelerating the formation of granulation tissue. On the seventh day of treatment under the influence of MSC and MSC-IG revealed faster formation and maturation of granulation tissue, reducing wound area and accelerating epithelialization processes.

4. On the 14th day of treatment and the 30th day of treatment, complete epithelialization of wounds was detected in 60 and 70 % of experimental animals using decasan, 75 % and 80 % with MSC and 90 % and 95 % with MSC-IG, compared with the control group, where epithelization occurred in only 10 and 30 % of experimental animals, respectively ($p<0.001$).

5. The results of the study proved the positive effect of MSC in the treatment of experimental chronic purulent-necrotic wounds, their high efficiency in combination with inert gases was established, which was confirmed by a significant increase and stabilization of vimentin expression in fibroblasts, CD34 in endothelial cells and ?SMA in myofibroblasts (0.910±0.031, 0.408±0.056, 1.850±0.092, $p<0.001$).

References

[1] Akita, S. (2019). Wound repair and regeneration: mechanisms, signaling. *International Journal of Molecular Sciences,* 20(24), 6328. doi: 10.3390/ijms20246328

[2] Arif, S., Attiogbe, E., & Moulin, V. J. (2021). Granulation tissue myofibroblasts during normal and pathological skin healing: The interaction between their secretome and the microenvironment. *Wound Repair and Regeneration,* 29(4), 563-572. doi: 10.1111/wrr.12919

[3] Bergant Suhodolcan, A., Luzar, B., & Kecelj Leskovec, N. (2021). Matrix metalloproteinase (MMP)-1 and MMP-2, but not COX-2 serve as additional predictors for chronic venous ulcer healing. *Wound repair and regeneration,* 29(5), 725-731. doi: 10.1111/wrr.12915

[4] Brenmoehl, J., Miller, S. N., Hofmann, C., Vogl, D., Falk, W., Scholmerich, J., & Rogler, G. (2009). Transforming growth factor-β1 induces intestinal myofibroblast differentiation and modulates their migration. *World journal of gastroenterology: WJG,* 15(12), 1431-1442. doi: 10.3748/wjg.15.1431

[5] Gaytan, F., Morales, C., Reymundo, C., & Tena-Sempere, M. (2020). A novel RGB-trichrome staining method for routine histological analysis of musculoskeletal tissues. *Scientific Reports,* 10(1), 1-13. doi: 10.1038/s41598-020-74031-x

[6] Guan, H., Dong, W., Lu, Y., Jiang, M., Zhang, D., Aobuliaximu, Y., ... & Lu, S. (2021). Distribution and antibiotic resistance patterns of pathogenic bacteria in patients with chronic cutaneous wounds in China. *Frontiers in medicine,* 8, 274. doi: 10.3389/fmed.2021.609584

[7] Guillamat-Prats, R. (2021). The role of MSC in wound healing, scarring and regeneration. *Cells,* 10(7), 1729. doi: 10.3390/cells1007172

[8] Han, G., & Ceilley, R. (2017). Chronic wound healing: a review of current management and treatments. *Advances in therapy,* 34(3), 599-610. doi: 10.1007/s12325-017-0478-y

[9] Kinsel, L. B., Szabo, E., Greene, G. L., Konrath, J., Leight, G. S., & McCarty, K. S. (1989). Immunocytochemical analysis of estrogen receptors as a predictor of prognosis in breast cancer patients: comparison with quantitative biochemical methods. *Cancer research*, 49(4), 1052-1056. PMID: 2643460

[10] Ko, U. H., Choi, J., Choung, J., Moon, S., & Shin, J. H. (2019). Physicochemically tuned myofibroblasts for wound healing strategy. *Scientific reports,* 9(1), 1-12. doi: 10.1038/s41598-019-52523-9

[11] Leavitt, T., Hu, M. S., Marshall, C. D., Barnes, L. A., Longaker, M. T., & Lorenz, H. P. (2016). Stem cells and chronic wound healing: state of the art. *Chronic Wound Care Management and Research,* 3, 7-27. doi: 10.2147/CWCMR.S84369

[12] Mathew-Steiner, S. S., Roy, S., & Sen, C. K. (2021). Collagen in Wound Healing. *Bioengineering,* 8(5), 63. doi: 10.3390/bioengineering8050063

[13] Marangoni, R. G., Korman, B. D., Wei, J., Wood, T. A., Graham, L. V., Whitfield, M. L., ... & Varga, J. (2015). Myofibroblasts in murine cutaneous fibrosis originate from adiponectin-positive intradermal progenitors. *Arthritis & rheumatology*, 67(4), 1062-1073. doi: 10.1002/art.38990

[14] Nourian Dehkordi, A., Mirahmadi Babaheydari, F., Chehelgerdi, M., & Raeisi Dehkordi, S. (2019). Skin tissue engineering: wound healing based on stem-cell-based therapeutic strategies. *Stem cell research & therapy*, 10(1), 1-20. doi: 10.1186/s13287-019-1212-2

[15] Sen, C. K. (2021). Human wound and its burden: updated 2020 compendium of estimates. *Advances in wound care,* 10(5), 281-292. doi: 10.1089/wound.2021.0026

[16] Suvarna, S. K., Layton, C., & Bancroft, J. D. (2020). *Bancroft's theory and practice of histological techniques* (Eighth edition). Oxford: Elsevier. doi: 10.1016/C2015-0-00143-5

[17] Tottoli, E. M., Dorati, R., Genta, I., Chiesa, E., Pisani, S., & Conti, B. (2020). Skin wound healing process and new emerging technologies for skin wound care and regeneration. *Pharmaceutics,* 12(8), 735. doi: 10.3390/pharmaceutics12080735

[18] Zhang, Z., & Lv, L. (2016). Effect of local insulin injection on wound vascularization in patients with diabetic foot ulcer. *Experimental and therapeutic medicine,* 11(2), 397-402. doi: 10.3892/etm.2015.291

РОЛЬ МІОФІБРОБЛАСТІВ У ЗАГОЄННІ ХРОНІЧНИХ РАН

Слободяник С. В., Вернигородський С. В., Хіміч С. Д., Школьніков В. С.

Хірургічна інфекція є однією з актуальних і найважливіших проблем сучасної медицини. Відсутність універсального засобу і методу лікування ран, складність вибору універсальної тактики ведення хворих з хронічними ранами визначає необхідність

подальшого пошуку нових методів лікування, що стимулюють репаративні процеси в хронічних ранах, в тому числі із застосуванням морфологічних методів дослідження. Роль клітинної регуляції в патогенезі відновлення морфофункціонального стану хронічної рани в умовах її пошкодження залишається не розкритою. Тому, метою нашого дослідження стала оцінка ролі міофібробластів у загоєнні хронічних гнійно-некротичних ран при лікуванні мезенхімальними стовбуровими клітинами за допомогою імуногістохімічного методу. В експерименті нами отримана модель хронічної гнійно-некротичної рани, яка відповідає усім вимогам щодо якісних показників при вивченні морфологічних змін в хронічних ранах та в подальшому може використовуватися як базова на доклінічному етапі досліджень. За допомогою гістологічного та імуногістохімічного методів вивчили стан хронічних гнійно-некротичних ран у 120 щурів. Хронічну рану моделювали за оригінальною методикою автора: під час формування стандартного дефекту шкіри в міжлопатковій ділянці щура діаметром 1 см, на оточуючі тканини накладалась ішемізуюча металоконструкція з ціллю зменшення кровотоку в ділянці рани, що призводило до значного уповільнення термінів загоєння. Лікування починали від 28 доби з початку накладання ран, що клінічно та гістологічно відповідало хронізації ранового процесу. Статистична обробка морфометричних параметрів здійснювалася за допомогою стандартного програмного пакета "Statistica 6.1". Встановлено, що позитивна динаміка загоєння хронічних ран, при застосуванні 0,025 % розчину декасану, спостерігалась переважно на ранніх термінах (3-7 доба), в той час як мезенхімальні стовбурові клітини (МСК) та МСК клоновані в інертних газах (МСК-ІГ) були ефективним на всіх етапах дослідження. Використання МСК та МСК-ІГ створюють сприятливі умови для нормального перебігу регенераторних процесів і епітелізації ран, забезпечуючи протинабряковий та протизапальний ефекти з активацією міофібробластів, що підвищує ефективність загоєння хронічних гнійно-некротичних ран. Показано перспективи використання МСК при лікуванні хронічних ран.

Ключові слова: *хронічні рани, лікування, мезенхімальні стовбурові клітини, мофібробласти, морфологічні зміни, імуногістохімія.*

DOI: 10.31393/morphology-journal-2022-28(2)-08 Reports of Morphology, Vol. 28, №2, Pages 57-61

ISSN 1818-1295 eISSN 2616-6194

REPORTS OF MORPHOLOGY

Official Journal of the Scientific Society of Anatomists, Histologists, Embryologists and Topographic Anatomists of Ukraine

journal homepage: https://morphology-journal.com

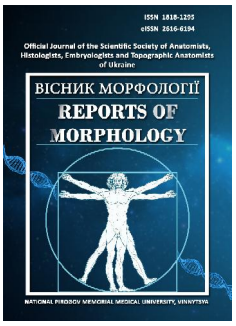

Pelvic circumference in young men and young women studying in higher education institutions of Bukovina, depending on the sport

Karatieieva S. Yu.[1], Slobodian O. M.[1], Muzyka N. Ya.[1], Hauriak O. D.[2], Chorna N. M.[1]

[1]HEI "Bukovinian State Medical University of the Ministry of Health of Ukraine", Chernivtsi, Ukraine
[2]Yuriy Fedkovych Chernivtsi National University, Chernivtsi, Ukraine

ARTICLE INFO
Received: 17 February 2022
Accepted: 23 March 2022

UDC: 611.96.06:572.087:796.07

CORRESPONDING AUTHOR
e-mail: Karatsveta@gmail.com
Karatieieva S. Yu.

CONFLICT OF INTEREST
The authors have no conflicts of interest to declare.

FUNDING
Not applicable.

In recent decades, anthropological research methods have been widely used by scientists to correctly predict the achievement of high sports results. The aim of the study is to find out the features of the pelvic circumference of young men (YM) and young women (YW), who study in higher education institutions in Bukovina, depending on the sport. Anthropometric parameters were studied for 115 first and second year students of higher education institutions in Chernivtsi, aged 16 to 21, including 78 (67.82 %) YM and 37 (32.18 %) YW, the main group - 75 (65.22 %), were students of I-II courses of the Faculty of Physical Culture and Human Health of Yuriy Fedkovych Chernivtsi National University, control group - 40 (34.78 %) - college students and students of the Faculty of Dentistry of Bukovina State Medical University. Among the students of the main group - 57 (76.00 %) YM and 18 (24.00 %) YW. Students of the main group, in addition to physical activity, which was included in the program of their specialty, additionally engaged in the following sports: football - 40 (53.34 %), of which YM - 36 (48.00 %), YW 4 (5.34 %), volleyball - 18 (24.00 %), of which YM - 9 (12.00 %), YW 9 (12.00 %), tennis - 10 (13.34 %), of which YM - 8 (10.67 %), YW 2 (2.67 %), basketball - 7 (9.32 %), of which YM - 4 (5.32 %), YW 3 (4.00 %), the control group consisted of 21 (52.50 %) YM and 19 (47.50 %) YW, which are loaded with hours of physical education, according to the curriculum of their specialty and additionally All students were determined to determine body weight and pelvic circumference according to the method of Bunak V. V. in the modification of Shaparenko P. P. Statistical analysis of the data was performed using a licensed program RStudio. Analyzing the average pelvic circumference of YM and YW, it is noteworthy that the average pelvic circumference among both study groups is much larger in YM compared to YW (representatives of the main group - respectively 83.40±3.01 cm and 78.31±3.01 cm; representatives of the control group - respectively 88.47±3.01 cm and 75.31±3.01 cm). In the main group, depending on the sport, volleyball players (YM - 86.11±3.02 cm; YW - 77.55±3.03 cm) and basketball players (YM - 85.50±3.03 cm; YW - 76.66±3.03 cm) have the largest pelvic circumference, followed by football players (YM - 81.52±3.02 cm, YW - 75.00±3.02 cm), and the smallest tennis players - 81.00±3.02 cm YM and 74.50±3.02 cm YW. Based on the regression analysis, it was found that weight is a significant factor for pelvic circumference.

Keywords: *athletes, anthropometry, pelvic circumference, sex differences.*

Introduction

In modern medicine, almost all branches are directly or indirectly related to anthropology. This characteristic has become especially important in connection with the development of various sports [1, 4, 6, 10, 11, 15, 16].

Highly productive athletes are extraordinary people who experience high physical and psychological stress during their professional life. However, to date, the prognostic value and dominance of total and partial body size in predicting the prospects for achieving high results in many sports have not been fully established [22].

Today, the theory of training athletes, based on the methodology of integrative approaches and opportunities of related disciplines, allows to provide such a systematization of knowledge, characterized by functional

completeness and absence of contradictions, allows to obtain knowledge accumulated in the theory of sports training, physiology, biochemistry, morphology, psychology, etc. [2].

The direction of management and control of training of athletes, their selection and orientation, modeling and forecasting unite the field of knowledge, which is intensively developed in the last two decades. This is due to the manifestation of the general trend and objectification of the training system of athletes, the introduction of scientific and technological progress, using the opportunities of general disciplines such as cybernetics, morphometry, systems approach, etc., finding reserves to improve the training system of athletes [5, 7-9, 13, 14, 17, 18, 21].

In this regard, the formation of a holistic system of knowledge requires consideration of management and control, selection and orientation, modeling and forecasting, as one of the key areas in the study of the theory of training athletes [19].

The purpose of the study is to find out the features of the pelvic circumference of young men and young women who study in higher education institutions in Bukovina, depending on the sport.

Materials and methods

We conducted a study of anthropometric parameters on 115 first and second year students of higher education institutions in Chernivtsi, aged 16 to 21, of which 78 (67.82 %) young men (YM) and 37 (32.18 %) young women (YW).

The Commission on Bioethics of the Bukovina State Medical University (Minutes № 6 of 18.03.2022) found that the studies were carried out in compliance with the basic provisions of the ICH GCP (1996), the Council of Europe Convention on Human Rights and Biomedicine (04.04.1997), the Helsinki Declaration Association for Ethical Principles of Conducting Scientific Medical Research with Human Participation (1964-2013) and Order of the Ministry of Health of Ukraine № 690 of 23.09.2009.

All subjects were divided into two groups: the main group - 75 (65.22 %), were students of I-II courses of the Faculty of Physical Culture and Human Health of Yuriy Fedkovych Chernivtsi National University, control group - 40 (34.78 %), were college students and students of the dental faculty of Bukovina State Medical University.

Among the students of the main group - 57 (76.00 %) YM and 18 (24.00 %) YW, who in addition to physical activity, which was included in the program of their specialty additionally engaged in the following sports: football - 40 (53.34 %), of which YM - 36 (48.00 %), YW 4 (5.34 %), volleyball - 18 (24.00 %), of which YM - 9 (12.00 %), YW 9 (12.00 %), tennis - 10 (13.34 %), of which YM - 8 (10.67 %), YW 2 (2.67 %), basketball - 7 (9.32 %), of which YM - 4 (5.32 %), YW 3 (4.00 %). The control group consisted of 21 (52.50 %) YM and 19 (47.50 %) YW, who are loaded with hours of physical education, according to the curriculum of their specialty and additionally did not play sports.

All students were determined body weight and pelvic circumference according to the method of Bunak V. V. in the modification of Shaparenko P. P. [20]. Determination of body weight was performed on floor scales (mechanical): for the most accurate results, weighing should be performed in the morning, on an empty stomach, after visiting the toilet. When weighing, students wore a minimum of clothing (underwear), stood on the scales so that the legs were symmetrical in relation to the center of the scales. The circumference of the pelvis (circumference) was measured with a centimeter tape in a supine position, bringing it under the buttocks, through the wings of the hip bones and the anterior surface of the pubic joint (increase).

The weight of the studied students of the main group is: female - 56.62±3.02 kg, male - 69.70±3.02 kg, where the greatest weight were students who played volleyball - 67.88±3.02 kg, of which 70.65±3.02 kg weight YM and 64.50±3.02 kg YW, football - 67.58±3.02 kg, of which 69.20±3.02 kg is the weight of YM and 63.56±3.02 kg of YW, basketball - 67.57±3.02 kg, of which 69.00±3.02 kg is the weight of YM and 63.10±3.02 kg of YW, tennis players weigh slightly less - 61.50±3.02 kg, of which 64.04±3.02 kg in YM and 58.51±3.02 kg in YW. The weight of students in the control group is: male - 77.04±3.02 kg, female - 56.10±3.02 kg.

In studying the distribution of pelvic circumference in the main group by sport, used the Kruskal-Wallis test (nonparametric ANOVA) to identify a significant difference in the average rates of respondents depending on the sport (as a central trend is considered the median distribution) [12]. To determine for which age groups there is a statistical difference between the medians - used the Conover-Iman test [3]. Statistical analysis of the data was performed using a licensed program RStudio.

Results

When comparing the pelvic circumference between males (83.40±3.01 cm) and females (78.31±3.01 cm) of the main group (Fig. 1), a statistically significant difference was found, as evidenced by the results of Welch's t-test: $t(39.72)=-3,221$, $p<0.05$.

When comparing the pelvic circumference between males (88.47±3.01 cm) and females (75.31±3.01 cm) of the control group (Fig. 2) also found a statistically significant difference, as evidenced by the results of the Welch t-test: $t(37.97)= -4.127$, $p<0.001$.

The values of the pelvic circumference, depending on the sport, are: YM volleyball players - 86.11±3.02 cm, and YW - 77.55±3.03 cm; basketball players YM - 85.50±3.03 cm, and YW - 76.66±3.03 cm; football players YM - 81.52±3.02 cm, and YW - 75.00±3.02 cm; tennis players YM - 81.00±3.02 cm, and YW - 74.50±3.02 cm.

The value of the pelvic circumference depending on the sport, regardless of sex, is presented in Figure 3. It seems that there is a significant difference in the average value of

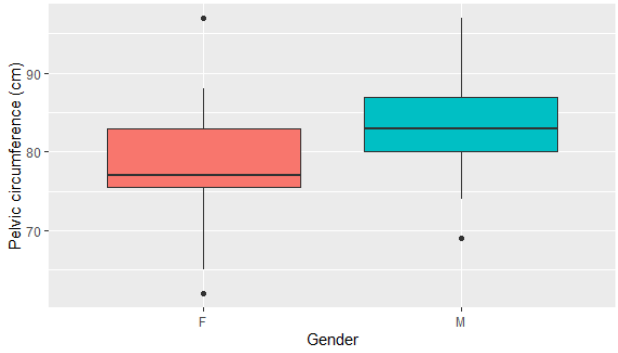

Fig. 1. Distribution of the pelvic circumference of the respondents of the main group by sex. F - female; M - male.

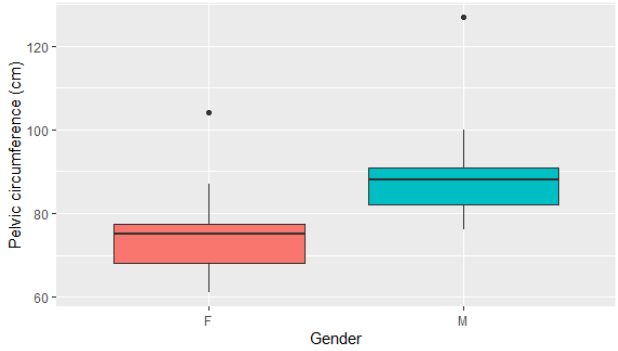

Fig. 2. Distribution of pelvic circumference of respondents in the control group by sex.

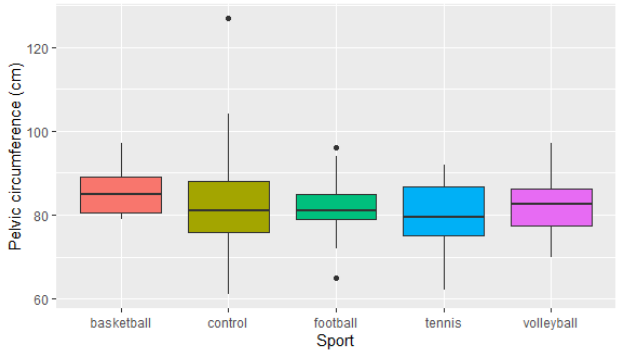

Fig. 3. Distribution of pelvic circumference of respondents by sport.

the pelvic circumference depending on the sport, including the control group. However, the results of the Kruskal-Wallis test are as follows - $\chi^2(6)=7.139$, $p=0.308$. Since $p<0.05$, the difference between the medians of the groups is not statistically significant.

Regression analysis shows that weight is a significant factor for pelvic circumference. The constructed model for predicting the circumference of the pelvis (coefficient of determination is 0.614, $p<0.001$) has the form of the following linear equation: $y = 44,76 + 0,562*x$, where y - pelvic circumference, x - weight.

Discussion

Much attention is paid to the study of the peculiarities of anthropometric and somatotypological indicators in athletes in modern sports medicine. Thus Olezhko V. G. [15] identified trends in changes in mass and age, proportions and circles of body parts and its composition in athletes of different sexes, depending on the groups of weight categories, as a result, obtained indicators of group models (III-x) morphofunctional state weightlifters, who testified that most of the indicators change with increasing weight category and have differences depending on the sex of athletes.

O. P. Khapitska and others [10] provide data on anthropometric and somatotypological indicators on the variability of hemodynamic parameters of the lower extremities of volleyball players.

I. Y. Gorskaya [6] studied the specifics of the morphological status of highly qualified pilots in bobsleigh, using anthropometry, a method of analyzing body composition (apparatus "Tanita"). Proved the feasibility of establishing the morphological status of high-skilled bobsleigh, conducted a comparative analysis (indicators of body length, body weight, girth, thickness of fat folds and the ratio of body components: fat, bone, muscle).

D. M. Kotko and others [11] studied changes in some anthropometric indicators in athletes - athletes in the stages of long-term training, including weight-growth index of Kettle, the relative amount of muscle tissue, the absolute amount of bone component of the body.

S. Cullen and others [4] studying the anthropometric profiles of elite athletes concluded that there are differences in anthropometric profiles between different athletes and different sports, which emphasizes the need to have available regulatory ranges for specific sports to ensure optimal monitoring of individual athletes. especially different between sports, as well as age, training status.

There are almost no works devoted to the study of the comprehensive parameters of the pelvis for sports.

We found that the average pelvic circumference among both study groups was significantly larger in YM compared to YW (representatives of the main group - respectively 83.40±3.01 cm and 78.31±3.01 cm; representatives of the control group - respectively 88.47±3.01 cm and 75.31±3.01 cm). In the main group, depending on the sport, volleyball players (YM - 86.11±3.02 cm; YW - 77.55±3.03 cm) and basketball players (YM - 85.50±3.03 cm; YW - 76.66±3.03 cm) have the largest pelvic circumference, followed by football players (YM - 81.52±3.02 cm, YW - 75.00±3.02 cm), and the smallest tennis players - 81.00±3.02 cm YM and 74.50±3.02 cm YW. Based on the regression analysis, it was found that weight is a significant factor for pelvic circumference.

Therefore, there is a need to further establish anthropometric parameters for specific sports, assessed by standardized methods, in accordance with the recommendations, to ensure optimal monitoring and

interpretation of anthropometric characteristics in athletes.

Further study of anthropometric parameters of students will allow to more correctly solve the problems of selection and sports orientation.

Conclusion

1. Comparison of the mean pelvic circumference of YM and YW shows that the average pelvic circumference among both study groups is much larger in YM compared to YW (representatives of the main group - respectively 83.40±3.01 cm and 78.31±3.01 cm; representatives of the control group - respectively 88.47±3.01 cm and 75.31± 3.01 cm).

2. By comparison, the largest pelvic circumference has volleyball players (YM - 86.11±3.02 cm; YW - 77.55± 3.03 cm) and basketball players (YM - 85.50±3.03 cm; YW - 76.66±3.03 cm), then football players (YM - 81.52± 3.02 cm; YW - 75.00±3.02 cm), and the smallest tennis players (YM - 81.00±3.02 cm; YW - 74.50±3.02 cm).

3. Based on the regression analysis, it was found that a significant factor for pelvic circumference is weight.

References

[1] Andriichuk, V. M. (2015). Порівняльна характеристика річних змін поздовжніх параметрів у курсантів, учнів та студентів на другому році навчання [Comparative characteristics of annual changes in longitudinal parameters in cadets, pupils and students in the second year of study]. *Клінічна анатомія та оперативна хірургія - Clinical anatomy and operative surgery,* 14(3), 37-39.

[2] Aragon, A. A., Schoenfeld, B. J., Wildman, R., Kleiner, S., VanDusseldorp, T., Taylor, L., ... & Antonio, J. (2017). International society of sports nutrition position stand: diets and body composition. *Journal of the International Society of Sports Nutrition,* 14(1), 1-19. doi: 10.1186/s12970-017-0174-y

[3] Conover, W. J., & Iman, R. L. (1979). *Multiple-comparisons procedures. Informal report* (No. LA-7677-MS). Los Alamos National Lab.(LANL), Los Alamos, NM (United States). doi: 10.2172/6057803

[4] Cullen, S., Fleming, J., Logue, D. M., O'Connor, J., Connor, B., Cleary, J., ... & Madigan, S. M. (2020). Anthropometric profiles of elite athletes. *Jurnal of Human Sport & Exercise*, 17(1), 145-155. doi: 10.14198/jhse.2022.171.14

[5] Gomez-Ezeiza, J., Tam, N., Torres-Unda, J., Granados, C., & Santos-Concejero, J. (2018). Anthropometric characteristics of top-class Olympic race walkers. *The Journal of Sports Medicine and Physical Fitness,* 59(3), 429-433. doi: 10.23736/S0022-4707.18.08363-9

[6] Horska, I. Yu. (2017). *Морфологический статус мужчин-бобслеистов высокой квалификации с учетом амплуа [Morphological status of highly qualified male bobsledders, taking into account the role].* Материалы VI международной научно-практической конференции "Проблемы развития физической культуры и спорта в новом тысячелетии", Екатеринбург (стр. 76-81). Екатеринбург - In Materials of the VI International Scientific and Practical Conference "Problems of Development of Physical Culture and Sports in the New Millennium", Yekaterinburg (pp. 76-81). Yekaterinburg.

[7] Karatieieva, S. Iu., Slobodian, O. M., Honchar, H. I., Penzai, S. A., & Karatieieva, A. Iu. (2020). Морфометричні дослідження в галузі спорту [Morphometric research in the field of sports]. *Клінічна анатомія та оперативна хірургія - Clinical anatomy and operative surgery*, 19(4), 65-71. doi: 10.24061/1727-0847.19.4.2020.54

[8] Karatieieva, S. Iu., Slobodian, O. M., Moseychuk, Yu. Yu., Hauriak, O. D., & Goy, R. S. (2021). Study of anthropometric and morphometric parameters in the training of atheletes. *Український журнал медицини, біології та спорту - Ukrainian Journal of Medicine, Biology and Sports,* 6(5(33), 16-22. doi: 10.26693/jmbs06.05.016

[9] Kendall, K. L., Fukuda, D. H., Hyde, P. N., Smith-Ryan, A. E., Moon, J. R., & Stout, J. R. (2017). Estimating fat-free mass in elite-level male rowers: a four-compartment model validation of laboratory and field methods. *Journal of sports sciences,* 35(7), 624-633. doi: 10.1080/02640414.2016.1183802

[10] Khapitska, O. P., Ivanytsia, A. O., Stefanenko, I. S., Sarafinyuk, L. A., & Moroz, V. M. (2017). Зміни реографічних показників гомілки у спортсменів різних видів спорту [Changes in rheographic parameters of the tibia in athletes of different sports]. *Фізіологічний журнал - Physiological Journal*, 63(1), 51-59.

[11] Kotko, D. M., Honcharuk, N. L., Shevtsov, S. M., Levon, M. M., Oksamytna, L. F., & Putro, L. M. (2021). Зміни деяких антропометричних показників у спортсменів-легкоатлетів на етапах багаторічної підготовки [Changes in some anthropometric indicators in athletes at the stages of long-term training]. *Науковий часопис НПУ імені Н.П. Драгоманова,* 3(133), 68-73. doi: 10.31392/NPU-nc.series 15.2021.3(133).15

[12] Kruskal, W. H., & Wallis, W. A. (1952). Use of ranks in one-criterion variance analysis. *Journal of the American statistical Association,* 47(260), 583-621. doi: 10.2307/2280779

[13] Logue, D., Madigan, S. M., Delahunt, E., Heinen, M., Mc Donnell, S. J., & Corish, C. A. (2018). Low energy availability in athletes: a review of prevalence, dietary patterns, physiological health, and sports performance. *Sports Medicine*, 48(1), 73-96. doi: 10.1007/s40279-017-0790-3

[14] Mountjoy, M., Sundgot-Borgen, J., Burke, L., Ackerman, K. E., Blauwet, C., Constantini, N., ... & Budgett, R. (2018). International Olympic Committee (IOC) consensus statement on relative energy deficiency in sport (RED-S): 2018 update. *International journal of sport nutrition and exercise metabolism,* 28(4), 316-331. doi: 10.1123/ijsnem.2018-0136

[15] Oleshko, V.H. (2003). *Морфофункціональні показники відбору важкоатлетів високої кваліфікації різних обтяжень-ових категорій та статі [Morphofunctional indicators of selection of highly qualified weightlifters of different weight categories and sex].* Педагогіка, психологія та медико-біологічні проблеми фізичного виховання і спорту: науковамонографія за редакцією проф. Єрмакова СС-Харків: ХДАДМ (ХХПІ) - Pedagogy, psychology and medical and biological problems of physical education and sports: scientific monograph edited by prof. Yermakova SS-Kharkiv: KhDADM (XXPI), (11), 45-53.

[16] Pastukhova, V. (2015). Дослідження антропометричних даних спортсменів-легкоатлетів на різних етапах підготовки [Research of anthropometric data of athletes at different stages of training]. *Теорія і методика фізичного виховання і спорту - Theory and methods of physical education and sports*, (1), 121-125.

[17] Perez, A. J. (2016). *Investigation: NFL improperly attempted to influence concussion research.* USA Today Sports, 2016. http://www.usatoday.com/story/sports/nfl/2016/05/23/nfl-concussion-research-investigation-nih /84787426/

[18] Sánchez Muñoz, C., Muros, J. J., Lopez Belmonte, Ó., & Zabala, M. (2020). Anthropometric characteristics, body composition and somatotype of elite male young runners. International journal of environmental research and public health, 17(2), 674. doi: 10.3390/ijerph17020674

[19] Sánchez-Muñoz, C., Muros, J. J., & Zabala, M. (2017). World and Olympic mountain bike champions' anthropometry, body composition and somatotype. *The Journal of Sports Medicine and Physical Fitness,* 58(6), 843-851. doi: 10.23736/S0022-4707.17.07179-1

[20] Shaparenko, P. F. (2000). *Антропометрія [Anthropometry].* Вінниця: Друкарня Вінницького державного медичного університету ім. М. І. Пирогова - Vinnytsia: Printing house of National Pirogov Memorial Medical University, Vinnytsya.

[21] Suydam, S. M., Cortes, D. H., Axe, M. J., Snyder-Mackler, L., & Buchanan, T. S. (2017). Semitendinosus tendon for ACL reconstruction: regrowth and mechanical property recovery. *Orthopaedic journal of sports medicine,* 5(6), 2-11. doi: 10.1177/2325967117712944

[22] Thomas, D. T., Erdman, K. A., & Burke, L. M. (2016). American College of Sports Medicine Joint Position Statement. Nutrition and Athletic Performance. *Medicine and science in sports and exercise,* 48(3), 543-568. doi: 10.1249/MSS.0000000000000852

ОСОБЛИВОСТІ ОКРУЖНОСТІ ТАЗА В ЮНАКІВ І ДІВЧАТ, ЯКІ НАВЧАЮТЬСЯ В ЗАКЛАДАХ ВИЩОЇ ОСВІТИ БУКОВИНИ, ЗАЛЕЖНО ВІД ВИДУ СПОРТУ

Каратєєва С. Ю., Слободян О. М., Музика Н. Я., Гауряк О. Д., Чорна Н. М.

Для коректного прогнозування досягнення високих спортивних результатів в останні десятиріччя науковцями широко використовуються антропологічні методи дослідження. Мета дослідження - з'ясувати особливості окружності таза юнаків і дівчат, які навчаються в закладах вищої освіти Буковини, залежно від виду спорту. Проведено дослідження антропометричних параметрів у 115 студентів першого та другого курсів закладів вищої освіти м. Чернівці, віком від 16 до 21 року, з них 78 (67,82 %) юнаки та 37 (32,18 %) дівчата. Основну групу - 75 (65,22 %), становили студенти I-II курсів факультету фізичної культури та здоров'я людини Чернівецького національного університету імені Юрія Федьковича, контрольну групу - 40 (34,78 %) - студенти коледжу та студенти стоматологічного факультету Буковинського державного медичного університету. Серед студентів основної групи - 57 (76,00 %) юнаків та 18 (24,00 %) дівчат. Студенти основної групи, окрім фізичного навантаження, яке входило в програму їхньої спеціальності додатково займались такими видами спорту: футбол - 40 (53,34 %), з них юнаків - 36 (48,00 %), дівчат 4 (5,34 %), волейбол - 18 (24,00 %), з них юнаків - 9 (12,00 %), дівчат 9 (12,00 %), теніс - 10 (13,34 %), з них юнаків - 8 (10,67 %), дівчат 2 (2,67 %), баскетбол - 7 (9,32 %), з них юнаків - 4 (5,32 %), дівчат 3 (4,00 %), Контрольну групу становили 21 (52,50 %) юнак і 19 (47,50 %) дівчат, які навантажені годинами фізкультури, відповідно до навчальної програми їхньої спеціальності та додатково спортом не займались Усім студентам було проведено визначення маси тіла та окружності таза за методикою Бунака В. В. у модифікації Шапаренка П. П. Статистичний аналіз отриманих даних проводили за допомогою ліцензованої програми RStudio. Аналізуючи середню величину окружності таза юнаків і дівчат звертає увагу те, що в середньому окружність таза серед обох досліджуваних груп значно більша у юнаків порівняно з дівчатами (представники основної групи - відповідно 83,40±3,01 см і 78,31±3,01 см; представники контрольної групи - відповідно 88,47±3,01 см і 75,31±3,01 см). В основній групі залежно від виду спорту найбільшу окружність таза мають волейболісти (юнаки - 86,11±3,02 см; дівчата - 77,55±3,03 см) та баскетболісти (юнаки - 85,50±3,03 см; дівчата - 76,66±3,03 см), далі футболісти (юнаки - 81,52±3,02 см; дівчата - 75,00±3,02 см), а найменшу тенісисти - 81,00±3,02 см юнаки та 74,50±3,02 см дівчата. На основі проведеного регресійного аналізу встановлено, що значимим фактором для окружності таза є вага.

Ключові слова: *спортсмени, антропометрія, окружність таза, статеві розбіжності.*

DOI: 10.31393/morphology-journal-2022-28(2)-09 Reports of Morphology, Vol. 28, №2, Pages 62-68

ISSN 1818-1295 eISSN 2616-6194

REPORTS OF MORPHOLOGY

Official Journal of the Scientific Society of Anatomists, Histologists, Embryologists and Topographic Anatomists of Ukraine

journal homepage: https://morphology-journal.com

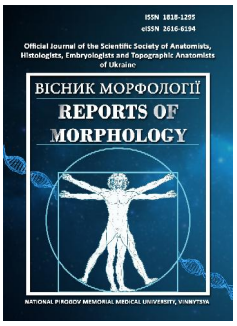

Variant anatomy of the mandibular canal topography

Oshurko A. P., Oliinyk I. Yu., Kuzniak N. B.

HEI "Bukovinian State Medical University of the Ministry of Health of Ukraine", Chernivtsi, Ukraine

ARTICLE INFO

Received: 21 February 2022

Accepted: 25 March 2022

UDC: 611.716.4.068

CORRESPONDING AUTHOR

e-mail: olijnyk1961@gmail.com

Oliinyk I. Yu.

CONFLICT OF INTEREST

The authors have no conflicts of interest to declare.

FUNDING

Not applicable.

This paper presents an analysis of 3D reconstruction models of the manifestation of variability of the mandible canal (canals) on both the left and right sides, their laying in the body of the mandible and the location, size and direction of the output canals. After all, the availability of minimally invasive techniques implemented in the research process helps to identify even minor anatomical variants or branches of the mandibular canal, which are quite common and do not allow the clinician to neglect them and require proper scientific evaluation. When planning reconstructive surgery on the mandible, the lack of high predictability to prevent functional complications, which are often irreversible (because the mandibular canal contains motor and sensory nerve fibers), forces us to reconsider the morphological fundamentality of its topography. Therefore, the aim of the work was to review computed tomography digital images, their analysis and identify possible anatomical variants of the canal (channels) of the mandible, as a basis for establishing its topographic features, on the left and right sides. After analyzing 426 digital CT scans of the mandible in males and females aged 25 to 75 years, 68 3D reconstruction models were reproduced using standardized X-ray diagnostic CT software Ez3D-I Original ver.5.1.9.0, used for visualizations of multimodal and multidimensional images, some of which are presented as the results of their own research. It is established that the entrance openings of the mandibular canals on both the left and right sides continue with one canal, however, in the projection of the second molar, the latter can be divided into two or three canals with high frequency. There is a difference in the diameters (Ø) of the canals and their opening - typical (in the projection of premolars on the right side) and atypical openings - in the projection of 3.6, 4.6 molars and central incisors, canines in the direction of the outlet and their location. There is no proper regular systematization of the number, topographic trajectory and size of the mandibular canals, their association or separation, as well as the direction of their exit, which requires additional vigilance not only during research but also in clinical dentistry or reconstructive surgery.

Keywords: *mandibular canal, computed tomography, morphometry, bone atrophy, human.*

Introduction

The question of the variability of complex anatomical structures in the modern scientific interpretation of the morphological norm or its deviation remains debatable [24, 26]. Scientific progress and the availability of minimally invasive techniques implemented in research processes help to identify even minor anatomical variations [6, 18], including the mandibular canal, which until now were considered abnormal manifestations or individual characteristics of the organism. At the same time, such interpretations do not reveal the main content, require understanding of the frequency and distribution of anatomical manifestations depending on sex, their synchronicity between left and right, as well as possible changes - from normal or pathological processes in the body [19, 27].

As scientific and practical experience shows, the anatomical variability of the branches of the mandibular canal is quite common, which does not allow to neglect it and requires proper scientific evaluation [5, 10].

Lack of theoretical experience leads to significant unpredictable functional complications (because the mandibular canal contains motor and sensory nerve fibers), which are often irreversible [14, 15]. An even more difficult problem is to find a solution to eliminate such complications and select methods of rehabilitation of patients that would not compromise their depth, even to

the complete loss of function [4, 29].

In response to these questions, priority is given to primary diagnosis using paraclinical radiological methods. Of course, magnetic resonance imaging remains in the first place in terms of the highest reliability, but the method of choice is the minimally invasive method of computed tomography (CT) [25, 30]. This approach reveals the understanding of the laying and length of the channel in the body of the mandible, morphology and configuration of branches as additional - bifid or trifid channels [17, 21]. Identification of the main trunk from the additional ones, with 3D reconstruction, becomes a basic informative support both for their topography [9] and areas of innervation, which extend to the bone of the mandible, teeth, surrounding soft tissues and their blood supply.

No less important tasks that have been left out of research are the effectiveness of traditional methods of local anesthesia, which directly depend on the variant and topographic anatomy of the mandibular canals, namely, their entry, laying and exit - guidelines for creating minimal and effective depot of anesthetics.

Therefore, supplementing existing progressive research with new, in particular, visualized 3D reconstruction models of variant anatomy of the mandibular canals, which formed the basis of this work, will update the views of modern researchers, teachers of morphological disciplines, give confidence to clinicians when planning and conducting reconstructive surgery.

The purpose of the work is to review, identify and analyze certain possible anatomical variants of the mandibular canal, as a fundamental basis in establishing its topographic features, on the left and right sides.

Materials and methods

This study analyzed 426 computed tomographic digital images of the mandible of patients who underwent routine diagnostic examinations and selected only 68 scans, without any changes that would distort the architecture of bone tissue, but had the best opportunities for analysis and provided proper informativeness in the study of possible morphotopographic features of its channel, on the left and right sides of males and females aged 25 to 75 years.

Computed tomography digital scans were performed using HEWLETT-SNCPUM1 computer equipment with 16.0 GB of RAM, 10 Pro for Workstations system software, 2019: 00391-70000-00000-AA425.

3D reconstruction models were reproduced using standardized X-ray diagnostic software Ez3D-I Original ver.5.1.9.0, which is used to visualize multimodal and multidimensional images, some of which are presented as the results of our own research.

Informed and signed by patients Informed consent to their participation in studies in compliance with the basic provisions of the GSR (1996), the Council of Europe Convention on Human Rights and Biomedicine (04.04.1997), the Helsinki Declaration of the World Medical Association on Ethical Principles for Human Scientific Research (1964-2013), orders of the Ministry of Health of Ukraine № 690 from 23.09.2009, № 616 from 03.08.2012 and approved by the decision of the Commission on Biomedical Ethics of Bukovinian State Medical University (Minutes № 2 from 21.10.2021).

Results

Traditionally, the mandibular canal is perceived as a monotubular morphological structure that originates with an inlet on the medial surface of the mandibular ramus and ends on its outer surface in the projection of the first or second premolars with a foramen, followed by intraosseous branching, to provide intraosseous branching to provide innervation and nutrition of the front group of teeth.

Morphological analysis of the materials of this work indicates the identified anatomical variability of the mandibular canal, which differs from the guidelines described in anatomical textbooks and are taken into account when teaching basic disciplines.

The presented 3D reconstruction models (Fig. 1) reveal the content of variant anatomy and provide answers to questions that have been little studied so far and remain far from complete.

Digital image analysis emphasizes the variability and asynchrony of the mandibular canal in a patient with variable

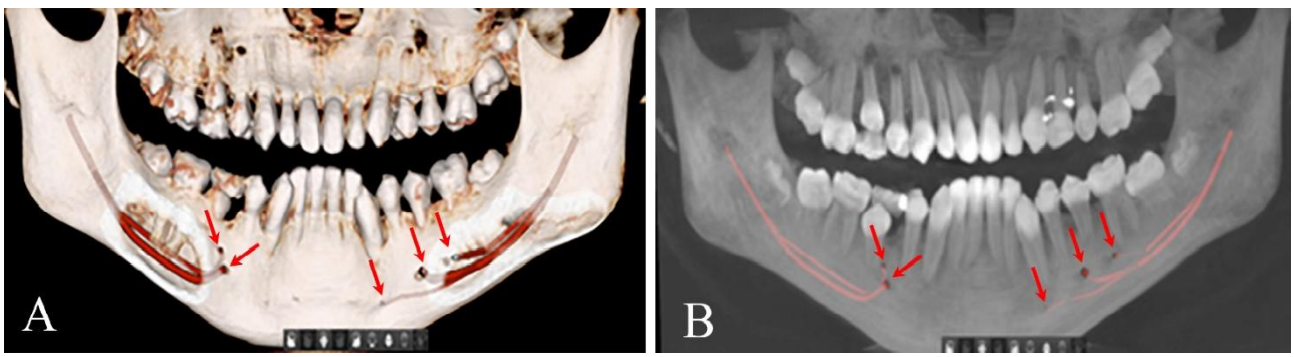

Fig. 1. A) 3D reconstruction model of bifid on the right side and trifide on the left side of the mandibular canal structure, bone image; B) 3D reconstruction model of bifide on the right side and trifide on the left side of the mandibular canal structure, X-ray image.

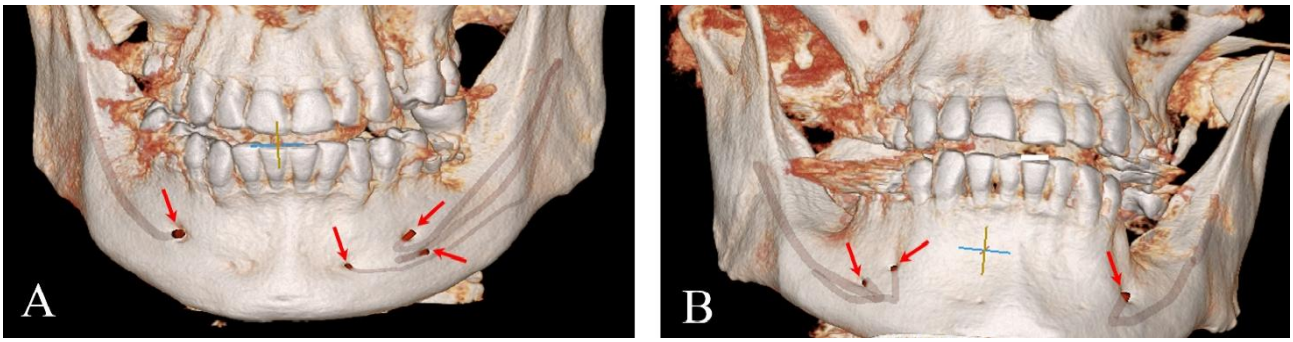

Fig. 2. A) 3D reconstruction model, typical topography on the right side and trifid - on the left side, the structure of the mandibular canals; B) 3D reconstruction model, bifid on the right side and typical on the left side, the structure of the mandibular canals.

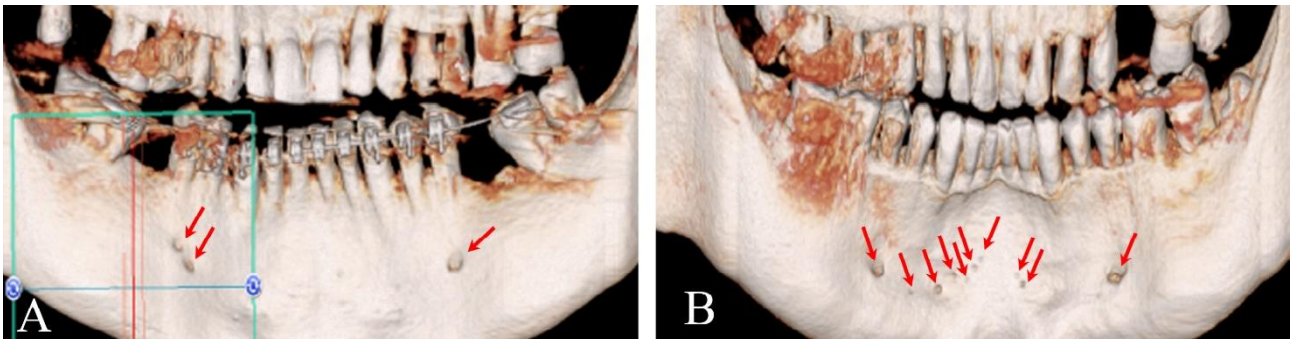

Fig. 3. 3D reconstruction model of variants of the canal foramens (s) of the mandible: A) double foramens on the right side and a single foramen on the left side; B) additional foramens of the mandibular canals in the projection of the central group of teeth.

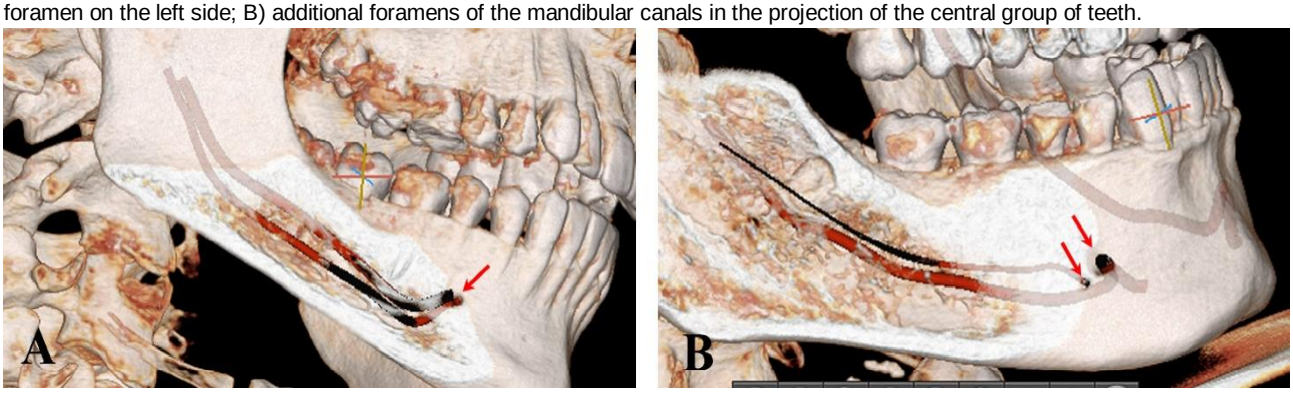

Fig. 4. 3D reconstruction model of modifications of the mandibular canals, their laying and projection of the foramens: A) opening the canals with one foramen; B) opening the channels with two foramens of different diameters and different directions.

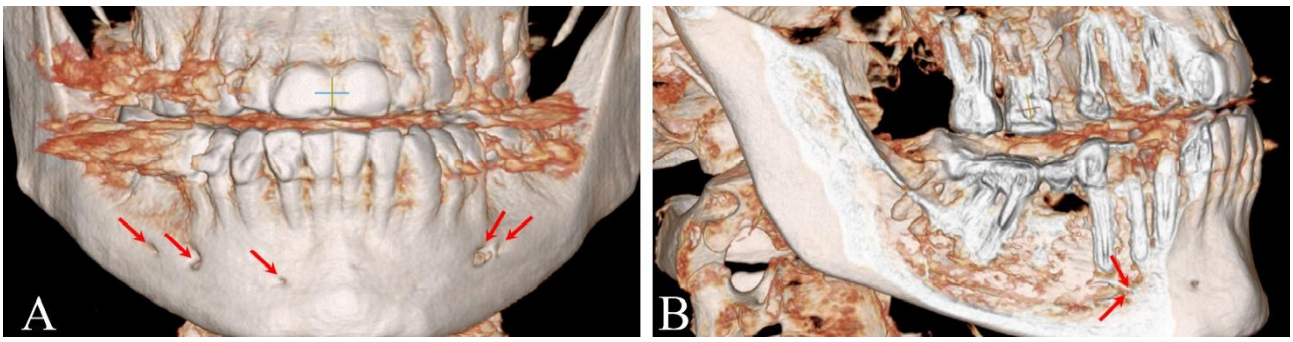

Fig. 5. 3D reconstruction model of variants of projections of foramen openings: A) opening of channels by exit foramens in projection of 4.1, 4.5, 4.6 teeth; B) the association of bifid canals in the body of the mandible with the next one foramen.

occlusion. The entrance openings of the mandibular canals on both the left and right sides continue with one canal, however, in the projection of the second molars they divide on the right side into two, enveloping the roots of the first molar, and on the left side into three canals (see Fig. 1). Also, there is a difference in the diameters (?) of the canals

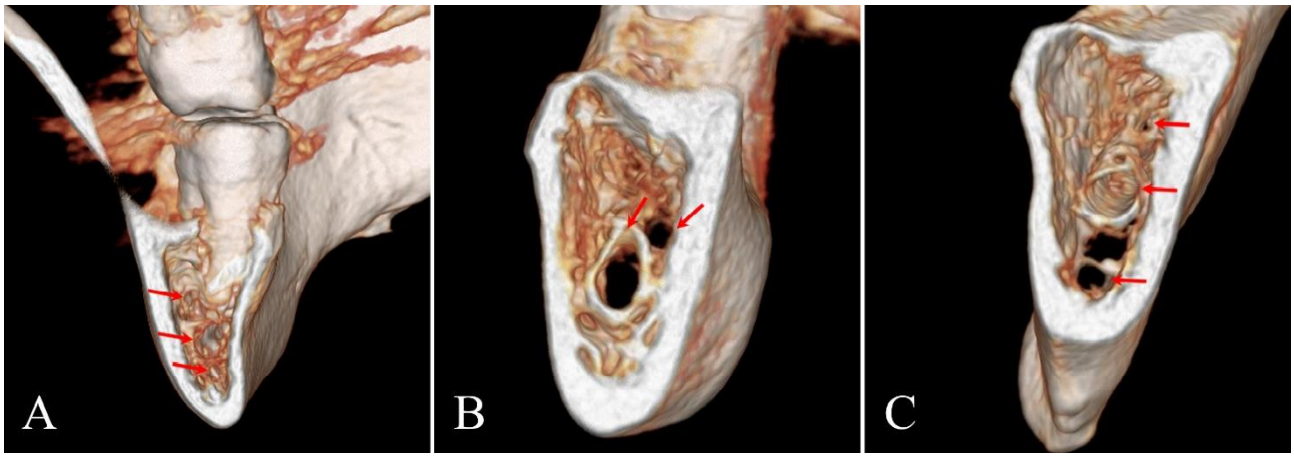

Fig. 6. 3D reconstruction model of the mandibular canals on coronal sections: A) trifid canal of the mandible, a person with a preserved dentition; B) bifid canal of the mandible, persons with loss of masticatory teeth from 6 months to 5 years; C) trifid canal of the mandible, persons with loss of masticatory teeth for more than 5 years.

and their foramens - typical, in the projection of premolars on the right side and atypical foramens, both in the direction of the outlet and their location on the left side.

Presented by computed tomography 3D reconstruction model (Fig. 2) of a patient with permanent occlusion and defects of the dentition confirms the asynchrony of the mandibular canals between the left and right sides, however, on the right side the length of the monochannel originates ends with the approach to the first premolar, and on the left side - one initial inlet and three different diameter channels (see Fig. 2A) and opens with two foramens obliquely in the direction from front to up and back. The third, bending in an arc to the bottom, leaves the body of the lower jaw with the approach to the mental tubercle (tuberculum mentale).

Opposite topographic characteristics of the channel are reflected by a 3D reconstruction model created by computed tomography (see Fig. 2B), originating left and right with single inlets and a typical outlet on the left side of the mandible and two different foramens on the right side, getting bifurcation only in the projection of the first molar.

It is impossible to determine a certain regularity of topographic features of the mandibular canal during survey digital CT scans due to their pronounced variability both in laying and in the location and diameters of the outlets (Fig. 3).

In most cases, the traditional morphological literature describes the projection of the exit opening of the mandibular canal only with a focus on premolars and possible branching of the canal in the body of the mandible, without leaving it. However, we have identified variants with numerous additional foramens (see Fig. 3B), which have a certain organizational morphological structure of small tubules, to provide innervation and nutrition of both hard and adjacent soft tissues.

There is no proper systematization of the specific topographic trajectory and size of the mandibular canals, their union or separation, and the direction of their exit, which requires additional vigilance not only during research but also in clinical dentistry (Fig. 4).

This confirmation is a 3D reconstruction model created by computed tomography (Fig. 5) of a patient with a restored defect of the dentition on the lower jaw on the right side. The location of one of the outlets of the canals (see Fig. 5A) is projected closer to the root of the second incisor, the others - between the first and second premolars and the third foramen in the projection of the medial root of the first molar.

It is important to note that a significant number of canals are combined in the body of the mandible into one, continuing and leaving it with one outlet (see Fig. 5B).

We also emphasize that the structure of the mandibular canals, in particular the surrounding tubular cortical layer, depends on the type of bone density and their "morphological form" - the time of tooth loss as an irreversible pathological factor leading to bone tissues atrophy (Fig. 6).

Discussion

Many scientific works are aimed at studying the morphological variations of the mandibular canal [2, 3, 31], which are substantiated in the studies and have proper evidence and confirmed by modern, even simple, radiological methods [8, 15]. However, attempts to differentiate the presence of specific anatomical structures (such as arteries, veins, nerves) in the existing mandibular canals by radiological methods are problematic, and the results are questionable, although there are clinical concerns about the invasiveness of surgery [16, 22].

It is known that the ramus of the mandible, which extends from its body at an obtuse angle upwards, on the inner surface contains a pterygoid tuberosity (tuberositas pterygoidea), just above which you can see the upward mandibular foramen (foramen mandibulae). From the inner surface it is limited by the lingula of the mandible (lingula mandibulae). This hole leads to the canal of the mandible,

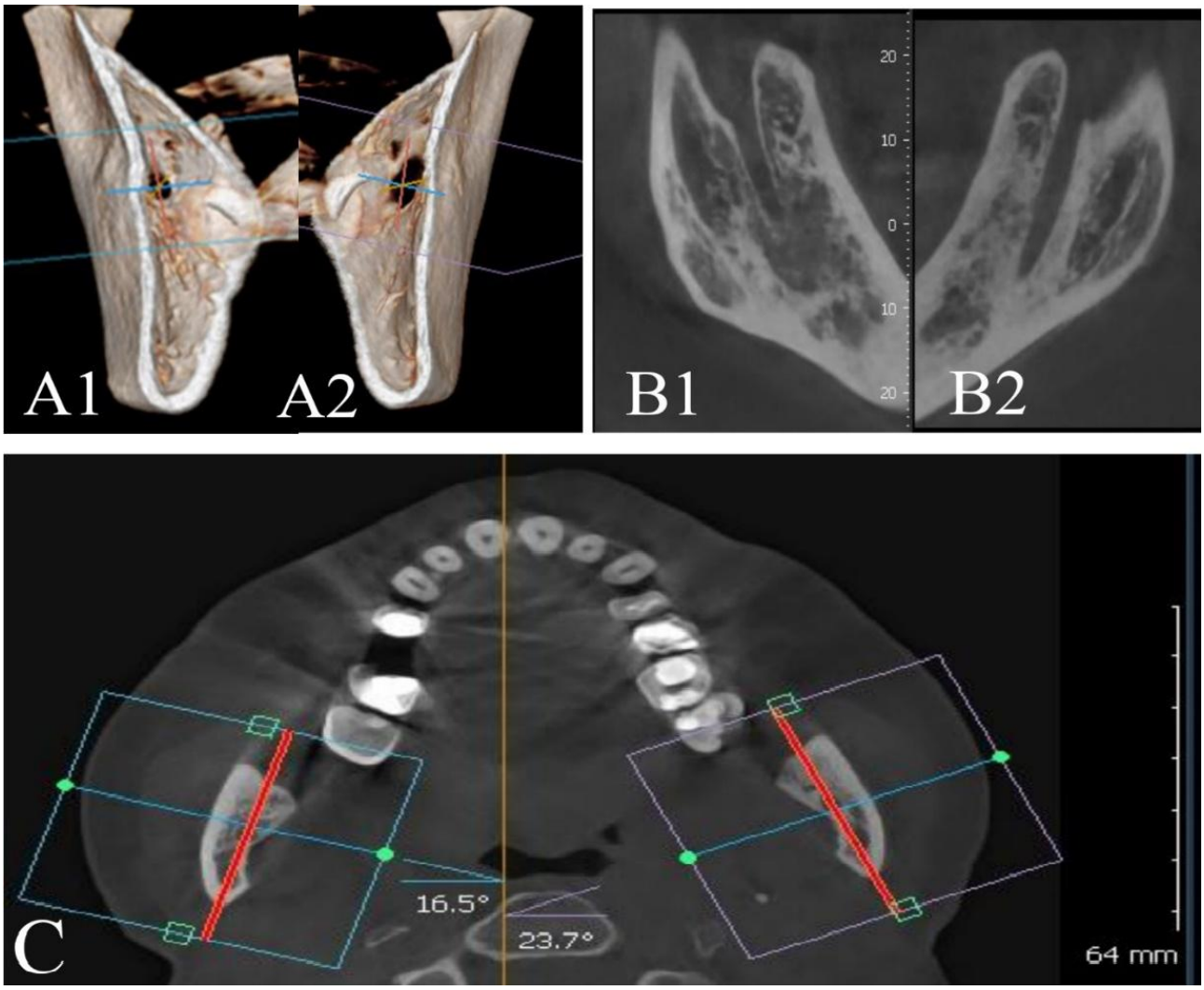

Fig. 7. X-ray method of research of the direction of mandibular canal laying, Ø°: A1, A2 - coronal section of the mandible; B1, B2 - coronal (smart) section; C - axillary (axial) section of the mandible.

which is laid in her body and ends on the outer surface of the chin hole, forming a through "tunnel" [8, 13, 16].

Bone atrophy leads to irreversible physiological processes, which are negatively reflected in the topographic features of the mandibular canal, even in relation to the most stable morphological structures, such as the angle of the mandible [20]. This study comprehensively characterizes the topographic variability of the mandibular canal in atrophy of bone tissue due to loss of the masticatory group of teeth.

We want to draw the researchers' attention to the fact that even asymmetric loss of one tooth leads to significant atrophy from inactivity on the corresponding side [7, 28] and is reflected, respectively, by changing the degree (Ø°) of the initial direction of the mandibular canal (Fig. 7). especially with end defects of the dentition, as a pathogenetic factor of bone atrophy.

These differences in topographic features and variability of channels should be taken into account, first, when analyzing digital images of both sides of the mandible, to increase the effectiveness of local anesthesia [11], as the initial stage of treatment, osteosynthesis, osteotomy and other reconstructive surgery.

The issues of formation of bone tissue of the mandible [12] as a fundamental platform for laying the canal (channels) of the mandible, the impact of somatic pathology [23] on its topographic variability and changes in morphometric values [1], morphological variability of channels, dependent from atrophy of bone tissue due to loss of the masticatory group of teeth.

Prospects for further research are the morphological identification of mandibular canals and their structures by functional purpose.

Conclusion

1. Variant anatomy of canal (channels) bifurcation of the mandible is manifested on both the left and right sides of the mandible.

2. The main canal of the mandible is well surrounded by a cortical layer, forming a rounded, slightly flattened (from the predominance of atrophic processes of bone tissue) tubular tunnel and clearly visualized during X-ray examinations.

3. The system of peripheral canals, tubules (branches) depends on the atrophy of bone tissue caused by tooth loss and is subject to "morphological degeneration from inactivity".

4. The variability of canal (channels) foramens of the mandible is differentiated by location, number, direction and size.

References

[1] Ahmed, A. A., Ahmed, R. M., Jamleh, A., & Spagnuolo, G. (2021). Morphometric Analysis of the Mandibular Canal, Anterior Loop, and Mental Foramen: A Cone-Beam Computed Tomography Evaluation. *Int J Environ Res,* 18(7), 3365. doi: 10.3390/ijerph18073365

[2] Borghesi, A., & Bondioni, M. P. (2021). Unilateral triple mandibular canal with double mandibular foramen: cone-beam computed tomography findings of an unexpected anatomical variant. *Folia Morphol* (Warsz), 80(2), 471-475. doi: 10.5603/FM.a2020.0057

[3] Costa, E. D., Peyneau, P. D., Visconti, M. A, Devito, K. L., Ambrosano, G. M. B., & Verner, F. S. (2019). Double mandibular canal and triple mental foramina: detection of multiple anatomical variations in a single patient. *Gen Dent,* 67(5), 46-49. PMID: 31454322

[4] De Castro, M. A. A., Vich, M. O. L., Abreu, M. H. G., & Mesquita, R. A. (2019). Cross-sectional study of mandibular canal branching in regions affected by dental inflammation with cone beam computed tomography. *Int J OdontoStomatol,* 13(2), 142-149. doi: 10.4067/S0718-381X2019000200142

[5] Dharmapala, R. M. A. U., Satharasinghe, D. M., Silva, S. P. I., & Jeyasugiththan, J. (2022). Medical Physics Determination of safe zone of the mandible for implant and bone harvesting (using CBCT) of mandible in a group of Sri Lankan subjects. *Journal of the National Science Foundation of Sri Lanka*, 50(1), 65-72. doi: 10.4038/jnsfsr.v50i1.10485

[6] Elnadoury, E. A., Gaweesh, Y. S. E-D., Abu El Sadat, S. M., & Anwar, S. K. (2022). Prevalence of bifid and trifid mandibular canals with unusual patterns of nerve branching using cone beam computed tomography. *Odontology,* 110, 203-211. doi: 10.1007/s10266-021-00638-9

[7] Fastovets, O., Sapalov, S., & Shtepa, V. (2020). Results of stress-strain states study in prosthetics of different types of atrophy of edentulous mandible. *Medicni Perspektivi,* 25(4), 146-158. doi: 10.26641/2307-0404.2020.4.221411

[8] Fuentes, R., Arias, A., Farfan, C., Astete, N., Garay, I., Navarro, P., & Dias, F. J. (2019). Morphological variations of the mandibular canal in digital panoramic radiographs: a retrospective study in a Chilean population. *Folia Morphol* (Warsz), 78(1), 163-170. doi: 10.5603/FM.a2018.0058

[9] Iwanaga, J., Takeshita, Y., Matsushita, Y., Hur, M. S., Ibaragi, S., & Tubbs, R. S. (2022). What are the retromolar and bifid/trifid mandibular canals as seen on cone-beam computed tomography? Revisiting classic gross anatomy of the inferior alveolar nerve and correcting terminology. *Surg Radiol Anat,* 44(1), 147-156. doi: 10.1007/s00276-021-02862-y

[10] Jena, S., Panigrahi, R., Pati, A. R., & Hasan, S. (2021). Prevalence, patterns and variations of anterior loop of inferior alveolar nerve|A CBCT based retrospective study. *Indian Journal of Otolaryngology and Head Neck Surgery,* 1-8. doi: 10.1007/s12070-021-02691-w

[11] Karamifar, K., Shirali, D., Saghiri, M. A., Ali Saghiri, M., & Paul, V. (2021). Abbott. Retromolar canal infiltration as a supplement to the inferior alveolar nerve block injection: an uncontrolled clinical trial. *Clin Oral Invest,* (25), 5473-5478. doi: 10.1007/s00784-021-03855-2

[12] Kawata, K., Narita, K., Washio, A., Kitamura, Ch., Nishihara, T., Kubota, S., & Takeda, S. (2021). Odontoblast differentiation is regulated by an interplay between primary cilia and the canonical Wnt pathway. *Bone,* (150), 116001. doi: 10.1016/j.bone.2021.116001

[13] Komal, A., Bedi, R. S., Wadhwani, P., Aurora, J. K., & Chauhan, H. (2020). Study of normal anatomy of mandibular canal and its variations in indian population using CBCT. *Journal of Oral and Maxillofacial Surgery,* 19(1), 98-105. doi: 10.1007/s12663-019-01224-x

[14] Ma, H., Van Dessel, J., Shujaat, S., Bila, M., Sun, Yi., Politis, C., & Jacobs, R. (2022). Long-term survival of implant-based oral rehabilitation following maxillofacial reconstruction with vascularized bone flap. *Int J Implant Dent*, (8), 15. doi: 10.1186/s40729-022-00413-7

[15] Miličević, A., Salarić, I., Đanić, P., Miličević, H., Macan, K., Orihovac, Ž., … & Macan, D. (2021). Anatomical Variations of the Bifid Mandibular Canal on Panoramic Radiographs in Citizens from Zagreb, Croatia. *Acta Stomatol Croat,* 55(3), 248-255. doi: 10.15644/asc55/3/2

[16] Moro, A., Abe, S., Yokomizo, N., Kobayashi, Y., Ono, T., & Takeda, T. (2018). Topographical distribution of neurovascular canals and foramens in the mandible: avoiding complications resulting from their injury during oral surgical procedures. *Heliyon,* 4(9), e00812. doi: 10.1016/j.heliyon.2018.e00812

[17] Ngeow, W. C., & Chai. W. L. (2020). The clinical anatomy of accessory mandibular canal in dentistry. *Clin Anat,* 33(8), 1214-1227. doi: 10.1002/ca.23567

[18] Nithya, J., & Aswath, N. (2020). Assessing the prevalence and morphological characteristics of bifid mandibular canal using cone-beam computed tomography - A retrospective cross-sectional study. *J Clin Imaging Sci*, (10), 30. doi: 10.25259/jcis_67_2019

[19] OkumuS, Ö., & Dumlu, A. (2019). Prevalence of bifid mandibular canal according to gender, type and side. *J Dent Sci,* 14(2), 126-133. doi: 10.1016/j.jds.2019.03.009

[20] Oshurko, A., Oliinyk, I., Kuzniak, N., Yaremchuk, N., & Makarchuk, I. (2021). Morphometric research significance in determination of variability of topographic relations of the mandible structures on the example of the sagittal section of its angle. *Clinical and experimental pathology,* 20(4), 58-65. doi: 10.24061/1727-4338.XX.4.78.2021.7

[21] Puche-Roses, M., Blasco-Serra, A., Valverde-Navarro, A. A., & Puche-Torres, M. (2022). Prevalence and morphometric analysis of the retromolar canal in a Spanish population sample: a helical CT scan study. *Med Oral Patol Oral Cir Bucal,* 27(2), 142-149. doi: 10.4317/medoral.25069

[22] Pucilo, M., Lipski, M., Sroczyk-Jaszczynska. M., Pucilo, A., & Nowicka, A. (2020). The anatomical relationship between the roots of erupted permanent teeth and the mandibular canal: a systematic review. *Surg Radiol Anat,* 42(5), 529-542. doi: 10.1007/s00276-019-02404-7

[23] Pylypchuk, I. (2021). Osteoporotic changes in bone and cartilaginous tissue in women with ovarian hypofunction.

Reports of Vinnytsia National Medical University, 25(4), 657-62. doi: 10.31393/reports-vnmedical-2021-25(4)-26

[24] Ramaglia, L., Blasi A., Galasso, L., Pezzella, V., Cuozzo, A., & Iorio-Siciliano, V. (2022). Prevalence and anatomical characteristics of bifid and trifid mandibular canals: a computed tomography analysis. *Research Sguare*, 1-14. doi: 10.21203/rs.3.rs-1561216/v1

[25] Reda, R., Zanza, A., Mazzoni, A., Cicconetti, A., Testarelli, L., & Di Nardo, D. (2021). An Update of the Possible Applications of Magnetic Resonance Imaging (MRI) in Dentistry: A Literature Review. *J. Imaging,* 7, 75. doi: 10.3390/jimaging7050075

[26] Shah, N. P., Murtadha, L., & Brown, J. (2018). Bifurcation of the inferior dental nerve canal: an anatomical study. *Br J Oral Maxillofac Surg,* 56, 267-271. doi: 10.1016/j.bjoms.2018.01.016 17

[27] Sonneveld, K. A., Mai, P. T., Hogge, M., Choi, E. Y., & Portnof, J. E. (2018). Bifid mandibular canal: A case review and retrospective review of cbcts. *Implant Dent,* 27, 682-686. doi: 10.1097/id.0000000000000819

[28] Stupnitsky, I.-O. R., Rozhko, M. M., & Stupnitsky R. M. (2021). Recovery of defects of the cellular progress of the lower jaw as a guarantee of successful orthopedic treatment. *Journal of Modern Dentistry,* 5, 58-62. doi: 10.33295/1992-576X-2021-5-58

[29] Yang, X. W., Zhang, F. F., Li, Y. H., Wei, B., & Gong, Y. (2017). Characteristics of intrabony nerve canals in mandibular interforaminal region by using cone-beam computed tomography and a recommendation of safe zone for implant and bone harvesting. *Clinical Implant Dentistry and Related Research,* 19(3), 530-538. doi: 10.1111/cid.12474

[30] Zhang, Y. Q., Zhao, Y. N., Liu, D. G., Meng, Y., & Ma, X. C. (2018). Bifid variations of the mandibular canal: cone beam computed tomography evaluation of 1000 Northern Chinese patients. *Oral Surg Oral Med Oral Pathol Oral Radiol*, 126(5), 271-278. doi: 10.1016/j.oooo.2018.06.008

[31] Zhou, X., Gao, X., & Zhang, J. (2020). Bifid mandibular canals: CBCT assessment and macroscopic observation. *Surg Radiol Anat*, 42(9), 1073-1079. doi: 10.1007/s00276-020-02489-5

ВАРІАНТНА АНАТОМІЯ ТОПОГРАФІЇ КАНАЛУ НИЖНЬОЇ ЩЕЛЕПИ

Ошурко А. П., Олійник І. Ю., Кузняк Н. Б.

У даній роботі представлено аналіз 3D реконструкційних моделей прояву варіативності каналу (каналів) нижньої щелепи як з лівої, так і з правої сторони, їх прокладання у тілі нижньої щелепи та локалізацію, розміри і напрямки вихідних каналів. Адже, доступність малоінвазивних технік, імплементованих у процеси дослідження, сприяють виявленню навіть незначних анатомічних варіантів чи розгалужень каналу нижньої щелепи, що є доволі частими і не дозволяють клініцисту нехтувати ними та потребують належної наукової оцінки. Під час планування реконструктивних хірургічних утручань на нижній щелепі брак високої прогностичності щодо запобігання функціональних ускладнень, які доволі часто бувають незворотними (через те, що канал нижньої щелепи містить рухові та чутливі нервові волокна), змушує переглядати морфологічну фундаментальність особливостей його топографії. Тому, метою роботи було проведення огляду комп'ютерно-томографічних цифрових зображень, їх аналізу та виявлення можливих анатомічних варіантів прокладання каналу (каналів) нижньої щелепи, як основи у встановленні його топографічних особливостей, із лівої та правої сторін. Після проведеного аналізу 426 цифрових КТ-сканувань нижніх щелеп в осіб чоловічої та жіночої статі віком від 25 до 75 років відтворено 68 3D реконстукційних моделей за допомогою стандартизованого рентгено-діагностичного КТ-програмного забезпечення Ez3D-I Original ver.5.1.9.0, що застосовується для візуалізації мультимодальних і багатовимірних зображень, окремі з яких подані як результати власних досліджень. Встановлено, що вхідні отвори нижньощелепних каналів як із лівої, так із правої сторін продовжуються одним каналом, проте, у проекції других великих корінних зубів, останні із великою частотою можуть розділятися на добре проектовані два-три канали. Наявна відмінність у діаметрах (Ø) каналів та їх відкриттям - типовим (у проекції малих корінних зубів з правої сторони) і нетиповим відкриттям - у проекції 3.6, 4.6 великих корінних зубів та центральних різців, іклів як за напрямком вихідного отвору, так і за їх розташуванням. Не прослідковується належної закономірної систематизації, щодо кількості топографічної траєкторії та розміру каналів нижньої щелепи, об'єднання чи їх розділення, а також напрямку їх виходу, що потребує додаткової пильності не лише під час дослідницьких робіт, а й навіть у клінічній стоматології чи реконструктивній хірургії.

Ключові слова: *канал нижньої щелепи, комп'ютерна томографія, морфометрія, атрофія кісткової тканини, людина.*

DOI: 10.31393/morphology-journal-2022-28(2)-10 Reports of Morphology, Vol. 28, №2, Pages 69-74

ISSN 1818-1295 eISSN 2616-6194

REPORTS OF MORPHOLOGY

Official Journal of the Scientific Society of Anatomists, Histologists, Embryologists and Topographic Anatomists of Ukraine

journal homepage: https://morphology-journal.com

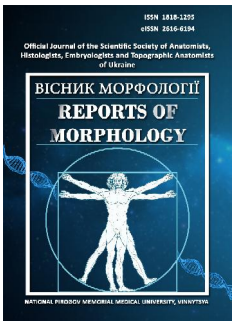

Discriminant models of the possibility of benign nevi occurrence and features in men depending on the characteristics of anthropo-somatotypological indicators

Haddad N. B. Yo.[1], Dmytrenko S. V.[1], Mateshuk-Vatseba L. R.[2], Khapitska O. P.[1], Kyrychenko V. I.[1]

[1]National Pirogov Memorial Medical University, Vinnytsya, Ukraine
[2]Danylo Halytsky National Medical University of Lviv, Lviv, Ukraine

ARTICLE INFO

Received: 23 February 2022
Accepted: 28 March 2022

UDC: 616.5-003.829-037-084-07

CORRESPONDING AUTHOR

e-mail: nabil.basim@gmail.com
Haddad N. B. Yo.

CONFLICT OF INTEREST

The authors have no conflicts of interest to declare.

FUNDING

Not applicable.

The multifactorial nature of the origin and development of nevi is the subject of debate so far. One way to understand this process and get an answer to this question is to use a constitutional method of research. The purpose of the study is to build and analyze discriminant models of benign nevi occurrence possibility in men depending on the characteristics of the structure and size of the body. For Ukrainian men aged 22 to 35 years with benign nevi (34 with melanocyte benign simple nevi; 27 with melanocyte benign dysplastic nevi; 14 with melanocyte benign congenital nevi; 17 with nonmelanocyte benign nevus) determined anthropometric indicators according to the scheme of Bunak V. V. (1941), components of the somatotype according to the Heath-Carter scheme (1990), as well as indicators of the component composition of body weight according to Matejko formulas (1921). The control group consisted of anthropometric and somatotypological indicators of 82 practically healthy men of the same age group selected from the data bank of the Research Center of National Pirogov Memorial Medical University, Vinnytsya. Discriminant analysis was performed in the licensed statistical package "Statistica 5.5". With the help of discriminant analysis, reliable models of the possibility of benign nevi depending on the characteristics of anthropometric and somatotypological indicators are built. It was found that healthy and patients with benign nevi of men can reliably interpret the obtained classification indicators between healthy and sick, and between patients with melanocyte simple or dysplastic nevi and other groups of benign nevi (discriminant function covers 75.7 % of cases; Wilks' Lambda statistics=0.125; p<0.001). Between groups of benign nevi, reliable interpretation of the obtained classification indicators is possible only between patients with melanocyte simple or dysplastic nevi and melanocyte congenital or non-melanocyte nevi (discriminant function covers 48.4 % of cases; Wilks' Lambda statistics=0.662; p<0.001), however, the totality of all anthropological variables has little discrimination. The models of healthy and sick men include the skinfold thickness (42.8 %), girth sizes (28.6 %), shoulder width and endomorphic component of the somatotype (14.3 % each); and among men with benign nevi, only girth sizes of the body. The greatest contribution to discrimination in models of healthy and sick men is made by the circumference of the forearm at the top, the width of the shoulders and the skinfold thickness on the side; and among patients with benign nevi - chest girth on inspiration. The obtained results indicate a significant influence of environmental factors on the occurrence of benign nevi.

Keywords: *skin diseases, benign nevi, anthropometric indicators, body circumference, transverse body dimensions, skinfold thickness, somatotypical indicators, Ukrainian men, discriminant models.*

Introduction

Cancer of the skin is of particular interest to the scientific community. In particular, this is due primarily to their multifactorial nature of origin, namely the various influences of external environmental factors. These factors become

more or less relevant depending on the type of pathology under consideration [19].

If we are talking about melanocyte pathologies (tumors based on melanin-producing tissue), such as nevi or melanoma, then such a factor as insolation comes to the fore [1]. However, new research data allow a deeper assessment of other factors that deserve attention. In this case, this applies to anthropometric data of the person, such as height, weight, body size, etc. [5, 11].

One possible explanation for this interaction may be the theory of direct involvement of adipose tissue in leptin metabolism, a complex and multi-chain process that includes various human systems and organs - brain, thyroid, adrenal, pancreas and others. In turn, leptin is one of the key factors in triggering melanocyte proliferation [10]. In turn, the amount of adipose tissue is directly related to the dimensions of the human body [2, 7].

The use of such a powerful research method as anthropometric can thus be a promising tool to find answers to questions about the possibility of occurrence, course of melanocyte pathologies, including nevi - pathologies of the skin and mucous membranes, much less studied than melanoma.

In addition, scientometric databases contain only isolated data on the prevalence of nevi, which complicates the understanding and overall assessment of the problem. Thus, it is noted that the prevalence of congenital melanocyte nevi, depending on the data of various studies ranges from 0.5 % to 31.7 %, and giant congenital melanocyte nevi occur in 1 in 20 thousand-500 thousand live births. The prevalence of melanocyte nevi among men and women is quite heterogeneous and is 2 to 3, respectively, and the average size of nevi varies between 3-4 cm; also melanocytic nevi are more common in African and Japanese ethnic groups [2].

The prevalence of dysplastic nevus in the Caucasian population is from 2 to 18 % [7].

Particular attention is paid to nevi due to the emergence of studies that confirm the relationship between the presence of nevi and the development of their degeneration into dangerous and high-lethal melanocyte skin pathologies, such as melanoma or neurodermal melanosis [8].

According to Alikhan A. and co-authors [2], the risk of malignancy of nevi with subsequent melanoma is from 1 to 5 % (for small and giant congenital nevi, respectively), and for neurodermal melanosis from 2.5 to 45 % (for giant congenital nevi).

Analysis of the database of 2159 cases of melanoma revealed that 1.3 % of them occurred on the background of congenital melanocyte nevi [3], and according to other studies for dysplastic nevus is from 34 to 59 % [7] and from 18 to 20 % depending on the type of melanoma spread [17].

It has also been found that genetically, nevi significantly increase the risk of basal cell carcinoma and squamous cell carcinoma [6].

Observations of 57 patients with nevi for 5.5 years revealed that 3.5 % of them developed melanoma during this period. The researchers estimated the risk of 5-year melanoma in this cohort of individuals was 4.8 % (95 % CI: 1.9-11.5%) [21].

Given the lack of work to study the relationship between anthropometric indicators and the frequency of nevi and the clinical importance of nevi as a prognostic factor for melanoma, there is an urgent need for clinical research to study it and the possibility of further practical application in practice.

The purpose of the study is to build and analyze discriminant models of benign nevi occurrence possibility of in men depending on the characteristics of the structure and size of the body.

Materials and methods

92 Ukrainian men aged 22 to 35 with benign nevi (34 with melanocyte benign simple nevi; 27 with melanocyte benign dysplastic nevi; 14 with melanocyte benign congenital nevi; 17 with non-melanocyte benign nevi) on the basis of the Military Medical Clinical Center of the Central Region and the Department of Dermatology and Venereal Diseases with a course of postgraduate education National Pirogov Memorial Medical University, Vinnytsya conducted clinical, laboratory and pathohistological examinations. The diagnosis of nevi was established according to a two-stage algorithm for the classification of pigmented tumors, which was adopted at the First World Congress of Dermatoscopy (Rome, 2001) [16].

All patients signed an informed consent to participate in the study. Committee on Bioethics of National Pirogov Memorial Medical University, Vinnytsya (protocol № 10 From 26.11.2020) found that the studies do not contradict the basic bioethical standards of the Declaration of Helsinki, the Council of Europe Convention on Human Rights and Biomedicine (1977), the relevant WHO regulations and laws of Ukraine.

All men with benign nevi were determined by anthropometric indicators according to the scheme of Bunak V. V. (1941), somatotype components according to the Heath-Carter scheme (1990), as well as indicators of the component composition of body weight according to the formulas Matejko (1921) [9]. The control group consisted of anthropometric and somatotypological indicators of 82 practically healthy men of the same age group were selected from the data bank of the research center of the National Pirogov Memorial Medical University, Vinnytsya.

Discriminant analysis was performed in the licensed statistical package "Statistica 5.5".

Results

Taking into account the indicators of body structure and size in practically healthy and patients with benign nevi of men, discriminant function covers 75.7 % of cases. Among

healthy and benign nevi men, the discriminant variables are the skinfold thickness (SFT) on the thigh (GBD), on the side (GB) and on the chest (GGR), endomorphic component of somatotype (FX), chest circumference on inspiration (OBGK1) and forearms at the top (OBPR1), as well as shoulder width (ACR). The largest contribution to discrimination between the healthy and benign nevi groups of men among the above indicators is the forearm girth in the upper part, shoulder width and SFT on the side. The set of all anthropological and somatotypological variables has a pronounced (Wilks' Lambda=0.125; p<0.001) discrimination between groups of healthy and benign nevi men.

For healthy and patients with benign nevi of men, classification indicators (Df) have been determined, which can be used to classify the subjects as healthy or patients with benign nevi. Below in the form of equations is the definition of classification indicators, where the attribution to healthy men is possible at a value of Df close to 166.2; to men with melanocyte simple nevi - at a Df value close to 159.7; to men patients with melanocyte dysplastic nevi - at a Df value close to 156.1; to men with melanocyte congenital nevi - at a Df value close to 167.6; to men with non-melanocyte nevi - at a Df value close to 168.8:

Df (*for healthy men*) = GBD x 1.157 - GB x 0.460 - FX x 6.371 + OBGK1 x 1.005 + ACR x 3.026 + OBPR1 x 4.311 - GGR x 0.804 - 166.2;

Df (*for men with melanocyte simple nevi*) = GBD x 0.194 + GB x 1.323 - FX x 14.59 + OBGK1 x 1.579 + ACR x 1.925 + OBPR1 x 3.795 + GGR x 0.191 - 159.7;

Df (*for men with melanocyte dysplastic nevi*) = GBD x 0.311 + GB x 1.193 - FX x 14.94 + OBGK1 x 1.814 + ACR x 1.869 + OBPR1 x 2.959 - GGR x 0.006 - 156.1;

Df (*for men with melanocyte congenital nevi*) = GBD x 0.143 + GB x 1.027 - FX x 14.00 + OBGK1 x 1.835 + ACR x 2.054 + OBPR1 x 3.000 + GGR x 0.217 - 167.6;

Df (*for men with non-melanocyte nevi*) = GBD x 0.299 + GB 1.052 - FX x 14.42 + OBGK1 x 1.737 + ACR x 2.021 + OBPR1 x 3.468 + GGR x 0.256 - 168.8;

where (here and hereafter), SFT - in mm; somatotype components - in points; circumferential body dimensions - in cm; body diameters - in cm

The statistical significance of discriminant functions of healthy and patients with benign nevi of men was determined using the criterion χ^2. The results of the χ^2 test indicate that taking into account the established anthropometric and somatotypological indicators it is possible to reliably interpret the obtained classification indicators between healthy and sick for all groups of benign nevi of men, as well as between men with melanocyte simple or dysplastic nevi and other groups.

Taking into account the indicators of anthropo-somatotypological indicators only in patients with benign nevi of men discriminant function covers 48.4 % of cases. Among men with benign nevi, the discriminant variables are upper arm circumference (OBPR1), inspiratory chest circumference (OBGK1), and expiratory chest circumference (OBGK2). The greatest contribution to discrimination between groups of men with benign nevi in men is chest girth on inhalation. The totality of all anthropological and somatotypological variables has a slight (Wilks' Lambda=0.662; $F_{(9.207)}$=4.241; p<0.001) discrimination between groups of men with benign nevi.

Below in the form of equations is the definition of classification indicators, where the attribution to men of patients with melanocyte simple nevi is possible with a Df value close to 118.8; to men patients with melanocyte dysplastic nevi - at a Df value close to 111.7; to men with melanocyte congenital nevi - at a Df value close to 123.2; to men with non-melanocyte nevi - at a Df value close to 124.4:

Df (*for men with melanocyte simple nevi*) = OBPR1 x 6.004 + OBGK1 x 2.676 - OBGK2 x 2.175 - 118.8;

Df (*for men with melanocyte dysplastic nevi*) = OBPR1 x 5.181 + OBGK1 x 2.842 - OBGK2 x 2.196 - 111.7;

Df (*for men with melanocyte congenital nevi*) = OBPR1 x 5.318 + OBGK1 x 3.111 - OBGK2 x 2.415 - 123.2;

Df (*for men with non-melanocyte nevi*) = OBPR1 5.767 + OBGK1 x 2.988 - OBGK2 x 2.393 - 124.4.

The results of the χ^2 test indicate that, taking into account the established anthropometric and somatotypological indicators, a reliable interpretation of the obtained classification indicators is possible only between patients with melanocyte simple or dysplastic nevi and other groups of benign nevi.

Discussion

Anthropometric researches about study the characteristics of certain dimensions or weights in people with nevi are not available in scientometric databases for the last decade. However, the results of examinations of persons with other types of skin pathology are quite encouraging.

A history of 70 Iraqi people with non-melanocyte skin cancer showed the following distribution: most people were 56-70 years old, illiterate, married, and working with a sufficient income. 11.4 % of respondents had a burdensome family history, and 62.9 % spent more than 4 hours in the sun every day. 72.9 % did not smoke and 98.6 % did not drink alcohol; 45.7 % had 1 blood group and slightly more than half of the participants had normal values of body mass index [1].

At the same time, no association was found between body mass index or waist circumference and the risk of glioma in adulthood. In young people, there is an association only with the body mass index (higher rates are associated with an increased risk of glioma). For women of all ages, there is a reduced risk of glioma in people with severe somatotype [5].

Taking into account age, height and height-to-sitting height ratios are significantly associated with the risk of melanoma (RR=1.40, 95 % CI=1.06-1.86 for $\geq$0.533 vs.<0.518; P for trend=0.02). An association has also been

found between a large type of somatotype during menarche and the risk of melanoma [11].

P. H. Lahmann and co-authors [12] conducted a 16-year follow-up of more than 1,000 individuals, of whom more than 500 developed skin cancer (334 - basal cell carcinoma, 188 - squamous cell carcinoma, 28 - melanoma). Statistical data showed a significant association between the risk of squamous cell carcinoma and melanoma and growth in men and basal cell carcinoma and growth in women.

Similar data were obtained from Nurses' Health (117,863 individuals) and Health Professionals Follow-up Study (51,111 individuals), which found an increased risk of basal cell and squamous cell skin cancer with an increase in height every 10 cm [13].

K. D. Meyle and others [14] analyzed the database of the Copenhagen School Register of Medical Records of 1930-1989 (372,636 people). During the observation period, 2329 people developed skin melanoma. The analysis of anthropometric indicators established a connection between the increased risk of melanoma and growth at the age of 7-13 years and birth weight.

An analysis of the literature on the relationship between the risk of melanoma and human growth clearly indicates its existence. This is confirmed by researchers from the United States, Norway, Canada, Israel, Italy and Australia [20].

A group of scientists analyzed 9 publications, which totaled almost a million people, of whom more than 50,000 developed non-melanocyte skin cancer. Statistical analysis of the data showed a nonlinear feedback between body mass index and non-melanocyte cancer risk (RR=0.88, 95 % CI: 0.85-0.91, I2=71.2 %, P-nonlinearity <0.001) [23].

Long-term follow-up of 71,645 women, more than 13,000 of whom developed nonmelanocyte skin cancer, revealed the factors most closely associated with the pathology. A body mass index greater than 25 kg/m^2 and a waist-to-thigh ratio greater than 0.80 are associated with a reduced risk of non-melanocytic cancer, only in the absence of excessive sun exposure [4].

Rezaiian F. and co-authors [18] found significant correlations between visceral fat percentage and waist circumference and risk of nonmelanocyte skin cancer by logistic regression analysis (OR: 1.10, 95 % CI: 1.024-1.190, p=0.01 and OR: 1.04, 95 % CI: 1.007-1.080, p=0.018, respectively).

One way or another, the values of body mass index, body fat and non-fat body mass are associated with the risk of cancer of the stomach, esophagus, liver, pancreas, lungs and uterus [22].

Thus, given the data of the above studies, and taking into account the known pathophysiological mechanisms, it becomes obvious that obesity is one of the key places in the trigger mechanism of both melanocyte and non-melanocyte skin tumors [10].

In the analysis of discriminant equations of healthy and patients with benign nevi men depending on anthropo-somatotypological indicators, we found that a reliable interpretation of the obtained classification indicators between healthy and patients with benign nevi, and between patients with melanocyte simple or dysplastic nevi and others benign nevi (discriminant function covers 75.7 % of cases; statistics Wilks' Lambda=0.125; p<0.001). In the analysis of discriminant equations only between men with benign nevi men found only slight discrimination (discriminant function covers 48.4 % of cases; statistics Wilks' Lambda=0.662; p<0.001) between patients with melanocyte simple or dysplastic nevi and melanocyte congenital or neonatal melanocytes.

Discriminant models in healthy and benign nevi male include SFT (42.8 %), girth (28.6 %), body diameter and somatotype components (14.3% each); and among men with benign nevi - only comprehensive body size (100 %). Moreover, the greatest contribution to discrimination in healthy and benign nevi of men is made by the girth of the forearm at the top, shoulder width and SFT on the side; and between groups of patients with benign nevi - chest girth on inspiration.

The high percentage of participation in SFT models and body circumference indicate a significant influence of environmental factors on the occurrence of this multifactorial disease [15].

Conclusion

1. Reliable discriminant models developed on the basis of anthropometric and somatotypological indicators allow to predict with high probability the possibility of benign nevi in Ukrainian men, as well as to separate melanocyte simple or dysplastic nevi (discriminant function covers 75.7 % of cases; statistics Wilks' Lambda=0.125; p<0.001). In the analysis of only sick men, significant slight discrimination between melanocyte simple or dysplastic nevi and melanocyte congenital or non-melanocyte nevi is possible (discriminant function covers 48.4% of cases; statistics Wilks' Lambda=0.662; p<0.001).

2. Discriminatory equations in healthy and patients with benign nevi men include SFT (42.8 %) and girth sizes (28.6 %); and between sick men - only the comprehensive size of the body.

References

[1] Ali, B. M., & Ahmed, H. A. (2018). Epidemiology of Non-Melanoma Skin Cancer Patients Attending at Hiwa Hospital in Sulaimani City, Iraq. *Kurdistan Journal of Applied Research*, 3(2), 44-48. doi: 10.24017/science.2018.2.7

[2] Alikhan, A., Ibrahimi, O. A., & Eisen, D. B. (2012). Congenital melanocytic nevi: where are we now?: part I. Clinical presentation, epidemiology, pathogenesis, histology, malignant transformation, and neurocutaneous melanosis. *Journal of the American Academy of Dermatology,* 67(4), 495.e1-495.e17. doi: 10.1016/j.jaad.2012.06.023

[3] Caccavale, S., Calabrese, G., Mattiello, E., Broganelli, P., Ramondetta, A., Pieretti, G., ... & Argenziano, G. (2021). Cutaneous melanoma arising in congenital melanocytic nevus: a retrospective observational study. *Dermatology,* 237(3), 473-478. doi: 10.1159/000510221

[4] Chan, A. A., Noguti, J., Pak, Y., Qi, L., Caan, B., Going, S., ... & Lee, D. J. (2019). Interaction of body mass index or waist?to?hip ratio and sun exposure associated with nonmelanoma skin cancer: A prospective study from the Women's Health Initiative. *Cancer,* 125(7), 1133-1142. doi: 10.1002/cncr.31810

[5] Cote, D. J., Downer, M. K., Smith, T. R., Smith-Warner, S. A., Egan, K. M., & Stampfer, M. J. (2018). Height, waist circumference, body mass index, and body somatotype across the life course and risk of glioma. *Cancer Causes & Control,* 29(8), 707-719. doi: 10.1007/s10552-018-1052-x

[6] Dusingize, J. C., Law, M. H., Pandeya, N., Neale, R. E., Ong, J. S., MacGregor, S., ... & Olsen, C. M. (2022). Genetically determined cutaneous nevi and risk of cancer. *International Journal of Cancer,* 150(6), 961-968. doi: 10.1002/ijc.33874

[7] Farber, M. J., Heilman, E. R., & Friedman, R. J. (2012). Dysplastic nevi. *Dermatologic clinics,* 30(3), 389-404. doi: 10.1016/j.det.2012.04.004

[8] Geller, A. C., Mayer, J. E., Sober, A. J., Miller, D. R., Argenziano, G., Johnson, T. M., & Swetter, S. M. (2016). Total nevi, atypical nevi, and melanoma thickness: an analysis of 566 patients at 2 US centers. *JAMA dermatology,* 152(4), 413-418. doi: 10.1001/jamadermatol.2016.0027

[9] Kalmin, O. V., & Galkina, T. N. (2020). *Медицинская антропология [Medical anthropology].* Высшее образование: Специалитет - Higher education: Specialitet.

[10] Karimi, K., Lindgren, T. H., Koch, C. A., & Brodell, R. T. (2016). Obesity as a risk factor for malignant melanoma and non-melanoma skin cancer. *Reviews in Endocrine and Metabolic Disorders*, 17(3), 389-403. doi: 10.1007/s11154-016-9393-9

[11] Kvaskoff, M., Bijon, A., Mesrine, S., Vilier, A., Clavel-Chapelon, F., & Boutron-Ruault, M. C. (2014). Anthropometric features and cutaneous melanoma risk: a prospective cohort study in French women. *Cancer epidemiology,* 38(4), 357-363. doi: 10.1016/j.canep.2014.05.008

[12] Lahmann, P. H., Hughes, M. C. B., Williams, G. M., & Green, A. C. (2016). A prospective study of measured body size and height and risk of keratinocyte cancers and melanoma. *Cancer epidemiology,* 40, 119-125. doi: 10.1016/j.canep.2015.12.006

[13] Li, X., Liang, L., Feng, Y. C. A., De Vivo, I., Giovannucci, E., Tang, J. Y., & Han, J. (2017). Height, height-related SNPs, and risk of non-melanoma skin cancer. *British journal of cancer,* 116(1), 134-140. doi: 10.1038/bjc.2016.366

[14] Meyle, K. D., Gamborg, M., Sørensen, T. I., & Baker, J. L. (2017). Childhood body size and the risk of malignant melanoma in adulthood. *American journal of epidemiology,* 185(8), 673-680. doi: 10.1093/aje/kww128

[15] Nikityuk, B. A., Moroz, V. M., & Nikityuk, D. B. (1998). *Теория и практика интегративной антропологии. Очерки [Theory and practice of integrative anthropology. Essays].* Киев-Винница, "Здоров'я" - Kiev-Vinnitsa, "Zdorov'ya".

[16] Potekayev, N. N., Shuginina, Y. K., Kuzmina, T. S., & Arutyunyan, L. S. (2011). *Дерматоскопия в клинической практике. Руководство для врачей [Dermatoscopy in clinical practice. A guide for doctors].* M: МДВ, 144 - M: MDV, 144.

[17] Reddy, K. K., Farber, M. J., Bhawan, J., Geronemus, R. G., & Rogers, G. S. (2013). Atypical (dysplastic) nevi: outcomes of surgical excision and association with melanoma. *JAMA dermatology,* 149(8), 928-934. doi: 10.1001/jamadermatol.2013.4440

[18] Rezaiian, F., Davoodi, S. H., Nikooyeh, B., Ehsani, A. H., Kalayi, A., Shariatzadeh, N., ... & Neyestani, T. R. (2021). Metabolic Syndrome and Its Components are Linked with Increased Risk of Non-Melanoma Skin Cancers in Iranian Subjects: A Case-Control Study. *Nutrition and Cancer,* 1-9. doi: 10.1080/01635581.2021.2012581

[19] Roh, M. R., Eliades, P., Gupta, S., & Tsao, H. (2015). Genetics of melanocytic nevi. *Pigment cell & melanoma research*, 28(6), 661-672. doi: 10.1111/pcmr.12412

[20] Vena, G. A., Cassano, N., Caccavale, S., & Argenziano, G. (2019). Association between melanoma risk and height: a narrative review. *Dermatology Practical & Conceptual,* 9(2), 82-89. doi: 10.5826/dpc.0902a02

[21] Viana, A. C. L., Goulart, E. M. A., Gontijo, B., & Bittencourt, F. V. (2017). A prospective study of patients with large congenital melanocytic nevi and the risk of melanoma. *Anais Brasileiros de Dermatologia,* 92, 200-205. doi: 10.1590/abd1806-4841.20175176

[22] Vithayathil, M., Carter, P., Kar, S., Mason, A. M., Burgess, S., & Larsson, S. C. (2021). Body size and composition and risk of site-specific cancers in the UK Biobank and large international consortia: A mendelian randomisation study. *PLoS medicine,* 18(7), e1003706. doi: 10.1371/journal.pmed.1003706

[23] Zhou, D., Wu, J., & Luo, G. (2016). Body mass index and risk of non-melanoma skin cancer: cumulative evidence from prospective studies. *Scientific reports,* 6(1), 1-8. doi: 10.1038/srep37691

ДИСКРИМІНАНТНІ МОДЕЛІ МОЖЛИВОСТІ ВИНИКНЕННЯ ТА ОСОБЛИВОСТЕЙ ПЕРЕБІГУ ДОБРОЯКІСНИХ НЕВУСІВ У ЧОЛОВІКІВ ЗАЛЕЖНО ВІД ОСОБЛИВОСТЕЙ АНТРОПО-СОМАТОТИПОЛОГІЧНИХ ПОКАЗНИКІВ

Хаддад Н. Б. Ю., Дмитренко С. В., Матешук-Вацеба Л. Р., Хапицька О. П., Кириченко В. І.

Мультифакторіальна природа виникнення та розвитку невусів є предметом дискусій вчених дотепер. Одним зі шляхів розуміння цього процесу і отримання відповіді на дане питання є застосування конституціонального методу дослідження. Мета дослідження - побудувати та провести аналіз дискримінантних моделей можливості виникнення доброякісних невусів у чоловіків залежно від особливостей показників будови та розмірів тіла. Українським чоловікам віком від 22 до 35 років, хворим на доброякісні невуси (34 із меланоцитарними доброякісними простими невусами; 27 із меланоцитарними доброякісними диспластичними невусами; 14 із меланоцитарними доброякісними вродженими невусами; 17 із немеланоцитарними доброякісними невусами) проведено визначення антропометричних показників за схемою Бунака В. В. (1941), компонентів соматотипу за схемою Хіт-Картера (1990), а також показників компонентного складу маси тіла за формулами Матейко (1921). Контрольну групу складали антропометричні та соматотипологічні показники 82 практично здорових чоловіків аналогічної вікової групи відібрані з банку даних науково-дослідного центру Вінницького національного медичного університету ім. М. І. Пирогова. Дискримінантний аналіз проведено в ліцензійному статистичному пакеті "Statistica 5.5". За допомогою дискримінантного аналізу побудовані достовірні моделі можливості виникнення доброякісних невусів в залежності від особливостей антропометричних і соматотипологічних показників. Встановлено, що у здорових і хворих на доброякісні невуси чоловіків можлива достовірна інтерпретація отриманих показників класифікації як між

здоровими та хворими, так і між хворими на меланоцитарні прості або диспластичні невуси та іншими групами доброякісних невусів (дискримінантна функція охоплює 75,7 % випадків; статистика Wilks' Lambda=0,125; p<0,001). Між групами доброякісних невусів достовірна інтерпретація отриманих показників класифікації можлива лише між хворими на меланоцитарні прості або диспластичні невуси та меланоцитарні вроджені або немеланоцитарні невуси (дискримінантна функція охоплює 48,4 % випадків; статистика Wilks' Lambda=0,662; p<0,001), однак сукупність усіх антропологічних змінних має незначну дискримінацію. До складу моделей у здорових і хворих чоловіків входять товщина шкірно-жирових складок (42,8 %), обхватні розміри тіла (28,6 %), ширина плечей та ендоморфний компонент соматотипу (по 14,3 %); а між хворими на доброякісні невуси чоловіками - лише обхватні розміри тіла. Найбільший внесок у дискримінацію в моделях здорових і хворих чоловіків вносять обхват передпліччя у верхній частині, ширина плечей та товщина шкірно-жирової складки на боку; а між хворими на доброякісні невуси - обхват грудної клітки на вдиху. Отримані результати вказують на значний вплив факторів зовнішнього середовища на виникнення доброякісних невусів.

Ключові слова: *захворювання шкіри, доброякісні невуси, антропометричні показники, обхватні розміри тіла, поперечні розміри тіла, товщина шкірно-жирових складок, соматотипологічні показники, українськи чоловіки, дискримінантні моделі.*

REQUIREMENTS FOR ARTICLES

For publication, scientific articles are accepted only in English only with translation on Ukrainian, which contain the following necessary elements: UDC code; title of the article (in English and Ukrainian); surname, name and patronymic of the authors (in English and Ukrainian); the official name of the organization (institution) (in English and Ukrainian); city, country (in English and Ukrainian); structured annotations (in English and Ukrainian); keywords (in English and Ukrainian); introduction; purpose; materials and methods of research; research results; discussion; conclusions; bibliographic references.

The title of the article briefly reflects its contents and contains no more than 15 words.

Abstract. The volume of the annotation is 1800-2500 characters without spaces. The text of an annotation in one paragraph should not contain general phrases, display the main content of the article and be structured. The abstract should contain an introductory sentence reflecting the relevance of the study, the purpose of the study, a brief description of the methods of conducting research (2-3 sentences with the mandatory provision of the applied statistical methods), a description of the main results (50-70% of the volume of the abstract) and a concise conclusion (1 sentence). The abstract should be clear without familiarizing the main content of the article. Use the following expressions: "Detected ...", "Installed ...", "Fixed ...", "Impact assessed ...", "Characterized by regularities ...", etc. In an annotation, use an active rather than passive state.

Keywords: 4-6 words (or phrases).

"Introduction"

The introduction reflects the state of research and the relevance of the problem according to the world scientific literature (at least 15 references to English articles in international journals over the past 5 years). At the end of the entry, the purpose of the article is formulated (contains no more than 2-3 sentences, in which the problem or hypothesis is addressed, which is solved by the author).

"Materials and methods"

The section should allow other researchers to perform similar studies and check the results obtained by the author. If necessary, this section may be divided into subdivisions. Depending on the research objects, the ethical principles of the European Convention for the protection of vertebrate animals must be observed; Helsinki Declaration; informed consent of the surveyed, etc. (for more details, see "Public Ethics and its Conflict"). At the end of this section, a "statistical processing of results" section is required, which specifies the program and methods for processing the results obtained by the automobile.

"Results"

Requirements for writing this section are general, as well as for all international scientific publications. The data is presented clearly, in the form of short descriptions, and must be illustrated by color graphics (no more than 4) or drawings (no more than 8) and tables (no more than 4), the information is not duplicated.

"Discussion"

In the discussion, it is necessary to summarize and analyze the results, as possible, compare them with the data of other researchers. It is necessary to highlight the novelty and possible theoretical or practical significance of the results of the research. You should not repeat the information already listed in the "Introduction" section. At the end of the discussion, a separate paragraph should reflect the prospects for using the results obtained by the author.

"Conclusion"

5-10 sentences that summarize the work done (in the form of paragraphs or solid text).

"Acknowlegements"

Submitted after conclusion before bibliographic references.

"References"

References in the text are indicated by Arabic numerals in square brackets according to the numerology in the list of references. The list of references (made without abbreviations) sorted by alphabet, in accordance with the requirements of APA Style (American Psychological Association Style): with the obligatory referencing of all authors, work titles, journal names, or books (with obligatory publication by the publishing house, and editors when they are available), therefore, numbers or releases and pages. In the Cyrillic alphabets references, give the author's surnames and initials in English (Cyrillic alphabet in brackets), the title of the article or book, and the name of the magazine or the publisher first to be submitted in the original language of the article, and then in square brackets in English. If available, doi indexes must be provided on www.crossref.org (at least 80% of the bibliographic references must have their own doi indexes). Links to online publications, abstracts and dissertations are not welcome.

After the list of references, it is necessary to provide information about all authors (in English, Ukrainian and Russian): last name, first name and patronymic of the author, degree, place of work and position, **ORCID number** (each of the authors of the ORCID personal number if absence - free creation on the official website http://www.orcid.org) to facilitate the readers of this article to refer to your publications in other scientific publications.

The last page of the text should include the surname, name and patronymic of the author, degree, postal address, telephone number and e-mail of the author, with which the editors will maintain contact.

Concluding remarks

The manuscript should be executed in such a way that the number of refinements and revisions during the editorial of the article was minimal.

When submitting the article, please observe the following requirements. The volume of the article - not less than 15 and not more than 25 pages, Times New Roman, 14 pt, line spacing - one and a half, fields - 2 cm, sheet A4. Text materials should be prepared in the MS Word editor (* .docx), without indentations. Math formulas and equations to prepare in the embedded editor; graphics - in MS Excel. Use the units of the International Measurement System. Tables and drawings must contain the name, be numbered, and references to them in the text should be presented as follows: (fig. 1), or (table 1). The drawings should be in the format "jpg" or "tif"; when scanned, the resolution should be at least 800 dpi; when scanning half-tone and color images, the resolution should be at least 300 dpi. All figures must be represented in the CMYK palette. The statistical and other details are given below the table in the notes. Table materials and drawings place at the end of the text of the manuscript. All elements of the text in images (charts, diagrams, diagrams) must have the Times New Roman headset.

Articles are sent to the editorial board only in electronic form (one file) at the e-mail address nila@vnmu.edu.ua

Responsible editor - Gunas Igor Valeryovich (phone number: + 38-067-121-00-05; e-mail: igor.v.gunas@gmail.com).

Signed for print 07.06.2022
Format 60x84/8. Printing offset. Order № 1375. Circulation 100.
Vinnytsia. Printing house “TVORY”, Nemyrivske shose St., 62a,
Vinnytsya, 21034
Phone: 0 (800) 33-00-90, (096) 97-30-934, (093) 89-13-852,
(098) 46-98-043
e-mail: tvory2009@gmail.com
http://www.tvoru.com.ua